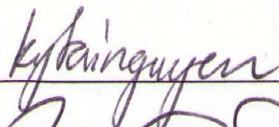


MULTI-LIGAND NANOPARTICLES FOR TARGETED DRUG DELIVERY TO
THE INJURED VASCULAR WALL

The members of the Committee approve the doctoral
dissertation of Soujanya Kona

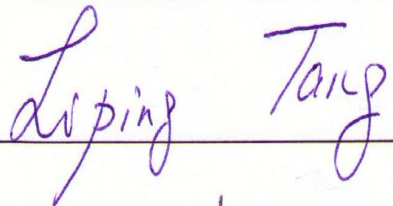
Kytai T. Nguyen
Supervising Professor



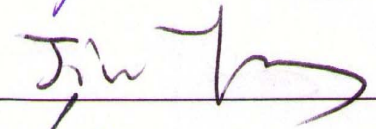
Robert C. Eberhart
Committee Chairperson



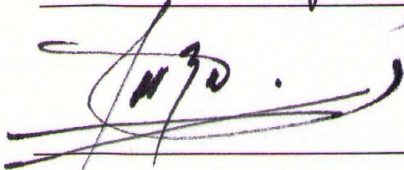
Liping Tang



Jian Yang



Mario Romero-ortega



Yaling Liu



MULTI-LIGAND NANOPARTICLES FOR TARGETED DRUG
DELIVERY TO THE INJURED VASCULAR WALL

by

SOUJANYA KONA

Presented to the Faculty of the Graduate School of
The University of Texas at Arlington in Partial Fulfillment
of the Requirements
for the Degree of

DOCTOR OF PHILOSOPHY

THE UNIVERSITY OF TEXAS AT ARLINGTON

August 2010

Copyright © by Soujanya Kona 2010

All Rights Reserved

ACKNOWLEDGEMENTS

I would like to thank Dr. Kytai T. Nguyen for providing me the opportunity to work in her laboratory. Her guidance and faith in my abilities enabled me to pursue this research independently. She, with her positive and optimistic outlook, has been a source of inspiration and a pillar of support throughout the duration of my graduate studies.

I would also like to thank my entire thesis committee (Dr. Robert C. Eberhart, Dr. Liping Tang, Dr. Jian Yang, Dr. Mario I. Romero-Ortega, and Dr. Yaling Liu) for their valuable time in reviewing my work and providing valuable advice. In addition, I would like to recognize our collaborator, Dr. Jing-Fei Dong of the Baylor College of Medicine, Houston, for providing me with purified glycolalicin and his expertise on platelet adhesion properties. I would also like to acknowledge all the lab members of the Nanomedicine and Tissue Engineering Laboratory. In particular, I would like to extend special thanks to Hao Xu for his help with the animal studies.

Last but not the least I would like to extend my heartfelt thanks to my entire family for their support and guidance. I would like to thank my parents, Mr. K.G.K. Sarma and (late) Mrs. K.Kamala for their continual guidance, support, unlimited love and encouragement in all my endeavors. I would also like to recognize my husband, Srikanth Voorakaranam, for all his love, support, and understanding.

April 29, 2010

ABSTRACT

MULTI-LIGAND NANOPARTICLES FOR TARGETED DRUG

DELIVERY TO THE INJURED VASCULAR WALL

Soujanya Kona, PhD

The University of Texas at Arlington, 2010

Supervising Professor: Kytai T. Nguyen

Pathological conditions like coronary artery disease, acute myocardial infarction, stroke, and peripheral artery diseases as well as cardiovascular interventions used in the treatment of coronary artery diseases such as angioplasty and stenting damage/injure the blood vessel wall, leading to inflamed or activated endothelial cells that have been implicated in events leading to thrombosis, inflammation, and restenosis. Oral administration of anti-coagulant and anti-inflammatory drugs causes systemic toxicity, bleeding, patient non-compliance, and inadequate amounts of drugs at the injured area. Though drug-eluting stents have shown therapeutic benefits, complications such as in-stent restenosis and late thrombosis still remain and are a cause for concern. Rapid growth in the field of nanotechnology and nanoscience in recent years has paved the

way for new targeted and controlled drug delivery strategies. In this perspective, the development of biodegradable nanoparticles for targeted intracellular drug delivery to the inflamed endothelial cells may offer an improved avenue for treatment of cardiovascular diseases.

The major objective of this research was to develop “novel multi-ligand nanoparticles,” as drug carriers that can efficiently target and deliver therapeutic agents to the injured/inflamed vascular cells under dynamic flow conditions. Our approach mimics the natural binding ability of platelets to injured/activated endothelial cells through glycoprotein Ib (GPIb) bound to P-selectin expressed on inflamed endothelial cells and to the subendothelium through GPIb binding to von Willebrand factor (vWF) deposited onto the injured vascular wall. Our design also exploits the natural cell membrane translocation ability of the internalizing cell peptide - trans-activating transcriptor (TAT) to enhance the nanoparticle uptake by the targeted cells. Our hypothesis is that these multi-ligand nanoparticles would show an increased accumulation at the injury site since GPIb specially binds to both P-selectin expressed on damaged endothelial cells and vWF deposited on injured subendothelium while the cell penetrating peptide – TAT would facilitate enhanced uptake of these nanoparticles by the damaged vascular cells.

To test this hypothesis, fluorescent drug loaded poly (D, L-lactic-co-glycolic acid) (PLGA)-polyethylene glycol (PEG) nanoparticles (PLGA-PEG NPs) were

formulated using a standard double emulsion method. We further conjugated GPIb and TAT via carbodiimide and avidin-biotin chemistry to the PLGA-PEG nanoparticles. Characterization of these nanoparticles indicated the average size to be about 200nm. Endothelial cell uptake studies indicated an optimal nanoparticle incubation time of one hour and optimal dose of 400 µg/ml. Biocompatibility results showed these particles to be non-toxic to endothelial cells. Moreover, dexamethasone release profiles from the nanoparticles demonstrated their ability to provide a sustained drug release over four weeks. Static and dynamic uptake studies of control, GPIb-conjugated, and GPIb-TAT-conjugated PLGA-PEG nanoparticles on activated endothelial cells exhibited an increased adhesion and uptake of GPIb-TAT conjugated PLGA-PEG nanoparticles compared to control nanoparticles. A similar trend of significantly higher adhesion of GPIb-TAT conjugated PLGA-PEG nanoparticles to the injured vessel wall was also observed in preliminary *ex-vivo* studies using the rat carotid injury model. These results suggest that “our novel multi-ligand NPs” would provide a unique active targeting strategy. This system would rapidly target and deliver therapeutic agents to the injured vascular wall under flow conditions. It could also serve as an effective therapeutic delivery system to treat the complications associated with cardiovascular diseases.

TABLE OF CONTENTS

ACKNOWLEDGEMENTS.....	iv
ABSTRACT	v
LIST OF ILLUSTRATIONS.....	xiii
LIST OF TABLES.....	xix
LIST OF ABBREVIATIONS.....	xx
CHAPTER	PAGE
1. INTRODUCTION.....	1
1.1 Cardiovascular Diseases	1
1.1.1 Existing Treatment Options.....	1
1.1.2 Limitations of Current Treatments for Cardiovascular Disease.....	3
1.2 Drug Delivery Particulate Systems.....	5
1.2.1 Characteristics of an Ideal Targeted Drug Delivery System.....	5
1.2.2 Nanoparticles for Drug Delivery	5
1.2.3 Polymers Used to Formulate Nanoparticles	6
1.2.4 Methods for Formulation of Biodegradable Nanoparticles	7
1.2.5 Other Drug Delivery Particulate Systems.....	9
1.2.6 Targeting Nanoparticles.....	11

1.2.7 Drawbacks with Using Nanoparticles for Drug Delivery	12
1.3 Endothelium and Strategies to Target the Injured Endothelium.....	13
1.4 Role of GPIIb/IIIa in Platelet Adhesion	16
1.5 Cell-Penetrating Peptides.....	19
1.6 Overview of Research Project	20
1.6.1 Goals/Objectives.....	20
1.6.2 Specific Aims.....	22
1.6.3 Innovative Aspects.....	23
1.6.4 Successful Outcome of the Project.....	24
2. FORMULATION AND CHARACTERIZATION OF <i>IN VITRO</i> PERFORMANCE OF DRUG-LOADED BIODEGRADABLE GPIIb-NANOPARTICLES.....	25
2.1 Introduction.....	25
2.2 Materials and Methods	27
2.2.1 Materials	27
2.2.2 Formulation of Nanoparticles	27
2.2.3 Characterization and <i>In Vitro</i> stability of PLGA NPs.....	28
2.2.4 Drug loading and <i>In vitro</i> Drug Release Studies	29
2.2.5 Culture of Human Aortic Endothelial Cells	30
2.2.6 Preparing P-selectin and vWF Coated Slides as well as Activated HAECs.....	30

2.2.7 Cellular Studies of PLGA NPs by HAECs.....	31
2.2.8 PLGA Nanoparticle Conjugation with Glycocalicin (GPIb).....	35
2.2.9 Adhesion and Cellular Uptake of GPIb-conjugated NPs under physiological flow conditions	36
2.2.10 <i>In Vitro</i> Anti-Inflammatory Study	37
2.2.11 Statistical Analysis.....	38
2.3 Results.....	39
2.3.1 Characterization and <i>In Vitro</i> Stability of PLGA NPs.....	39
2.3.2 Drug Release Profile.....	41
2.3.3 Characteristics of cellular studies of NPs by HAECs	41
2.3.4 GPIb conjugated NPs improved adhesion on coated surfaces and cellular uptake by HAECs under physiological flow conditions.....	47
2.3.5 <i>In Vitro</i> Anti-inflammation Study	52
2.4 Discussion.....	54
2.5 Limitations.....	58
3. GPIb-TAT CONJUGATED NANOPARTICLES FOR TARGETED DRUG DELIVERY TO VASCULATURE	59
3.1 Introduction.....	59
3.2 Materials and Methods	60
3.2.1 Materials	60
3.2.2 Formulation of PLGA-PEG NPs	61

3.2.3 Characterization and <i>In Vitro</i> Stability of PLGA-PEG NPs	62
3.2.4 Drug Loading and <i>In vitro</i> Drug Release Studies.....	63
3.2.5 Culture of Human Aortic Endothelial Cells	64
3.2.6 Determination of Suitable Cell Penetrating Peptide for Conjugation to NPs	64
3.2.7 Preparing P-selectin– and vWF– Coated Slides and Activation of HAECs	65
3.2.8 Cellular Studies of PLGA–PEG NPs using HAECs	65
3.2.9 Conjugation of Glycocalicin and TAT Peptide to PLGA-PEG NPs	67
3.2.10 Comparative Studies of Adhesion and Cellular Uptake of Conjugated NPs	68
3.2.11 <i>In Vitro</i> Anti-Inflammatory Study	70
3.2.12 <i>Ex vivo</i> localization and retention of the GPIb-TAT-conjugated NPs	71
3.2.13 Statistical Analysis.....	72
3.3 Results.....	72
3.3.1 Characterization and <i>In Vitro</i> stability of the NPs	72
3.3.2 Drug Release Profile.....	76
3.3.3 Determination of suitable cell penetrating peptide for conjugation to NPs	76
3.3.4 Characteristics of cellular studies of PLGA-PEG NPs by HAECs.....	83

3.3.5 Comparative Studies with GPIb-TAT conjugated NPs under static and physiological flow conditions.....	85
3.3.6 <i>In Vitro</i> Anti-inflammation Study	91
3.3.7 Mechanisms of Nanoparticle Uptake.....	92
3.3.8 <i>Ex Vivo</i> Retention Study.....	94
3.4 Discussion.....	95
3.5 Conclusions.....	98
4. CONCLUSIONS, LIMITATIONS AND FUTURE WORK.....	99
REFERENCES	103
BIOGRAPHICAL INFORMATION.....	145

LIST OF ILLUSTRATIONS

Figure	Page
1.1 Mechanism of EDC Action	12
1.2 Interactions of platelet GPIIb/IIIa with P-selectin, vWF and P-selectin-bound vWF to injured endothelium.....	18
1.3 Schematic Representation of Multi-Ligand Nanoparticles Targeting Injured Vascular Wall for Drug Delivery	21
2.1 Schematic illustration of GPIIb conjugated nanoparticles mimicking the binding characteristics of platelets to target the injured endothelium	26
2.2 Scheme of the Parallel Plate Flow Chamber. The chamber has a polycarbonate slab (A), silicone gasket (B) and glass slides (C). The system was held in place by vacuum generated by the vacuum pump connected to the vacuum port. The continuous flow syringe pump was connected to the inlet port to create the required shear stress. This system was used for cellular studies while a similar set-up for coated surfaces used the circular flow chamber.....	33
2.3 Schematic of the chemical reactions used to attach GPIIb (glycocalicin) to carboxylated PLGA NPs.....	35
2.4 Characterization of PLGA NPs (A) Scanning Electron Microscopy (SEM) Image (B) Transmission Electron Microscopy (TEM) Image.....	39
2.5 <i>In vitro</i> stability of the NPs over 5 days. Control NPs and GPIIb–conjugated NPs either in PBS or in 100% FBS, were incubated at 37°C over five day period. NP suspensions were collected to measure NPs size using ZetaPALS dynamic light scattering. Values represent mean ± standard deviation (n=3).....	40
2.6 <i>In vitro</i> Release Profile of Dexamethasone from the drug loaded PLGA NPs at 37°C. Values represent mean ± standard deviation (n=4).....	41

2.7 Nanoparticle biocompatibility study. Cells were exposed to the nanoparticles for 24 hours and cells not exposed to nanoparticles served as controls (100% cell viability). ** indicates significant differences compared to the control samples (p< 0.001). All values are represented as mean ± SD (n=4)	42
2.8 Effects of particle size on uptake by HAECs. Values were obtained after one hour of incubation with NP solutions. * indicates significant differences compared to 200 nm NPs samples (p<0.05)s.....	43
2.9 Effects of NP concentration and time on cellular uptake. Values were obtained after incubating with NP solutions either for one hour or with 100 µg/ml.....	44
2.10 Color overlay of Z-stack of NP uptake by HAECs. Plasma membranes were labeled with FM [®] 4-64 FX and imaged using TRIC filter (Ex(λ) 565 nm/Em(λ) 744 nm). Fluorescent NPs were imaged with FITC filter (Ex(λ) 488 nm/Em(λ) 525 nm). Scale bar= 20 µm.....	45
2.11 Effect of temperature on uptake of different sized particles by HAECs. Values were obtained after one hour pre-incubation at respective temperatures followed by NP incubation. Results are represented as mean ± SD (n=4). * indicates significant difference of 200 nm particles compared to 37°C samples (p< 0.05); # indicates significant difference of 500 nm particles compared against 37°C samples (p< 0.05); ≠ indicates significant difference of 1000 nm particles versus 37°C samples (p< 0.05)	46
2.12 Effect of shear stress on cellular uptake by HAECs. Values were obtained after 30 minutes of flow with 200 nm NP solutions and are represented as mean ± SD (n=4). * indicates significant differences compared to static samples (p< 0.05)	47
2.13 Glycocalicin conjugation onto PLGA NPs (A) Fluorescent NPs imaged using the green filter via Cytoviva microscope (B) Cytoviva image obtained using both green and red filters.....	48
2.14 GPIb-conjugated particle adhesion to (A) P-selectin and (B) vWF coated surfaces using different size particle samples. Values represent mean ± SD (n=4). ** denotes the significant differences with respect to the same particle group of static samples (p< 0.001)	49

2.15 Adhesion of control and GPIIb-conjugated NPs onto P-selectin and vWF coated surfaces at a shear stress of 5 dyne/sq. cm for 15 minutes. Values are represented as mean \pm SD (n=4). * indicates the significant difference compared to the control NPs samples (p< 0.05).....	50
2.16 Adhesion and Uptake of GPIIb-conjugated and control NPs by activated HAECs under shear stresses. Cells were activated with 25mM histamine just before flow. Measurements were made after 30 minutes of flow. Values represent mean \pm SD (n=3). * indicates the significant differences compared to the same nanoparticle group of static samples (p< 0.05). # denotes the significant difference between GPIIb-conjugated NPs with control NPs (p< 0.05).....	51
2.17 (A) Z-stack Confocal Image of cellular uptake of control NPs (B) Z-stack Confocal Image of cellular uptake of GPIIb-conjugated NPs. Fluorescent NPs were imaged using a FITC filter, while plasma membranes were stained with FM [®] 4-64 FX red membrane dye and imaged using TRIC filter. Images on the far right represent the color overlay of FITC and TRIC filters. Scale Bar = 20 μ m.	52
2.18 <i>In vitro</i> anti-inflammatory study comparing control, free DEX, DEX encapsulated PLGA NPs and GPIIb-conjugated - DEX encapsulated PLGA NPs. Values represent mean \pm standard deviation (n=4). * indicates significant differences of GPIIb-conjugated NPs compared to control NP samples (p< 0.05).....	53
3.1 Illustration showing the reaction for conjugation of PEG to PLGA NPs.....	62
3.2 Schematic of the conjugation of GPIIb and TAT to the PLGA-PEG NP.....	67
3.3 FTIR spectra of PLGA NPs, PEG polymer and PLGA-PEG NPs	73
3.4 Nanoparticle Characterization using TEM (A) PLGA NPs (B) PLGA-PEG NPs (C) GPIIb-conjugated PLGA-PEG NPs (D) GPIIb-TAT-conjugated PLGA-PEG NPs.....	74
3.5 Stability of formulated NPs over 5 days at 37 ^o C (A) PBS and (B) 100% FBS. Values represent mean \pm standard deviation (n=3)	75
3.6 <i>In vitro</i> Release Curve of Dexamethasone from PLGA-PEG NPs at 37 ^o C. Values represent mean \pm standard deviation (n=4)	76

3.7 Uptake of various CPPs in HAECs after incubation for one hour. FITC intensity was determined by normalizing fluorescence intensity of each treatment with its cell numbers. Values are represented as mean \pm standard deviation (n=4).....	78
3.8 Cytotoxicity of various CPPs in HAECs as determined by MTS assays after incubation for 24 hours. Values are represented as mean \pm standard deviation (n=4).....	78
3.9 Uptake of various CPP-conjugated PLGA NPs by HAECs after incubation for one hour (200 μ g/ml). Uptake was determined by normalizing FITC fluorescence intensity with respective cell numbers. Values represent mean \pm standard deviation (n=4). * indicates significant differences compared to the control samples (p< 0.05).....	79
3.10 Cytotoxicity of various CPP-conjugated PLGA NPs in HAECs after incubation for 24 hours at a concentration of 200 μ g/ml. Viability was assessed by MTS assay. Values are represented as mean \pm standard deviation (n=4). * indicates significant differences compared to the control samples (p< 0.05).....	80
3.11 Effect of dose and incubation time on cellular uptake of TAT peptide. Values were obtained after incubating with TAT for either upto 1 hour or upto 5 μ M.....	81
3.12 HAEC viability after exposure to TAT peptides for 24 hours at 37°C.....	82
3.13 Half-life of TAT peptides in HAECs.....	82
3.14 Fluorescence microscope image of cellular uptake of FITC-labeled TAT by HAECs. Cells were incubated with 5 μ M of peptide for 30 minutes. After fixation, cells were counterstained with DAPI and the cellular distribution of peptide was visualized with fluorescence microscope. Scale = 100 μ m.....	83
3.15 PLGA-PEG NPs biocompatibility study. Cells not exposed to NPs act as controls (100% cell viability). * indicates significant differences compared to the control samples (p< 0.05). Values are expressed as mean \pm SD (n=4).....	84
3.16 Effect of PLGA-PEG NP dose and incubation time on HAEC uptake. Values were obtained after incubating with NPs solutions either for one hour or with 300 μ g/ml of NPs.....	85

3.17 Evidence of TAT peptide and GPIb conjugation to PLGA-PEG NPs using Cytoviva imaging (A) PLGA-PEG NPs (B) Fluorescent NPs imaged using green filter (C) Image obtained using both green and red filters	86
3.18 Quantification of ligand detachment from the conjugated NPs over one week. Values are presented as mean \pm SD (n=4). The total amount of protein bound to the nanoparticles served as the control sample	86
3.19 Adhesion of control, GPIb-conjugated NPs and GPIb-TAT conjugated NPs on P-selectin and vWF coated surfaces at shear stress of 10 dyne/cm ² for 30 minutes. Values represent mean \pm SD (n=4). ** indicates the significant difference compared to the control NPs samples (p< 0.001)	88
3.20 Comparison of cellular biocompatibility of control, GPIb-conjugated and GPIb-TAT-conjugated NPs (NP concentration = 300 μ g/ml) on control and activated HAECs. Values are represented as mean \pm SD (n=4)	89
3.21 Comparison of uptake of control, GPIb-conjugated, and GPIb-TAT-conjugated NPs by either control or activated HAECs under static experimental conditions Values represent mean \pm SD (n=4). * indicates the significant differences compared to the control NPs of respective cell type.....	89
3.22 Shear stress regulated uptake of double-conjugation, single- conjugation and control NPs by activated HAECs. 25 mM histamine was used to activate the cells just before flow. After 30 minutes of flow, the NPs were quantified as described in section 3.2.8. Values represent mean \pm SD (n=3). * indicates the significant differences compared to the static control NP sample.....	90
3.23 Confocal Images of cellular uptake of (A) control NPs (B) GPIb-conjugated NPs, and (C) GPIb-TAT-conjugated NPs. The fluorescent NPs were imaged via a FITC filter, while the FM 4-64 FX [®] stained plasma membranes were imaged with a TRIC filter. Images represent the overlay of both the filters.....	91
3.24 <i>In vitro</i> anti-inflammatory study comparing control, free DEX, and GPIb-TAT-conjugated DEX-encapsulated NPs. Values are represented	

as mean \pm standard deviation (n=4). * indicates significant differences compared to 0 hour control NP samples (p< 0.05).....	92
3.25 Effects of various inhibitory agents on cellular uptake of GPIb-TAT-conjugated PLGA-PEG NPs. <i>Inb.1</i> (chlorpromazine), <i>Inb.2</i> (filipin) and <i>Inb. 3</i> (amiloride). Positive control represents cells incubated with all three inhibitors while negative controls were not exposed to any of the inhibitors. Values represent mean \pm standard deviation (n=4). * indicates significant differences compared to the negative control sample (p< 0.05).....	93
3.26 Retention of PLGA-PEG NPs and GPIb-TAT conjugated NPs in rat carotid artery injury model. Values are correspond to mean \pm standard deviation (n=6). * indicates significant differences compared to the control NPs sample (p< 0.05).....	94
3.27 <i>Ex vivo</i> images of rat carotid arteries using (A) Control NPs, (B) GPIb NPs and (C) GPIb-TAT NPs imaged using the KODAK FX Pro imaging system, after washing with PBS for 3 minutes.....	95

LIST OF TABLES

Table	Page
3.1 Size, polydispersity and Zeta potential of various NP formulations	74
3.2 Zeta Potential of various cell penetrating peptides	77
3.3 Coating Efficiency using Passive Coating Method	87

LIST OF ABBREVIATIONS

ADP.....	Adenosine Diphosphate
BSA.....	Bovine Serum Albumin
CABG	Coronary Artery Bypass Graft
CAD	Coronary Artery Disease
CDC	Centers for Disease Control and Prevention
CVD	Cardio Vascular Disease
Caco-2.....	Human Colon Adenocarcinoma Cell Line
DES.....	Drug Eluting Stent
DEX	Dexamethasone
DI	Deionized
DLS.....	Dynamic Light Scattering
EC	Endothelial Cell
ECAM.....	Endothelial Cell Adhesion Molecule
ECM.....	Extracellular Matrix
EDC.....	1-ethyl-3-(3-dimethylaminopropyl) carbodiimide
FBS	Fetal Bovine Serum
FDA.....	Food and Drug Administration

FITC.....	Fluorescein Isothiocyanate
GPIb.....	Glycoprotein Ib
HAEC.....	Human Aortic Endothelial Cells
ICAM.....	Intercellular Adhesion Molecule
IgG.....	Immunoglobulin G
LSGS.....	Low Serum Growth Supplement
mAbs.....	Mouse Antibodies
MES.....	2-Morpholinoethanesulfonic Acid
MWCO.....	Molecular Weight Cut-off
NHS.....	N-Hydroxysuccinimide
NPs.....	Nanoparticles
O.....	Oil Phase
PBS.....	Phosphate Buffered Saline
PCI.....	Percutaneous Coronary Intervention
PEG.....	Poly Ethylene Glycol
PLGA.....	Poly (lactic-co-glycolic) Acid
PSGL-1.....	P-Selectin Glycoprotein Ligand-1
PTC.....	Percutaneous Transluminal Coronary
PTCA.....	Percutaneous Transluminal Coronary
	Angioplasty
PVA.....	Polyvinyl Alcohol
RES.....	Reticular Endothelial System

RITC	Rhodamine Isothiocyanate
SEM	Scanning Electron Microscopy
sLe ^x	Sialyl-Lewis ^x
TAT	Trans-activating Transcriptor
TEM	Transmission Electron Microscopy
VCAM.....	Vascular Cell Adhesion Molecule
VSMC	Vascular Smooth Muscle Cell
vWF	Von Willebrand Factor
W	Water Phase
W/O/W	Water-Oil-in-Water
W/V	Weight by Volume

CHAPTER 1
INTRODUCTION

1.1 Cardiovascular Diseases

According to the Center for Disease Control and Prevention (CDC), cardiovascular diseases (CVD) still remain the leading cause of death across the globe. In 2006 alone, more than half a million Americans died of CVD.¹ A recent study estimates the cost of CVD in 2010 in the United States would be \$316.4 billion.² Risk factors for CVD include high cholesterol, high blood pressure, diabetes, smoking, alcohol, obesity, poor diet, and physical inactivity due to sedentary lifestyle in the current technological society. Most of these risks can be eliminated or minimized by changes in diet and current life-style as well as in health awareness.

1.1.1 Existing Treatment Options

Various pathological conditions like acute myocardial infarction, stroke, peripheral artery diseases, and coronary artery disease (CAD) trigger events that lead to thrombosis, inflammation, and stenosis.³⁻⁵ Of these, CAD has been implicated the most in triggering these adverse events and in 2005 alone, about 400 thousand people died of CAD.⁶⁻⁸ CAD is caused by the build up of plaque in the coronary arteries that restricts

the blood flow to the heart muscle. This causes the heart to be deprived of oxygen, leading to symptoms ranging from mild chest pain to fatal heart attack.⁹ This build-up of plaque is known as atherosclerosis. Depending on the amount of plaque built up and patient diagnosis, current treatments for CAD include drug therapy and/or surgical interventions like coronary artery bypass graft (CABG) or percutaneous transluminal angioplasty (PTCA). In order to provide symptomatic relief and to directly address the causes of the disease, pharmacotherapy is adopted as the first step for CAD treatment. Pharmacological therapies for treating cardiovascular diseases include drug-based therapies consisting of anticoagulant and antiplatelet agents such as aspirin, beta-blockers, angiotensin-converting enzyme inhibitors, vasodilators, calcium-channel blockers, statins, cyclooxygenase inhibitors, peroxisome proliferator-activated receptors' agonists, and lipid-lowering drugs.^{10, 11} These medications are used to treat patients of cardiovascular diseases along with changes in diet and lifestyle. However, if drug therapy is not effective, interventional therapy is required.

The extent of arterial occlusion determines the interventional procedure: use of either coronary artery bypass graft (CABG) or angioplasty and/or stents. CABG is a highly invasive procedure where the occluded artery is bypassed by grafting an autologous conduit taken from the healthy saphenous vein or internal mammary artery. CABG is often the preferred treatment option for severely occluded arteries that have a high degree of plaque buildup or in cases of multivessel coronary artery disease.^{12, 13} Alternatively, percutaneous coronary intervention (PCI), a much less invasive

procedure, is routinely used for treatment of CAD with lesser plaque buildup. In case of angioplasty, a balloon catheter is inserted and guided through the artery to the site of occlusion where it is then expanded by hydraulic pressure to open up the artery.^{9, 14-16} In the past decade, angioplasty has been accompanied by the deployment of metallic stents made of stainless steel or nickel-titanium to provide support to the expanded artery.

1.1.2 Limitations of Current Treatments for Cardiovascular Disease

Even though current treatments for CAD and CVD are effective in reducing the risks of major cardiac failure, many limitations still exist that need to be overcome. A major concern of PCI involves the risk of neointimal hyperplasia and subsequent restenosis – the re-narrowing of the treated artery as well as inflammation and thrombosis.^{17, 18} The sequence of events leading to restenosis is attributed to the damage of the arterial wall caused by interventions. This damage includes dysfunction, disruption, or inflammation of endothelial cells (ECs) that stimulates platelet deposition and promotes the migration and proliferation of smooth muscle cells (SMCs) from the subendothelium to the injured vessel wall, leading to subsequent neointimal hyperplasia. The injury is also heightened by deposition of platelets, migration of SMCs, macrophages, and neutrophils at the injury site, where they release chemokines.¹⁹⁻²² This encourages further migration and proliferation of SMCs and remodeling of the extracellular matrix, leading to restenosis.²⁰⁻²⁷ In addition, it also generates elastic recoil of the vessel and vessel remodeling.^{28, 29} Thus, in most instances, patients may have to undergo further coronary intervention due to in-stent restenosis

within six months of surgery.^{30, 31} To prevent platelet adhesion and SMC ingrowth, oral administration of anticoagulants and anti-inflammatory drugs have been used.^{32, 33} However, problems associated with oral administration include systemic toxicity, patient incompliance, bleeding complications, and insufficient drug levels at the targeted artery for sufficient time periods to inhibit migration and proliferation of SMCs.

Over the years, use of drug eluting stents has shown great promise in reducing the incidence of restenosis following PCI.³⁴ Drug eluting stents are of two types – stents that are directly coated with drugs, and stents, which have a drug loaded polymeric coating. Various drugs, such as paclitaxel, rapamycin, sirolimus, dexamethasone, and curcumin, have been either directly coated on stents or incorporated into polymer coating of metallic stents to treat vascular thrombosis and restenosis.³⁵⁻⁴³ These drug eluting stents have been shown to drastically reduce the chances of restenosis by delivering the drug over an extended period of time. Even though such stents show important benefits, there are concerns about complications associated with their use such as loss of endothelialization, delayed healing, hypersensitivity reactions, and higher incidences of late thrombosis partially due to impaired endothelial functions.⁴⁴ Significant research has shown that patients implanted with drug eluting stents (DES) have a higher risk of fatal occlusions and myocardial infarctions compared to those having bare metal stents (BMS).⁴⁵⁻⁴⁷ For instance, one study compared the risk of late stent thrombosis (>30 days) in DES to BMS and found that the risk of late stent

thrombosis was significant (50% DESs vs 14% BMSs) when antiplatelet therapy was discontinued. In addition, 25% of patients on aspirin monotherapy and 25% of patients on dual antiplatelet therapy exhibited late angiographic stent thrombosis, while none were observed in patients with BMS.⁴⁸ In light of these concerns, it is important to develop an alternative therapy to overcome these limitations.

1.2 Drug Delivery Particulate Systems

1.2.1 Characteristics of an Ideal Targeted Drug Delivery System

In order to accomplish site-specific drug delivery, an ideal targeted drug delivery system (DDS) relies on the interaction between specific physiological receptors and physical attachment of the DDS system to the desired or targeted site.⁴⁹ In addition, the targeted DDS should be able to deliver a sufficient dose of the drug at the interested/diseased site and be able to maintain the therapeutic amount for a required period of time.⁵⁰ Moreover, an ideal DDS should be able to escape detection and clearance by the immune system while in circulation.⁵¹ It is also beneficial if the material used for DDS is bioresorbable so that it can be cleared by the body naturally.

1.2.2 Nanoparticles for Drug Delivery

In the past few years, the rapid growth of nanotechnology and nanoscience has greatly expanded the clinical opportunities for new therapies. Recently, nanoparticles (1-1000 nm) have been developed for use as potential therapeutic transporter of drugs

for treatment of various diseases – from CVD to cancer. The drugs can either be encapsulated inside these nanocarriers or covalently coupled to the surfaces of these nanocarriers. It is essential that the nanoparticles, especially degradable nanocarriers, and their degradation products, do not elicit any unfavorable immunogenic responses when administrated *in vivo*. Thus, the selection of materials for formulation of nanoparticles plays a vital role in the properties and characteristics of nanoparticles, and should be considered strictly before designing any nanoparticle-based DDS. Based on the application, the materials used to prepare nanoparticles can be biodegradable or non-biodegradable; however, biodegradable materials are preferred for drug delivery applications.

1.2.3 Polymers Used to Formulate Nanoparticles

Polymers used in the preparation of nanoparticles can be either natural or synthetic. Natural polymers exhibit properties similar to the body matter, and thereby cause less toxicity compared to synthetic materials. However, these polymers are difficult to handle and mould owing to their complex structure.⁵² They are also easily degraded by various factors like proteases, temperature, and pH changes, to name a few. Some examples of natural materials used in the formulation of nanoparticles include collage, gelatin, and chitosan. On the other hand, synthetic polymer materials are favorable due to their ability to be manipulated so that they can be fabricated to have varying mechanical and biocompatible properties as well as degradability.⁵³ In addition, material properties of synthetic polymers are well-defined and can be modified and

controlled for different applications.⁵⁴ However, the synthetic polymers trigger immune responses due to the body's innate reaction towards foreign substances. The most common polymers used in the formulation of nanoparticles are polyesters such as poly (lactic acid) (PLA), poly (glycolic acid) (PGA), and their copolymers poly (lactic-co-glycolic acid) (PLGA). These polymers exhibit high mechanical strength and non-toxic degradative properties.^{54, 55} These polymers have been approved by the FDA for applications such as biodegradable sutures, bone pins and dental implants.^{56, 57} Polymers used for nanoparticle formulation can be either biodegradable or non-biodegradable. Biodegradable polymers are preferred due to their ability to be broken down and subsequently eliminated from the body over a period of time. For example, PLGA undergoes a hydrolytic scission of the ester bonds in the polymer chains and degrades into its constituent components of lactic acid and glycolic acid, which are the by-products of various metabolic pathways in the body, and the body effectively clears the two monomers with minimal systemic toxicity.⁵⁵

1.2.4 Methods for Formulation of Biodegradable Nanoparticles

Various techniques are used in the formulation of biodegradable nanoparticles. Of these, two methods that are commonly used are emulsion-solvent evaporation and nanoprecipitation.⁵⁸⁻⁶⁰ The evaporative emulsion method of nanoparticle formulation involves the use of a single or double emulsion process.⁵⁹ The single emulsion process is used for making hydrophobic drug-loaded nanoparticles while the double emulsion process is used to encapsulate aqueous soluble drugs. In the evaporative emulsion

method, the polymer and water-insoluble drugs are dissolved in an organic solvent like acetone, ethyl acetate, chloroform or dichloromethane to make an oil phase (o). This oil phase is added to an aqueous surfactant phase and sonicated to form the primary oil-in-water emulsion (o/w), ensuing nanoparticle formation. To formulate nanoparticles using the double emulsion method, the water-soluble drugs/proteins are mixed in water (water phase, w) while the polymer is dissolved in the oil phase (o). These two different phases are then emulsified using external ultrasonic energy (sonication). This forms the primary emulsion which is then added to an aqueous phase containing a stabilizer or surfactant, and is further sonicated to give the secondary water-in-oil-in-water emulsion (w/o/w), resulting in the formation of nanoparticles. Any remaining organic solvent is allowed to evaporate before recovering the nanoparticles through ultracentrifugation or filtration.^{61, 62}

A second popular method for preparing nanoparticles is nanoprecipitation, which uses aqueous miscible organic solvents to drive spontaneous nanoparticle formation. In this process both the polymer and the drug are dissolved in the amphiphilic solvent and then mixed into a continuous aqueous phase that has the surfactant. This causes the dissolved polymer in the water-miscible organic phase to spontaneously diffuse into the aqueous phase leading to the rapid formation of dispersed nanodroplets within an aqueous matrix. These precipitated nanoparticles are then solidified through solvent evaporation under reduced pressure, and particles are recovered by centrifugation or filtration.^{58, 63} The key criteria in determining the suitable

method for formulating nanoparticles and the effectiveness of formulation techniques are particle size and distribution, toxicity of materials used, reproducibility, surface morphology, surface chemistry, surface charge, drug encapsulation efficiency, drug release kinetics, and hemodynamic properties of the particle.^{50, 64} Viewed from this perspective, the emulsion-solvent evaporation method fits the norm for an effective nanoparticle formulation method. The technique offers great flexibility in the choice of solvents and surfactants with lower concentrations required to form the emulsions.⁵⁸ The nanoparticles formed using this process have a narrow size distribution and the process has been shown to be consistent and reproducible.^{58, 59} Another advantage of this method over other methods is its ability to encapsulate a wide spectrum of materials. Since nanoprecipitation relies heavily on gradient driven diffusion to form the nanoparticles, the loading of the drug or other substance into the particles is dependent on its affinity to the aqueous phase.⁵⁸

1.2.5 Other Drug Delivery Particulate Systems

Recent spurt in the field of nanotechnology has seen the development of many systems that can have potential applications in the field of DDS. Examples of such DDS include liposomes, micelles, and microparticles, to name a few.^{56, 65-71} Liposomes are colloidal formations with properties similar to the membranes in cells. They have a lipid bilayer that encapsulates an aqueous core into which water soluble drugs or proteins can be loaded.⁶⁶ Recently, liposomes have been formulated using pH-sensitive lipids, cationic lipids, and other surface modifications in order to improve the efficacy of these

carriers.⁷² Micelles contain a single lipid layer with a hydrophobic core and hydrophilic heads near the surface.^{73, 74} Microparticles (1-1000 μm) are larger in size compared to nanoparticles. This allows for a higher drug loading capacity per particle in the microparticles.^{55, 75-77}

However, of all these particulate DDS, nanoparticles continue to be the preferred option for intracellular drug delivery. The major advantage of nanoparticles as compared to microparticles is their size which enables them to remain in circulation for a longer duration of time.^{78, 79} Added to this is their ability to accumulate at diseased tissues like tumors resulting in augmented drug delivery.⁸⁰ Microparticles (due to their large size), polymeric liposomes, and micelles (with surface properties comparable to those of the lipid bilayer), are rapidly cleared from circulation through the reticular endothelial system (RES), reducing their effectiveness as drug carriers.^{81, 82} Various studies have shown the advantages of nanoparticles over microparticles. For instance, NPs cause little or no local inflammation^{53, 81, 83, 84} and pose a reduced risk of arterial occlusion because of their small size.⁵⁹ *In vitro* studies on different cell types (vascular smooth muscle cells (VSMC), human colon adenocarcinoma cell line (Caco-2), and endothelial cells (ECs)) have shown that cellular uptake by these cells is better with particles of smaller size.^{59, 85, 86}

1.2.6 Targeting Nanoparticles

Nanoparticles can be targeted to the area of interest by either active or passive means. Active targeting involves attaching antibodies or other targeting moieties including peptides or proteins, to the nanoparticle surface. As ligands are more stable under experimental conditions and less prone to batch-to-batch variations that are often observed in antibodies, in addition to being minimally immunogenic, they are the preferred choice.^{51, 64, 87, 88} Various methods can be used for conjugating molecules to the nanoparticles. However, the most successful method engages carbodiimide chemistry and/or avidin-biotin affinity. As the carbodiimide chemistry is often used for covalent binding of carboxylic acid groups and amine groups, this method is especially useful for conjugating ligands to PLGA nanoparticles. Due to its high water solubility and ability to activate carboxyl groups to form bonds with different functional groups, 1-ethyl-3-(3-dimethylaminopropyl) carbodiimide (EDC) is a popular choice for use in bioconjugation. EDC binds directly to the ligand via an amide linkage (Figure 1.1) by a zero-length crosslinking procedure.⁸⁹

Another method for incorporating ligands on nanoparticles makes use of the avidin-biotin affinity. Avidin (egg white), a tetramer protein having four identical subunits, has a high-affinity binding site for biotin, with a dissociation constant of 10^{-15} M.⁹⁰ In this reaction process, biotin (vitamin H) is used to modify the targeting ligand through its carboxylic group with a NHS ester. This biotinylated ligand is then allowed to associate with avidin, resulting in four biotinylated conjugates per avidin. This highly

selective type of carbodiimide and avidin/biotin chemistry can also be used for formulating targeted nanoparticles.

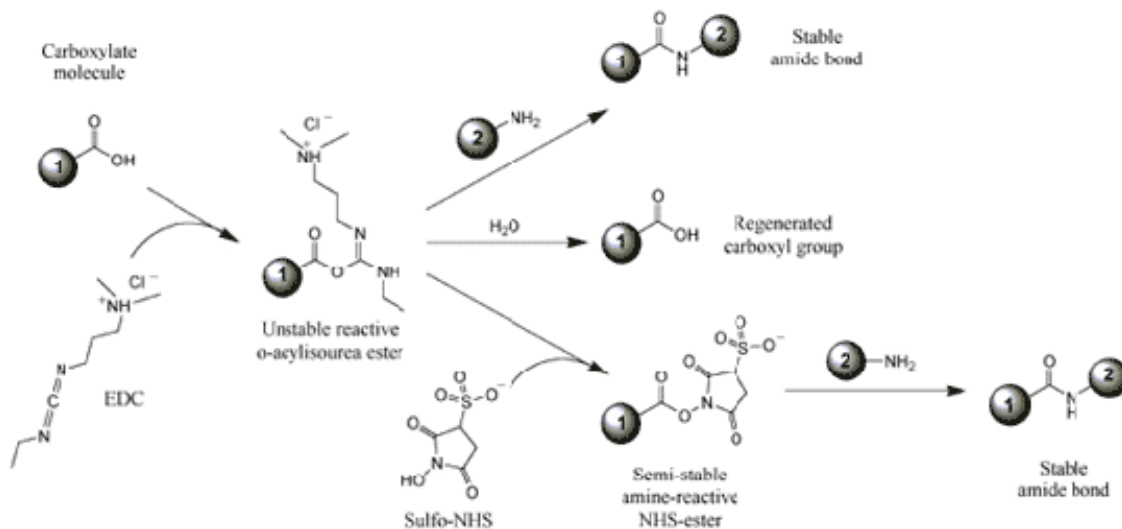


Figure 1.1 Mechanism of EDC Action.⁹¹ EDC activates the carboxyl group on the nanoparticle and forms an amine-reactive O-acylisourea intermediate that is stabilized by sulfo-NHS. The amine reactive NHS-ester then reacts with the amine group of the ligand to form a stable amide bond conjugating the ligand to the nanoparticle.

1.2.7 Drawbacks with Using Nanoparticles for Drug Delivery

The use of nanoparticles for targeted sustained drug delivery has shown promising results *in vitro*. However, nanoparticle drug delivery to cardiovascular systems has the major limitation that NPs do not arrest on the vascular wall efficiently when exposed to the high shear stresses of blood flow that are usually seen *in vivo*. In fact, studies demonstrate that increasing the shear stress rate above 300 s^{-1} causes a significant decrease in the adhesion of particles onto the endothelium.^{92, 93} Preliminary studies conducted in our lab also confirmed this observation.⁹⁴ Therefore, adherence to the targeted surface under high shear forces is a vital step that needs to be addressed

while developing an effective nanoparticle-based therapeutic delivery system for targeting of the vascular system.

One potential approach towards addressing this limitation is to mimic blood components such as red blood cells, leukocytes, and platelets. For instance, nanoparticles that mimic the main structural and functional features of the red blood cells have been recently investigated.⁹⁵ In addition to having the ability to carry oxygen, these RBC-mimicking particles can encapsulate drugs and imaging agents. Other studies have focused on developing particles that can imitate circulating leukocytes.^{96, 97} Another potential strategy would be to mimic nature, specifically the function of platelets that adhere to the damaged vessel wall very efficiently even in regions of high wall shear stress.⁹⁸⁻¹⁰⁰

1.3 Endothelium and Strategies to Target the Injured Endothelium

Endothelium is a thin layer of cells that line the inner lumen of the blood vessels forming a non-thrombogenic barrier between the circulating blood cells and the arterial wall of the blood vessel. This non-thrombogenic function of endothelium can be attributed to heparin sulphate that acts as a cofactor for antithrombin III – a protease enzyme that acts to cleave several factors in the coagulation cascade.¹⁰¹ Along with other vascular and blood cells, endothelial cells (ECs) are also involved in various vascular functions such as vasodilation and vasoconstriction, hemostasis, inflammation,

and thrombosis. Regular endothelial functions are regulated by release of various endothelium-derived factors such as prostacyclin, nitric oxide, thromboxane A₂, and growth factors.¹⁰²⁻¹⁰⁴ An impaired endothelium can cause CVD like atherosclerosis, inflammation and increased adhesion of platelets and other blood components to the activated endothelium.¹⁰⁵⁻¹¹⁴

When ECs get injured or activated, they cause an increased expression of endothelial cell adhesion molecules (ECAMs) on the cell surface.^{113, 115-119} Appearance of these ECAMs triggers a cascade of events that stimulate the adhesion of blood cells such as platelets and leukocytes onto the injured endothelium.¹²⁰⁻¹²³ The increased expression of ECAMs can be triggered by exposure to histamine, thrombin, or by PCI, and this augmented expression can cause increased platelet adhesion through ECAM-mediated processes.^{122, 124} P-selectins are one type of ECAMs that are over-expressed when ECs become activated. P-selectins are stored in intracellular bodies inside the cells and are transported from these storage bodies to the plasma membranes within a few seconds,¹²⁵⁻¹²⁸ where they interact with blood platelets and leukocytes through glycoprotein (GP) I α and P-selectin glycoprotein ligand-1 (PSGL-1), respectively. This results in the rolling adhesion of the platelets and leukocytes on to the activated endothelium.^{56, 125}

A targeted approach to delivering drugs is the new paradigm of DDS to treat CVD, and this has been studied extensively in recent years for targeting therapeutics to

the inflamed endothelium. The research has focused mainly on targeting the ECAMs in diseased endothelium. For instance, one approach used immunoliposomes conjugated with AbH18y7, an antibody for E-selectin, to deliver the drugs.⁷² This study made use of the increased expression of E-selectin in activated ECs to target the drug and found that liposomes conjugated with AbH18y7 exhibited a 275 fold increase in cellular adhesion to activated ECs compared to unactivated ECs.⁷² When the liposomes were loaded with the cytotoxic agent doxorubicin, they showed a significant decrease in cell survival of activated ECs but showed minimal effect on survival of unactivated ECs.⁷² A different approach to targeting inflamed endothelium made use of ligands or humanized monoclonal antibodies (mAbs) against P-selectin and E-selectin for conjugation to microparticles.^{56, 65, 76, 77, 92, 129-132} The ligands used in the selectin studies were Sialyl-Lewis^x (sLe^x) - a carbohydrate found on neutrophils and PSGL-1, present on leukocytes surface.^{56, 77, 132} SLe^x-conjugated microparticles were shown to mimic the rolling behavior of leukocytes on surfaces coated with purified P-selectin, and this rolling adhesion was found to be dependent on the ligand surface density.⁵⁶ An *in vivo* study on mice using PSGL-1 coated microparticles found an increased adhesion of the microparticles by P-selectin expressed on activated endothelium.¹³² Also, conjugation of recombinant PSGL-1 to PEGylated biodegradable microparticles and nanoparticles also showed the selective adhesion of these particles to cytokine-activated endothelium *in vitro* and in animal models.^{65, 130} The promising results of using “leukocyte-inspired particles” for targeted drug delivery initiate new strategies for improving site-specific drug therapy. Even though platelets show a better adherence to activated ECs under

high shear conditions than leukocytes,¹³³ currently there is no targeting strategy that takes advantage of this property or mimics the platelet binding to target the injured vascular wall for drug delivery.

1.4 Role of GPIIb α in Platelet Adhesion

Platelets play a critical role in the early stages of inflammation – a key factor in CVD. Under healthy circumstances, platelets, leukocytes and blood components flow within the lumen of the blood vessels without adhering to the ECs lining the lumen of these vessels. However, when ECs become activated or inflamed upon injury caused to the vessel during angioplasty and/or stenting or due to atherosclerotic plaque rupture,³⁻⁵ there is an increase in the adhesion of platelets and leukocytes to the ECs due to an increased ECAM expression on the ECs. Atherosclerotic plaque rupture leads to the exposure of the underlying extracellular matrix (ECM) leading to platelet adhesion mediated by von Willebrand Factor (vWF) and collagen.^{134, 135} Occlusion of the artery due to thrombus formation can also cause platelet deposition on the artery wall through plasma vWF, and this can be attributed to the shear forces created by blood flow in the blocked vessel.¹³⁴ On attachment to activated or injured ECs, platelets express and release proinflammatory cytokines that cause further interactions between ECs and leukocytes.¹³⁶⁻¹³⁹

Platelets adhere to activated endothelium or the subendothelium through various binding proteins that are present on its surface. The adhered platelets then release chemicals like adenosine diphosphate (ADP), thromboxane A₂, and others, which lead to platelet activation followed by further platelet aggregation. Activation of platelets is caused by conformational changes in its structure causing them to become sticky and allowing them to aggregate by interacting with blood plasma proteins.¹⁴⁰ This process also leads to accumulation of circulating leukocytes to the injury site setting off the inflammatory cascade.

Of the various proteins present on the platelet surface, GPIb-IX-V complex is the primary platelet adhesion molecule that aids in their binding to the P-selectin of the injured ECs or the vWF deposited on the subendothelium.¹³⁴ GPIb-IX-V complex is made up of four glycoproteins – GPIb α , GPIb β , GP-IX and GP-V.¹⁴¹⁻¹⁴³ Of these, GPIb α has binding regions for P-selectin and vWF.^{134, 141} The complex is also responsible for attachment of the platelets to the injured endothelium under high shear conditions.^{125, 144} The expression of ECAMs like P-selectin, E-selectin, VCAM-1 and ICAM-1 by activated ECs mediate the adhesion of platelets through GPIb α .^{145, 146} Thus, GPIb α ligand of platelets can bind to both P-selectin expressed by activated ECs as well as vWF deposited on the subendothelium (Figure 1.2).

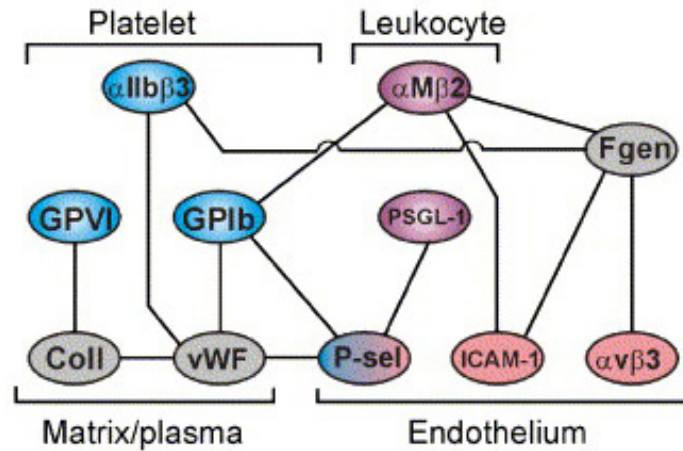


Figure 1.2 Interactions of platelet GPIIb α with P-selectin, vWF and P-selectin-bound vWF to injured endothelium¹³⁴

The N-terminal domain of GPIIb α , consists of approximately 300 amino acids which include the binding regions responsible for adhesion to vWF and P-selectin. Under normal physiological flow conditions, where shear stress in arterial tree averages 15–20 dynes/cm²,¹⁴⁷⁻¹⁴⁹ platelets can adhere to blood vessel walls at shear stresses of upto 60 dyne/cm². Under pathological conditions such as blood vessel injury, adhesion can take place even at shear forces of 100 dyne/cm².^{4, 150} This indicates that GPIIb α ligand is highly effective in adhering platelets to endothelial and subendothelial regions.¹⁵⁰ Hence, targeting therapeutic nanoparticles to activated endothelium by mimicking platelet (GPIIb α) binding affinity to both P-selectin and vWF would provide a better targeting option than mimicking leukocytes. This strategy can be used to develop a controlled nanoparticle DDS to injured vasculature as well as to the leaky endothelium observed in tumors.

1.5 Cell-Penetrating Peptides

The cell membrane exhibits poor permeability to various drugs and DNA which in turn translates into low therapeutic efficacy. This barrier can be overcome by use of cell-penetrating peptides (CPPs), which have shown considerable success in the transport of biologically active molecules into the cells.^{151, 152} CPPs are typically short cationic sequences of amino acids and can be made from natural or synthetic sources.¹⁵³ Studies have shown that CPPs can efficiently improve the intracellular delivery of proteins,^{154, 155} nuclear materials like plasmid DNA, oligonucleotides, siRNA (short interfering RNA) and PNA (peptide nucleic acid),¹⁵⁶⁻¹⁵⁸ as well as liposome nanoparticles¹⁵⁹⁻¹⁶¹ into cells both *in vivo* and *in vitro*. The choice of CPPs is determined by the application and the common peptides under investigation include trans-activating transcriptional activator (TAT), polyarginine, penetratin, and transportan.¹⁵⁷

Cellular uptake studies on different cell types such as SK-BR-3 cells, HeLa cells, IMR-90 cells, U937 cells, and H9 cells, using the HIV-1 TAT peptide which has 9 to 16 amino acids, have shown that these peptides are readily taken up by the studied cells with a cytotoxic effect being observed at concentrations greater than 5 μM , depending on cell type and incubation time.¹⁶² TAT peptide can pass through biological membranes by a mechanism that is independent of transporters and receptor-mediated endocytosis.^{163, 164} Additionally, uptake studies of cell-penetrating peptide – TAT47-57-streptavidin (TAT-SA, 60 kD) in living cells with various fluorescent endocytic markers

and inhibiting agents suggest that TAT-SA is internalized into cells efficiently, using both clathrin-mediated endocytosis and lipid-raft-mediated macropinocytosis.¹⁶⁵ Furthermore, PLA nanoparticles conjugated to TAT peptide bypass the efflux action of P-glycoprotein and increase the availability of the encapsulated protease inhibitor in the central nervous system, while maintaining therapeutic drug levels in the brain for a sustained period.¹⁶⁴

1.6 Overview of Research Project

1.6.1 Goals/Objectives

The overall goal of this project was to develop novel multi-ligand nanoparticles that can be targeted to the injured vascular wall and exhibit better adhesion onto the injured vessel wall under physiological flow conditions as well as to stimulate the cellular uptake of the nanoparticles by the injured endothelial cells and/or the sub-endothelium for drug delivery. Based on observations of platelet interactions and physiology, we selected GPIb as the ligand for conjugating to the drug-encapsulated biodegradable nanoparticles to increase their binding to the vascular wall under high shear. GPIb α would also aid in the specific binding of the nanoparticles to the P-selectin expressed on activated ECs and vWF deposited on the subendothelium. Additionally, the cell internalizing peptide TAT would enhance the nanoparticle uptake by the targeted cells. A schematic representation of our proposed design is shown in Figure 1.3. We chose dexamethasone (DEX) as our model drug since it has been proven to be

an immune suppressant that decreases the development of the intimal hyperplasia¹⁶⁶ and has been shown to consist of well-known potent anti-inflammatory and antiproliferative properties.^{167, 168} By delivering DEX intracellularly, the activity of eNOS is inhibited leading to excessive vasoconstriction¹⁶⁹ and this also blocks the function of the adhesion molecules.¹⁶⁸

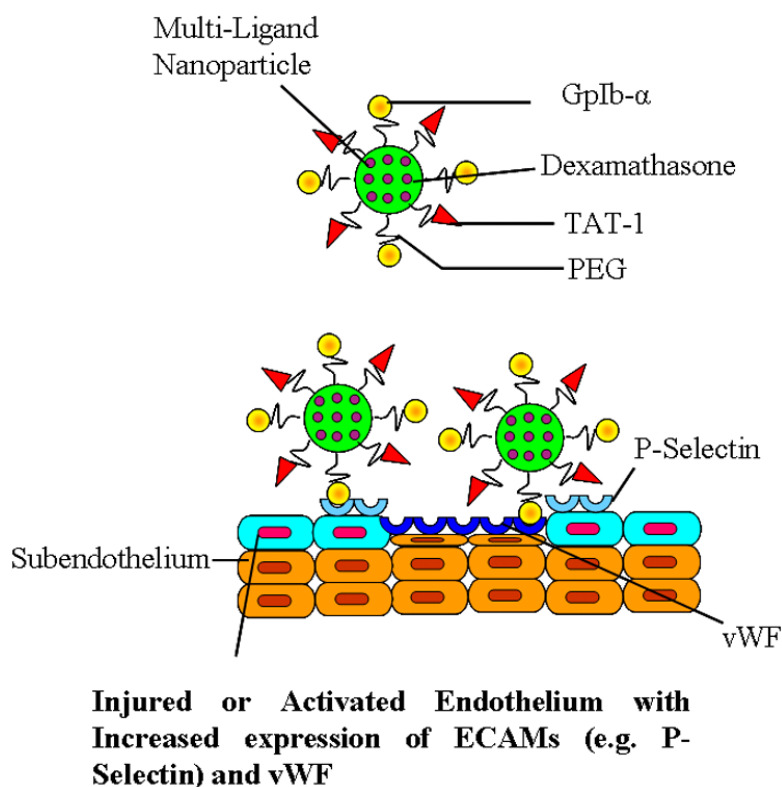


Figure 1.3 Schematic Representation of Multi-Ligand Nanoparticles Targeting Injured Vascular Wall for Drug Delivery

Our design of multi-ligand nanoparticles that efficiently target the injured vessel wall and adhere better under physiological flow conditions, in addition to being internalized by the vascular cells in increased amounts, is based on the following observations:

- After vascular injury due to plaque rupture, cardiovascular interventions or other pathophysiological cardiac conditions, significant P-selectin expression is observed on the damaged endothelium^{106, 130, 131, 168, 170-173} and excess vWF deposition on the luminal surface of the injured blood vessel were seen compared to the normal vessel wall.^{134, 174, 175}
- GPIb serves as an attachment molecule of platelets to the injured vessel wall (either through P-selectin expressed on activated ECs or through vWF deposited on the damaged vessel wall) under physiological flow conditions, especially those of high wall shear stresses.^{134, 143, 176-179}
- The HIV-1 trans-activating transcriptor (TAT) peptide can pass through biological membranes by a mechanism that is independent of transporters and receptor-mediated endocytosis.^{164, 180}
- Drugs that stimulate endothelium (antioxidant vitamins – C & E, eNOS substrate, L-arginine or its co-factor),¹⁸¹⁻¹⁸³ anti-platelet/anti-thrombotic drugs (Prasugrel, Clopidogrel or Aspirin),¹⁸⁴ or anti-inflammatory/anti-proliferative agents (Paclitaxel, Estradiol, Sirolimus or glucocorticoids like dexamethasone, Prednisolone, etc.)¹⁸⁵⁻¹⁹⁰ can be loaded in nanoparticles.

1.6.2 Specific Aims

To achieve our goal, the following **specific aims** will be undertaken.

Aim 1. Formulate and investigate the efficacy of drug-loaded biodegradable GPIb-nanoparticles *in vitro*.

Aim 2. Prepare novel drug-loaded multi-ligand nanoparticles and investigate selective binding and effectiveness of these novel nanoparticles *in vitro*.

Aim 3. Preliminary *ex vivo* studies to determine the effectiveness of these novel nanoparticles, using rats as the animal model.

1.6.3 Innovative Aspects

The innovative aspect of this proposal is to design multiple-ligand targeted nanoparticles that mimic the platelet adhesive properties to recruit these particles selectively to the site of damaged vasculature under physiological flow conditions (multi-ligand nanoparticles, Figure 1.3). The major advantage of using multi-ligand nanoparticles for targeting drug delivery, compared to current targeting strategies including anti-P-selectin antibodies, is that GPIb specially binds to both P-selectin expressed on damaged ECs and vWF deposited on injured subendothelium under flow conditions, thereby accumulating more nanoparticles as drug carriers to the injured arterial site for drug delivery. Also, while GPIb anchors the nanoparticles to the cell wall, the cell internalizing peptide – TAT – facilitates enhanced uptake of nanoparticles by the targeted cells for intracellular drug delivery. In this sequentially triggered and synergistic strategy, GPIb acts as a catch-bond enabling the nanoparticles to be anchored specifically to the injured vascular wall under high flow conditions similar to the adherence properties of platelets onto the injured artery, and the penetrating peptide aids as a facilitator to increase intracellular nanoparticle uptake into the injured cells similar to the penetration properties of HIV-1 virus into the immune cells.

1.6.4 Successful Outcome of the Project

A successful outcome of this study will provide a means to efficiently deliver therapeutic agents to the injured vessel wall in order to either reduce the inflammation of ECs and deposition of platelets, to stimulate endothelial healing, and/or prevent the migration and proliferation of smooth muscle cells (SMCs). Nanoparticles developed in this project can also be used as models to investigate the mechanisms of the platelet-endothelial cell interactions. In addition, results from this work will also provide new knowledge about the combined use of targeting and penetrating peptides for intracellular drug delivery applications. The clinical relevance of this research is that targeted nanoparticles could provide an alternative to systematic drug delivery, via oral and injection routes, to the injured vascular wall and/or complement drug eluting stents.

CHAPTER 2
FORMULATION AND CHARACTERIZATION OF *IN VITRO* PERFORMANCE OF
DRUG-LOADED BIODEGRADABLE GPIb-NANOPARTICLES

2.1 Introduction

Recently, various nanoparticles have been developed for targeted and controlled drug delivery to treat coronary artery diseases. For example, E-selectin immunoliposomes loaded with doxorubicin significantly decreased cell survival in activated ECs, but had no effect on inactivated ECs.⁷² Sialyl-Lewis^x (SLe^x)-conjugated microparticles were able to roll successfully on P-selectin coated surfaces similar to leukocytes.^{96, 191-193} Recombinant PSGL-1 conjugated to PEGylated biodegradable microparticles and NPs exhibited selective adhesion to cytokine-activated endothelium *in vitro* and in animal models.^{130, 170} However, targeting strategies to the vasculature via nanoparticles are limited in that the nanoparticles do not arrest efficiently to the vascular wall under blood flow.^{92, 194} In this chapter we present a targeted drug delivery system that mimics the platelet GPIb binding to the P-selectin and vWF of the injured vessel wall under high shear conditions.⁹⁸⁻¹⁰⁰ Our hypothesis is that these GPIb-conjugated nanoparticles would exclusively attach to the injured vascular wall under high shear conditions (Figure 2.1).

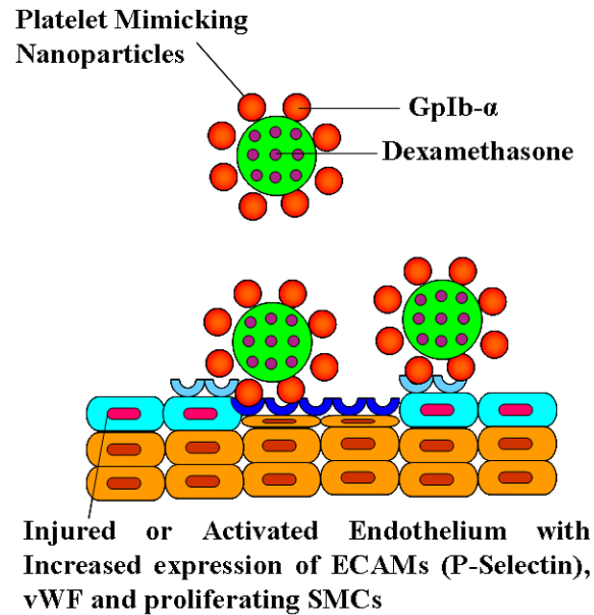


Figure 2.1 Schematic illustration of GPIb conjugated nanoparticles mimicking the binding characteristics of platelets to target the injured endothelium

In this study, we formulated and characterized GPIb-conjugated and dexamethasone-loaded biodegradable poly (D, L-lactic-co-glycolic acid) (PLGA) nanoparticles. For our studies, we chose dexamethasone (DEX) as the model drug since it has been proven to be an immune suppressant that decreases the development of the intimal hyperplasia.¹⁶⁶ Cellular uptake of the nanoparticles was investigated on human aortic endothelial cells (HAECs). The cellular uptake of these particles was determined by both fluorescent measurements and confocal microscopy imaging. Furthermore, GPIb α conjugated PLGA NPs were investigated for their effectiveness in adhering to P-selectin and vWF coated surfaces and for their cellular uptake by HAECs under physiological flow conditions using the parallel plate flow chamber. GPIb α –

conjugated, drug loaded NPs were also examined for their ability to reduce inflammation of activated HAECs.

2.2 Materials and Methods

2.2.1 Materials

Poly (D, L-lactic-co-glycolic acid) (PLGA) (inherent viscosity – 0.4dl/g, copolymer ratio 50:50) with carboxyl end groups, was purchased from Lakeshore Biomaterials (Birmingham, AL). Chemicals, if not specified, were purchased from Sigma-Aldrich (St. Louis, MO). Low serum growth supplement (LSGS, 2 % fetal bovine serum, hydrocortisone (1 µg/ml), human epidermal growth factor (10 ng/ml), basic fibroblast growth factor (3 ng/ml), and heparin (10 µg/ml)) was purchased from Invitrogen (Carlsbad, CA). HAECs were purchased from PromoCell GmbH, Germany. Cell culture media, buffers, and supplements including trypsin-EDTA, Medium 199 (M199), fetal bovine serum (FBS) and penicillin-streptomycin were acquired from Invitrogen Corporation (Carlsbad, CA). Glycocalicin (the external fraction of platelet GPIb α), provided by our collaborator at Baylor College of Medicine, Dr. Jing-Fei Dong, was isolated from human blood as described previously.^{195, 196}

2.2.2 Formulation of Nanoparticles

PLGA NPs were formulated using a double emulsion–solvent evaporation method. In brief, 3% aqueous DEX solution (30mg of DEX in 300µl of DI water) was

emulsified in 3% PLGA solution (90 mg of PLGA in 3 ml chloroform containing 100 μ l of 0.005 mg/ml of 6-coumarin solution) using a probe sonicator (Misonix Inc., 3000, Farmingdale, NY) to form a primary emulsion. This primary emulsion was then added to an aqueous solution of 5% PVA (0.24g PVA in 12ml DI water) to create the double emulsion which was allowed to stir overnight at room temperature allowing organic solvent evaporation. NPs were recovered by ultracentrifugation at 30,000 rpm (Beckman Coulter, Inc., Fullerton, CA) followed by washing to remove residual PVA and non-trapped drug and then lyophilized. NPs without DEX and 6-coumarin dye were formulated in a similar way. 500nm and 1 micron sized NPs were formulated in a similar manner using 1% and 0.5% of PVA, respectively.

2.2.3 Characterization and *In Vitro* stability of PLGA NPs

We characterized the formulated NPs for their morphology, particle size, polydispersity, and surface charge (zeta potential) using scanning electron microscopy (SEM, Hitachi S-3000N), transmission electron microscopy (TEM, JEOL 1200 EX Electron Microscope) and ZetaPALS dynamic light scattering (DLS) detector (Brookhaven Instruments, Holtsville, NY) at room temperature. In addition, we also performed *in vitro* studies of long-term stability and protein binding on our formulated NPs. For studying the stability of NPs in PBS, the NPs were suspended in PBS and incubated at 37°C for 5 days with particle size measured every 24 hours. In addition, NPs were suspended in 100 % fetal bovine serum (FBS) and 10 % (v/v) human plasma

solution for 120 hours at 37°C to determine the stability and protein binding of our NPs in serum and human plasma. Particle sizes were measured every 24 hours using DLS.

2.2.4 Drug loading and *In vitro* Drug Release Studies

To determine the loading efficiency of drugs in the NPs, 1 mg of the freeze-dried particles were dissolved in mixture of chloroform and DI water which allowed the drug to escape the PLGA NPs into the aqueous phase. This solution was then used to determine the amount of drug in the solution and the value obtained was compared to the total amount of DEX used in the nanoparticle formulation to determine the loading efficiency of the NPs.

For *in vitro* drug release studies, stock solutions of drug-loaded NPs were prepared in 0.1 M PBS. 1 ml of stock solution was placed inside dialysis bags (Spectrum Laboratories Inc.) with molecular weight cut-off of 1,000 (since the molecular weight of dexamethasone is 392.5 Dalton) and dialyzed against PBS at 37°C for 21 days. At predetermined intervals, 1 ml of dialysate was collected from each sample and replaced with 1 ml of fresh PBS. The collected dialysate was stored at -20°C for analysis. To determine the amount of DEX released, absorbance of the samples was read at 242 nm. The amount of released drug was determined against a standard DEX curve and correlated to the loading amount to determine the cumulative percentage drug release.

2.2.5 Culture of Human Aortic Endothelial Cells

HAECs were cultured in M199 supplemented with 10% FBS, 1% penicillin-streptomycin and LSGS (complete M199). Upon reaching confluence, cells were either passaged or used for experiments. Cells up to passage 9 were used for the cellular studies. Since prior research has shown that the use of high serum (greater than 1%) media increased the rate of endocytosis and exocytosis of PLGA NPs,^{197, 198} we used low serum (1% serum) M199 for all the nanoparticle cellular studies.

2.2.6 Preparing P-selectin and vWF Coated Slides as well as Activated HAECs

To prepare P-selectin coated surfaces, 35mm non-treated culture dishes were incubated with 500 μ l of 20 μ g/ml P-selectin (R&D Systems) overnight at 4°C while vWF coated surfaces were incubated with 500 μ l of 5 μ g/ml vWF (Calbiochem) under the same conditions. This was followed by 1 hour incubation with a 1% BSA solution to block nonspecific binding. Two-thirds of the culture dishes were then washed gently with a PBS solution to remove any unbound P-selectin and vWF and used immediately for experiments. The remaining one third of the culture dishes were further incubated with the respective antibodies against either P-selectin or vWF for one hour at room temperature, in order to serve as a negative control, and then washed prior to use in the experiment. To prepare activated HAECs, cells were seeded on glass slides as described earlier and then treated with 25 mM histamine for 12 minutes at physiological temperature (37°C) to stimulate the expression of P-selectin by HAECs. These activated cells were then used immediately for experiments.

Coated culture dishes (either P-selectin or vWF for surface studies) were assembled in a circular flow chamber (GlycoTech, Gaithersburg, MD) while pre-etched glass slides with activated HAEC monolayer for cell studies, were assembled into the parallel plate flow systems for cellular studies. We used circular flow chamber for non-cellular surface flow studies as opposed to parallel plate flow system to minimize the cost as well as the amount of protein required for coating. However, for cellular studies we used the parallel plate flow chamber as this system not only provides sufficient surface for the cells to grow but also provides enough cells for bioassays.

2.2.7 Cellular Studies of PLGA NPs by HAECs

To determine the biocompatibility of our formulated NPs on HAECs, we incubated HAECs with various NP concentrations (0-1000 $\mu\text{g/ml}$). Following 24 hours of exposure to the NPs, cell viability was assessed using the MTS assay (Promega Corp.) following the manufacturer's instructions.

To determine cellular uptake of NPs, HAECs were seeded onto 24-well plates at a seeding density of 30,000 cells/well and allowed to grow for 2 days. Complete media was replaced with low serum media at least overnight prior to the experiments to quiescent the cells. The first study was conducted to determine the effect of particle sizes on cellular particle uptake by HAECs. Particles ranging from 200-1000 nm in size were suspended in low serum growth medium at the concentration of 200 $\mu\text{g/ml}$. Media from the 24-well plate was replaced with the particle suspensions, and HAECs were

incubated for one hour. A second study was done to optimize the NP concentration. For this as well as all other studies, NPs in the size range of 100 nm–200 nm were used. NP solutions (0-300 µg/ml) were prepared in low serum growth medium and incubated with HAECs for one hour. The third study evaluated the effect of incubation time on cellular uptake of NPs. HAECs were incubated with 100 µg/ml NPs solution for different periods of time (0–6 hours).

To study the temperature dependent uptake of different size nanoparticles, HAECs were seeded in 24–well plates at a seeding density of 30,000 cells/well and were allowed to grow for two days. For the experiment, cells were first pre-incubated for one hour at three different temperatures, 4°C, 37°C, and 42°C, and then incubated with 200 µg/ml of 200-1000 nm sized particles for an additional one hour at the respective temperatures.

To examine the effects of shear stress on uptake of NPs by HAECs, we seeded the cells on pre-etched glass slides at a density of 10^5 cells/cm² and allowed to reach confluence. Then HAECs on glass slides were exposed to varying (0-20 dyne/cm²) shear stresses (since the average wall shear stress of coronary arteries in coronary artery disease or after coronary stent deployment has been reported to be in the range of 12-15 dyne/sq. cm¹⁹⁹⁻²⁰¹) of media containing PLGA NPs (200 nm) at a concentration of 200 µg/ml for 30 minutes using the parallel plate flow chamber system (Figure 2.2) as described previously.²⁰² Cells in a static condition served as the controls.

We chose the parallel plate flow chamber due to its ability to generate constant levels of shear stress. In brief, the parallel plate flow chamber consisted of a polycarbonate rectangular slab, with a silicon gasket. Glass cover slides were placed on top of the gasket (Figure 2.2). The system was held together by the aid of a vacuum pump (Gast Manufacturing, Inc., Benton Harbor, MI), and shear stress was generated using a continuous flow syringe pump (Harvard Systems, Holliston, MA). Wall shear stress (τ) for the flow chamber was calculated from the following equation:

$$\tau = 6Q\mu / bh^2$$

where Q is the volumetric flow rate, μ is the fluid viscosity, b is the channel width, and h is the channel height.

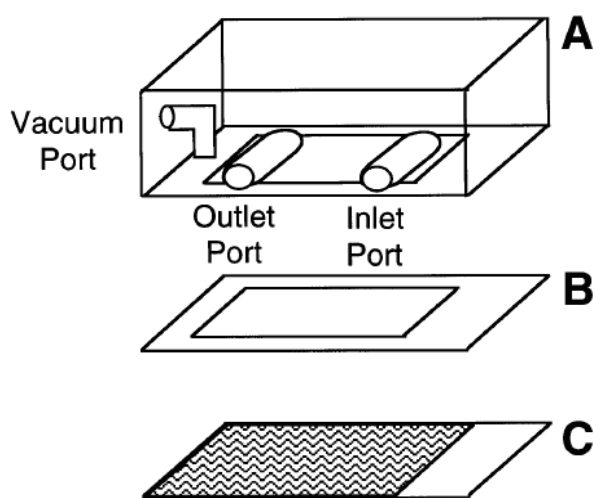


Figure 2.2 Scheme of the Parallel Plate Flow Chamber. The chamber has a polycarbonate slab (A), silicone gasket (B) and glass slides (C). The system was held in place by vacuum generated by the vacuum pump connected to the vacuum port. The continuous flow syringe pump was connected to the inlet port to create the required shear stress. This system was used for cellular studies while a similar set-up for coated surfaces used the circular flow chamber.

After experiments, cells were washed carefully 3 times with cold PBS to remove any adhering NPs. The cells were then incubated with 1% Triton[®] X-100 for one hour in order to lyse them. The cell lysate was then used to determine cell number via the Pierce BCA protein assay (Fisher Scientific, Hampton, NH), following manufacturer's instructions and a standard curve was generated using known number of cells. In order to quantify NPs uptaken by HAECs, the fluorescent intensity of NPs in cell lysates as well as the nanoparticle standards was measured at EX 480 nm/EM 510 nm using the microplate reader (Infinite M200, Tecan USA, Inc.). The NPs uptaken by HAECs was calculated by normalizing the particle concentration with the cell number of each cell lysis sample. The determined optimal time and dosage were used for all further studies.

Intracellular localization of the NPs was visualized using confocal microscopy. For confocal experiments, cells were incubated with 200 µg/ml of NP solutions for one hour. Cover slips were then washed with cold PBS, followed by the addition of cold FM[®] 4-64 FX (5 µg/ml, Invitrogen) in PBS for 5 minutes to stain cell membranes in red. Cells were then fixed with paraformaldehyde and imaged using confocal laser scanning microscope (Leica) equipped with FITC (Ex(λ) 488 nm/Em(λ) 525 nm) and TRIC filters (Ex(λ) 565 nm/Em(λ) 744 nm). Slice thickness was set at 0.1 µm, with an average of 32 slices taken per cell image. The images were analyzed using ImageJ software (NIH, ImageJ 1.40).

2.2.8 PLGA Nanoparticle Conjugation with Glycocalicin (GPIb)

NPs were conjugated with glycocalicin, the external fraction of platelet GPIb α , using carbodiimide chemistry and avidin-biotin affinity (Figure 2.3).

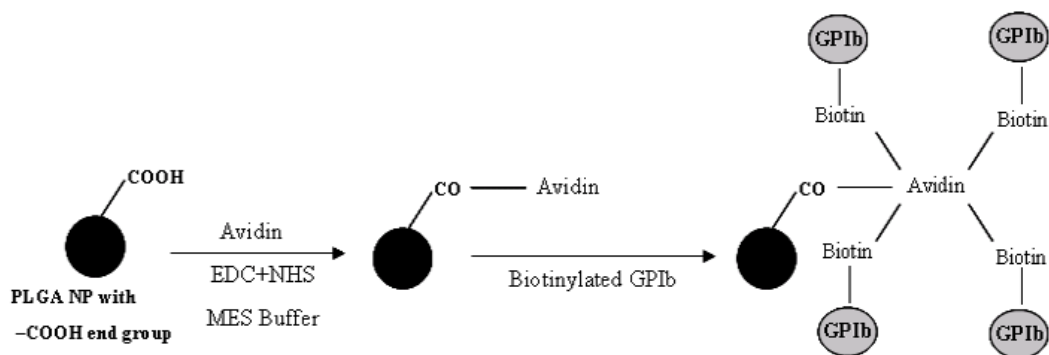


Figure 2.3 Schematic of the chemical reactions used to attach GPIb (glycocalicin) to carboxylated PLGA NPs

Initially, glycocalicin was biotinylated using the Biotin-X-NHS kit (EMD Biosciences, Inc., San Diego, CA), following the manufacturer's instructions. Next, the PLGA NPs were added to EDC solution (prepared in 0.1 M MES buffer, pH 4.75) and incubated at room temperature for five hours to ensure activation of carboxyl groups. This was followed by addition of avidin (EMD Biosciences, Inc.) to the NP solution and overnight interaction. Biotinylated glycocalicin prepared previously was added to the avidin-conjugated NPs and reacted at room temperature under gentle agitation, for another two hours. Conjugated-NPs were then purified by ultracentrifugation. Extreme care was taken to avoid exposure of the NPs to light throughout the entire procedure. In order to confirm the conjugation of glycocalicin onto the NPs, 100 μ l of 30 μ g/ml primary mouse antibody monoclonal against glycocalicin (HIP1, BioLegend) was

incubated with glycolalicin-conjugated NPs in PBS for one hour. After washing, Texas-Red[®] conjugated secondary antibody (anti-mouse IgG1, BioLegend) was added to the NPs solution and incubated for one hour, followed by extensive washing. The NPs were then imaged using Zeiss cyto viva microscope. In addition, we also characterized these GPIb-conjugated NPs for their stability and protein binding using PBS, 100 % FBS, and 10 % human plasma, as described above.

2.2.9 Adhesion and Cellular Uptake of GPIb-conjugated NPs under physiological flow conditions

Coated culture dishes (either P-selectin or vWF) were assembled in a circular flow chamber (GlycoTech, Gaithersburg, MD) for surface studies, while pre-etched glass slides with activated HAECs monolayer were assembled into the parallel plate flow systems for cellular studies. For surface flow studies, we used the circular flow chamber as this required very small amounts of protein for coating the surface, thereby reducing the experimental cost. However, the parallel plate system was used for cellular studies to provide the cells with ample surface to grow and to also ensure that adequate amount of cells are available for carrying out bioassays.

We compared the adhesion of different sizes of conjugated particles (200 nm - 1000 nm) to P-selectin and vWF-coated surfaces under varying shear stress conditions (0-25 dyne/cm²). In addition, we performed a comparative non-cellular flow study, where the flow chamber was set to produce 5 dyne/cm² of shear stress, and two groups

of NPs were used, namely control NPs and GPIb-conjugated NPs. After the flow experiments, the amount of NPs bound to the surfaces were measured using a spectrofluorophotometer.

We also performed comparative cellular uptake studies of control NPs and GPIb conjugated PLGA NPs under static and flow conditions to evaluate the effectiveness of our GPIb-conjugated NPs. HAEC, seeded in a 24-well plate were incubated with 200 $\mu\text{g/ml}$ of respective nanoparticle solution for four hours at 37°C. Cells incubated with low serum media alone served as controls. To study the targeting efficacy of our conjugated NPs to cells under flow conditions, the shear stress was varied between 0-25 dyne/cm^2 . The NP solutions were diluted to 100 $\mu\text{g/ml}$ concentration in low serum media. Activated HAECs seeded on the glass slides were exposed to low serum media with either non-conjugated (control) or GPIb-conjugated NPs under various levels of shear stress. Samples in the static condition served as controls. Following flow experiments, cells were washed with PBS, lysed, and analyzed for cellular uptake of the NPs as described earlier. For confocal imaging, after the completion of the experiments, cells were prepared as described before.

2.2.10 *In Vitro* Anti-Inflammatory Study

To compare the anti-inflammatory property of GPIb-conjugated-DEX encapsulated NPs, DEX-encapsulated control NPs and free DEX in media, we performed an *in vitro* anti-inflammatory study. HAECs were seeded in 6-well plates at

a density of 50,000 cells/well for two days, after which cells were quiescent. Cells were then activated with 25 mM histamine. Solutions of control NPs and GPIb-conjugated NPs at 200 µg/ml and free DEX at 25 µg/ml were prepared in low serum growth media. HAECs incubated with low serum media served as controls, while other groups were incubated with solutions consisting of free DEX, control NPs, or GPIb-conjugated NPs. After experiments, the cells were detached using EDTA and washed. The cells were then incubated with APC-conjugated monoclonal primary mouse antibodies (BD Pharmingen, San Jose, California) against P-selectin for one hour and then washed. The mean fluorescence intensity of the cells was measured by flow cytometry. Since over-expressed ECAMs like P-selectin^{145, 203-206} have been implicated for their role in inflammation of vascular endothelium, we chose P-selectin as the marker for studying the anti-inflammatory effects of our NPs.

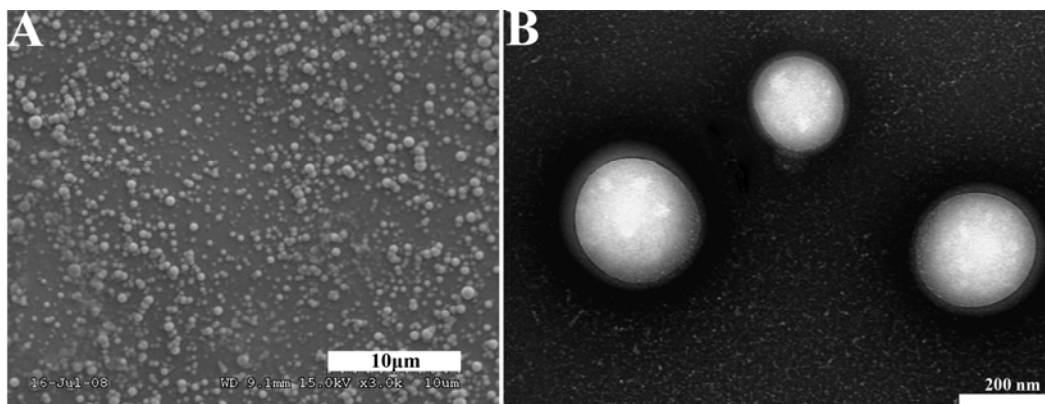
2.2.11 Statistical Analysis

Results were analyzed using one way ANOVA and t-tests with $p < 0.05$ (StatView 5.0 software, SAS Institute). Post-hoc comparisons were made using the Fisher's least significant differences (LSD). All the results are represented as mean \pm standard deviation (SD).

2.3 Results

2.3.1 Characterization and *In Vitro* Stability of PLGA NPs

After formulation, we characterized the NPs for their size and surface charge and also performed studies to determine their stability in different physiological fluids. The mean hydrodynamic diameter of the NPs was measured to be 187.3 ± 2.2 nm using ZetaPALS, with a polydispersity index of 0.032 ± 0.006 . The surface charge of the NPs was found to be -30.02 ± 0.53 mV. SEM (Figure 2.4A) and TEM (Figure 2.4B) images of these particles also confirm the average distribution and size of the particles.



Size (nm)	187.3 ± 2.2
Polydispersity	0.032 ± 0.006
Zeta Potential (mV)	-30.02 ± 0.53

Figure 2.4 Characterization of PLGA NPs (A) Scanning Electron Microscopy (SEM) Image (B) Transmission Electron Microscopy (TEM) Image

The DLS size measurements of both control NPs and GPIb-conjugated NPs in PBS over a five-day period demonstrated that the NPs remained stable over the period

with no significant changes in size and polydispersities (Figure 2.5). In addition, the protein binding and long term stability of control NPs and GPIIb-IIIa-conjugated NPs in both FBS (Figure 2.5) and dilute human plasma (results not shown) showed that the NPs maintained their shape and stability over the 5 days period after an initial 10-20 nm increase in size.

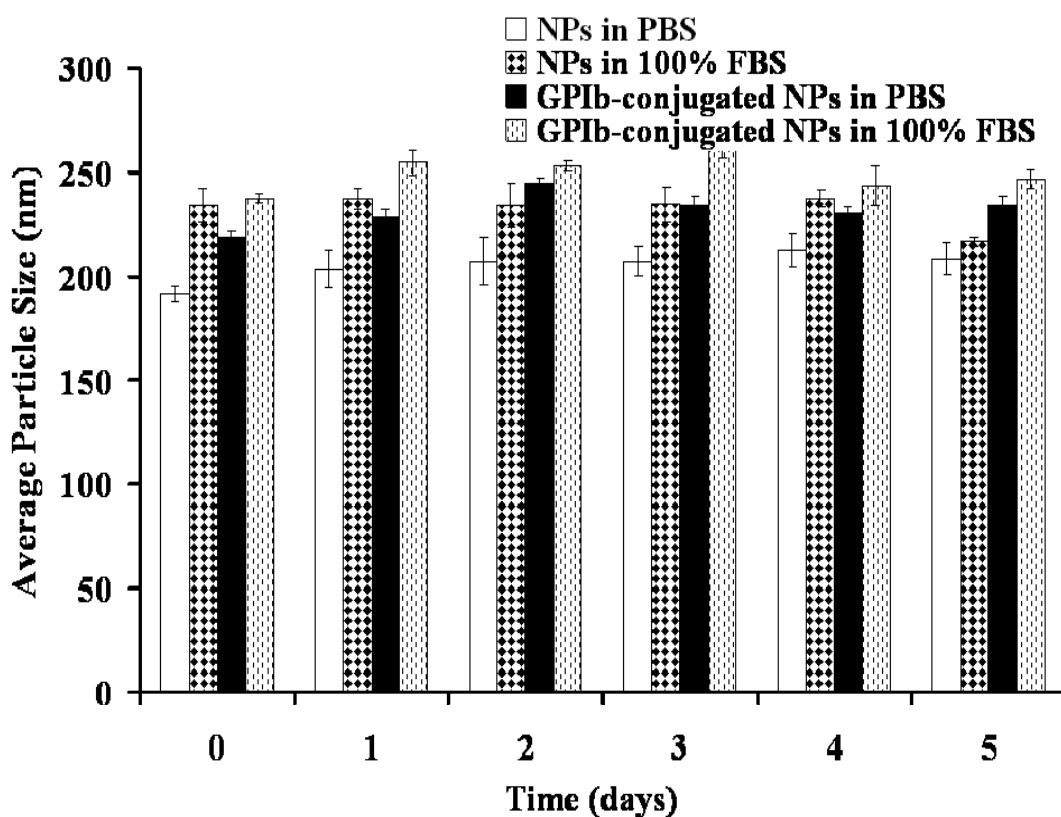


Figure 2.5 *In vitro* stability of the NPs over 5 days. Control NPs and GPIIb-IIIa-conjugated NPs either in PBS or in 100% FBS, were incubated at 37°C over five day period. NP suspensions were collected to measure NPs size using ZetaPALS dynamic light scattering. Values represent mean \pm standard deviation (n=3)

2.3.2 Drug Release Profile

To determine the efficacy of the drug-loaded NPs as a sustained drug delivery carrier, we performed an *in vitro* drug release study. The amount of DEX released from the NPs at different times was measured and correlated to the initial loading to get the cumulative drug release. Results indicated a triphasic drug release with the NPs showing the ability for a sustained drug release for up to 3 weeks (Figure 2.6). The loading efficiency of DEX into the PLGA NPs was calculated to be about 66.5%.

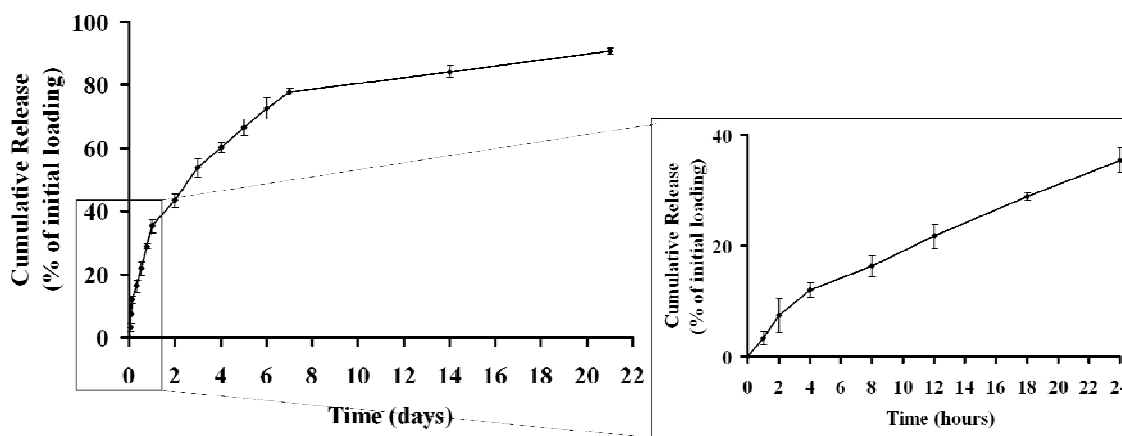


Figure 2.6 *In vitro* Release Profile of Dexamethasone from the drug loaded PLGA NPs at 37°C. Values represent mean \pm standard deviation (n=4)

2.3.3 Characteristics of cellular studies of NPs by HAECs

We evaluated the cellular viability of our drug-free NPs after 24 hours incubation of HAECs with the NPs using the MTS assay. As seen from the results (Figure 2.7), about 90% cell viability (relative to the control cells, 100% cell viability) was observed for cells exposed to concentrations of upto 500 $\mu\text{g}/\text{ml}$ and around 70%

viability at high concentrations of NPs (1000 $\mu\text{g/ml}$). These results suggest that our NPs are relatively biocompatible.

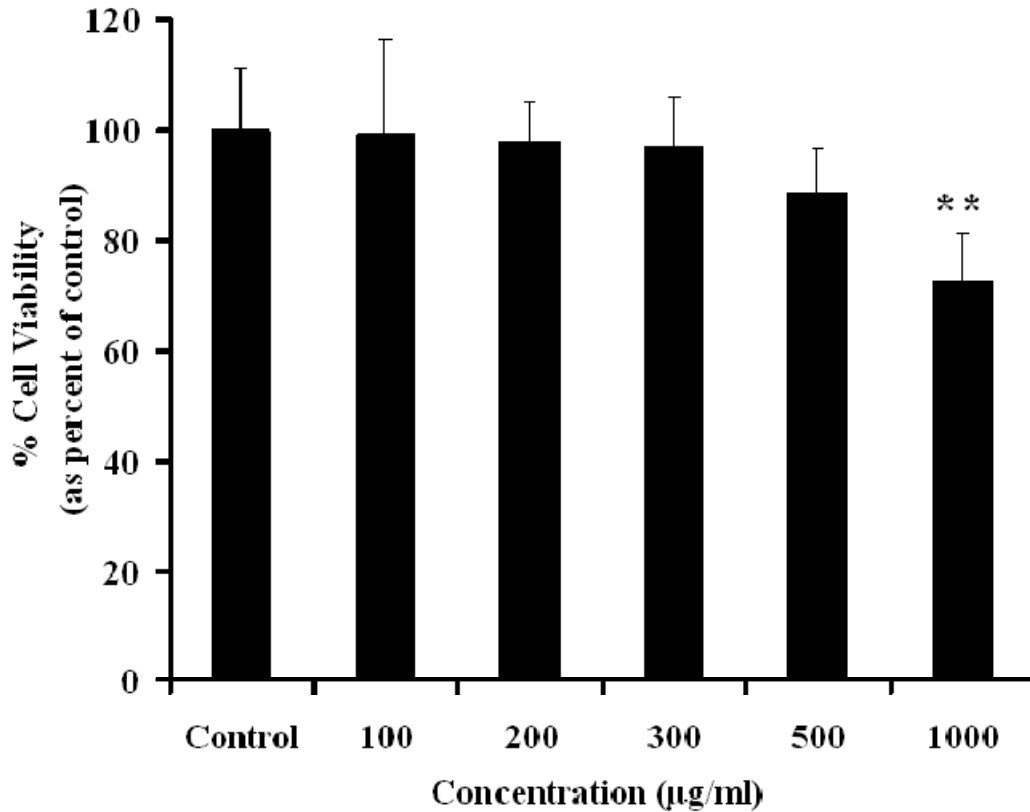


Figure 2.7 Nanoparticle biocompatibility study. Cells were exposed to the nanoparticles for 24 hours and cells not exposed to nanoparticles served as controls (100% cell viability). ** indicates significant differences compared to the control samples ($p < 0.001$). All values are represented as mean \pm SD ($n=4$)

To characterize the cellular uptake of PLGA particles, we investigated the effects of particle size, concentration, incubation time, and levels of shear stress on the particle uptake of HAECs. To determine the effects of particle size on cellular uptake by HAECs, we performed experiments using NPs of different sizes (200-1000 nm). Results displayed a clear trend of decreased cellular uptake with an increase in particle

size. The 1000 nm particles showed the least uptake while the 200 nm NPs exhibited the highest uptake by HAECs (Figure 2.8).

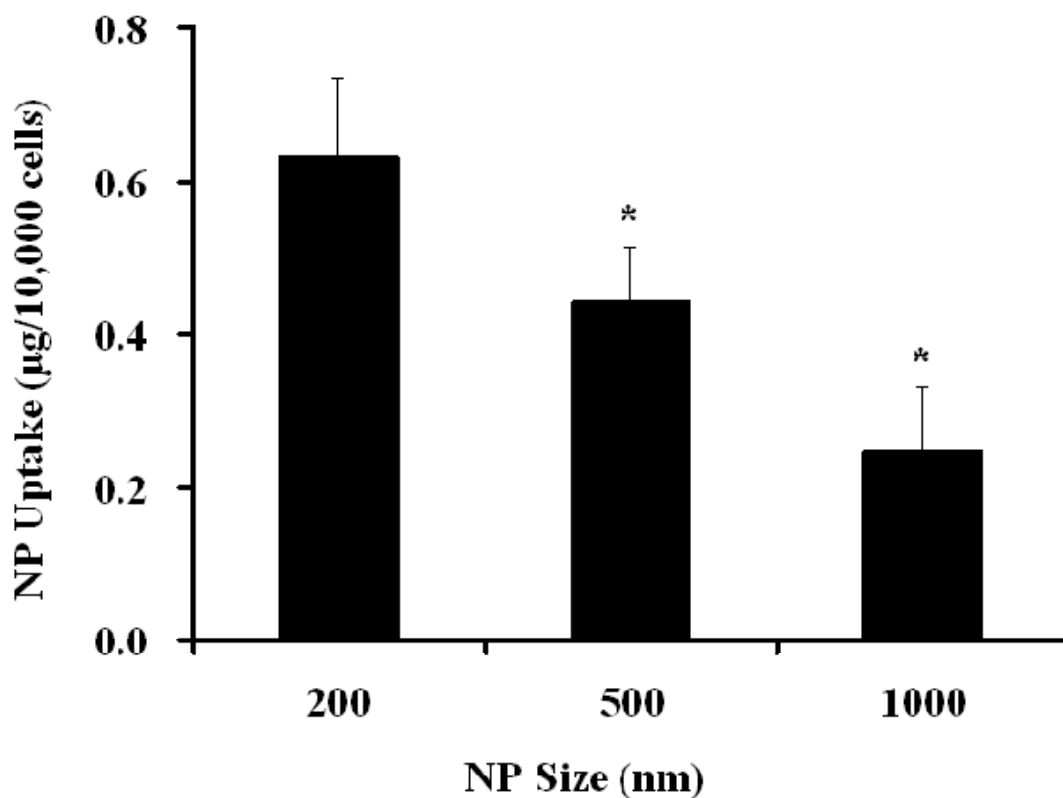


Figure 2.8 Effects of particle size on uptake by HAECs. Values were obtained after one hour of incubation with NP solutions. * indicates significant differences compared to 200 nm NPs samples ($p < 0.05$).

In addition, cellular uptake of NPs displayed a dependence on both concentration and incubation time. HAEC cellular uptake attained saturation at NP concentrations of 300 µg/ml (Figure 2.9) while a saturation of NP uptake was observed after 4 hours of incubation (Figure 2.9).

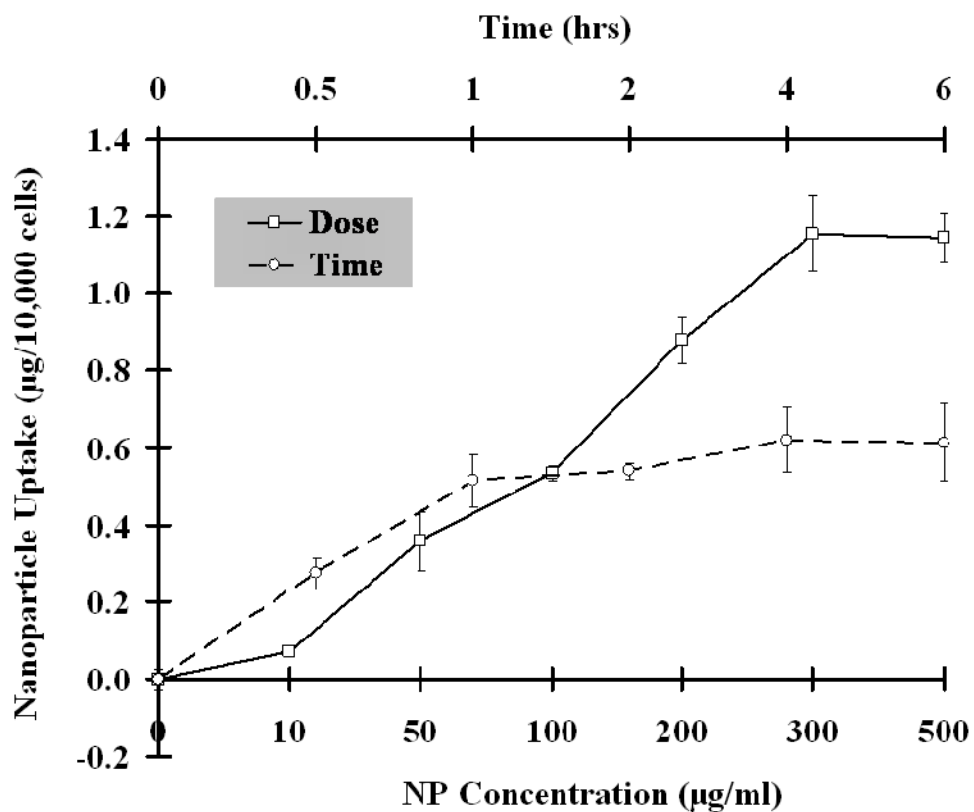


Figure 2.9 Effects of NP concentration and time on cellular uptake. Values were obtained after incubating with NP solutions either for one hour or with 100 µg/ml.

We employed confocal microscopy to confirm cellular uptake and intracellular localization of the NPs (Figure 2.10). Images at the middle point of the cell confirmed that the fluorescent PLGA NPs were localized inside cells.

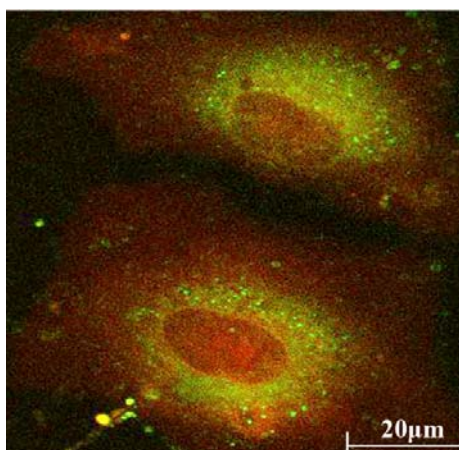


Figure 2.10 Color overlay of Z-stack of NP uptake by HAECs. Plasma membranes were labeled with FM[®] 4-64 FX and imaged using TRIC filter (Ex(λ) 565 nm/Em(λ) 744 nm). Fluorescent NPs were imaged with FITC filter (Ex(λ) 488 nm/Em(λ) 525 nm). Scale bar= 20 μ m.

Our studies on the temperature effects on cellular uptake of different sized particles by HAECs showed the uptake to be temperature dependent, as evident from the decrease in the cellular uptake at lower and higher temperatures of incubation (Figure 2.11). However, the 200 nm and 500 nm particles showed nearly same uptake at 42°C and at 4°C the 500 nm and 1micron particle showed a slightly higher uptake compared to the 200 nm size particles. From these results we can infer that the uptake of the nanoparticles is an active process that requires the expenditure of energy by the cells, and this is supported by our findings of decreased cellular uptake at both low (4°C) and high (42°C) temperature of incubation.

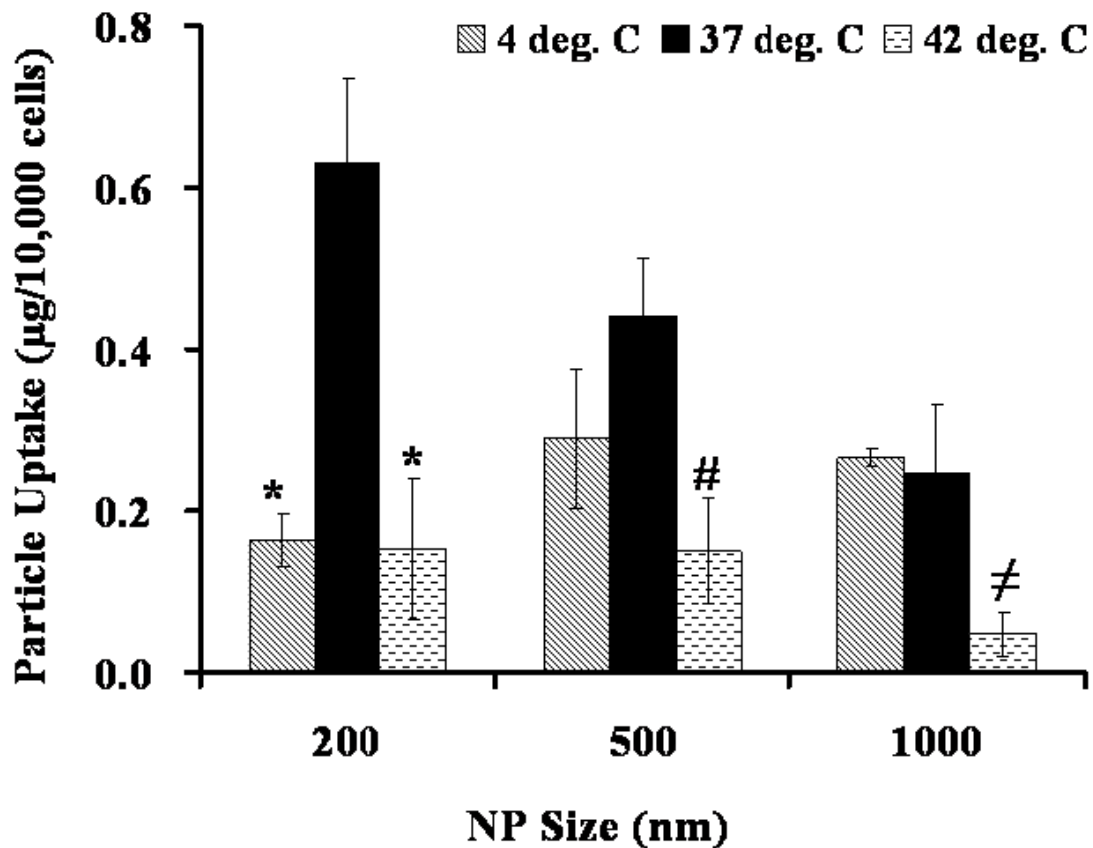


Figure 2.11 Effect of temperature on uptake of different sized particles by HAECs. Values were obtained after one hour pre-incubation at respective temperatures followed by NP incubation. Results are represented as mean \pm SD ($n=4$). * indicates significant difference of 200 nm particles compared to 37°C samples ($p < 0.05$); # indicates significant difference of 500 nm particles compared against 37°C samples ($p < 0.05$); \neq indicates significant difference of 1000 nm particles versus 37°C samples ($p < 0.05$).

To investigate the effects of shear stress on cellular uptake of NPs by HAECs, we used the parallel plate flow system to produce various shear stress levels. We observed a decrease in the cellular uptake of NPs with an increasing magnitude of shear stress (Figure 2.12), indicating that an inverse correlation exists between nanoparticle uptake and shear stress levels.

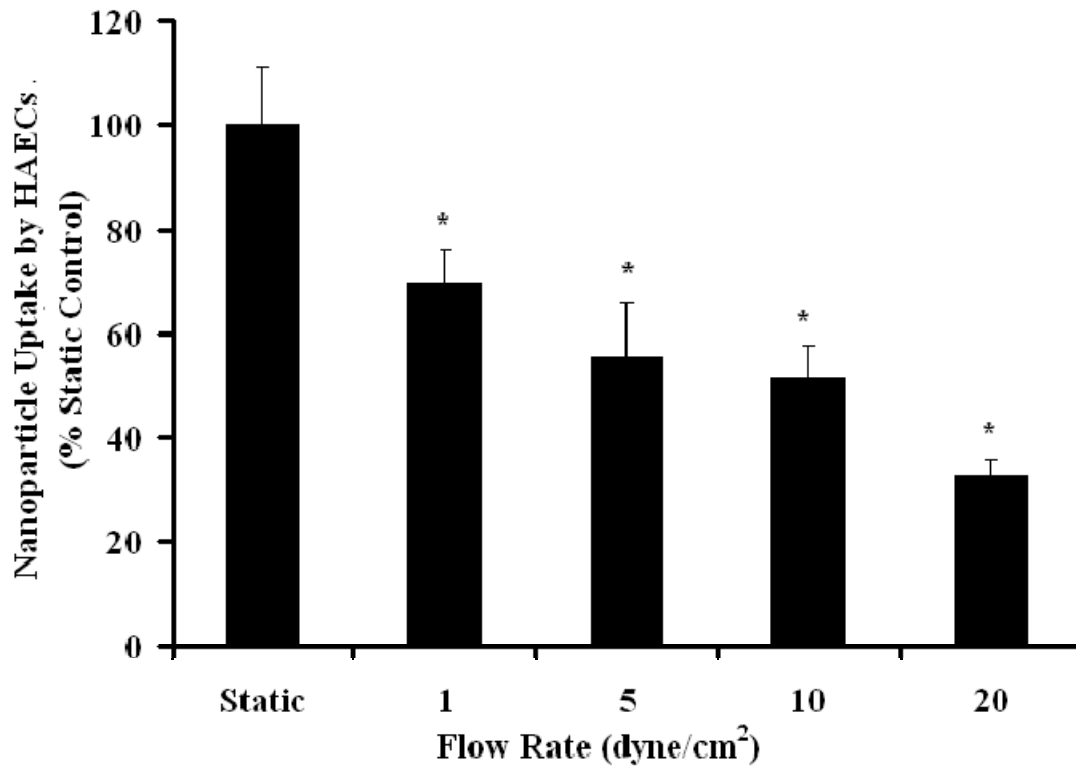


Figure 2.12 Effect of shear stress on cellular uptake by HAECs. Values were obtained after 30 minutes of flow with 200 nm NP solutions and are represented as mean \pm SD ($n=4$). * indicates significant differences compared to static samples ($p < 0.05$)

2.3.4 GPIb conjugated NPs improved adhesion on coated surfaces and cellular uptake by HAECs under physiological flow conditions

We used the imaging method as opposed to flow cytometry to confirm the conjugation of glycolalicin to our NPs because the size of our NPs is much below the detection limit of the available flow cytometry. Cytoviva images (Figure 2.13) showed the presence of red fluorescence around the NPs which can be attributed to the presence of Texas Red[®] fluorescent secondary antibodies against GPIb antibodies. This indicated that we successfully conjugated glycolalicin onto our NPs.

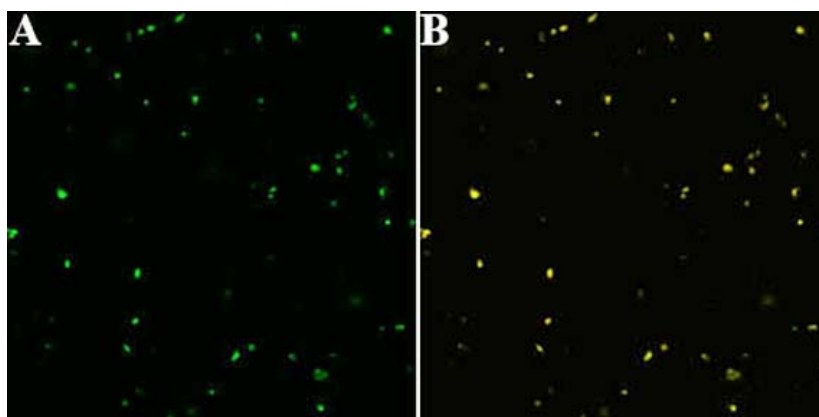


Figure 2.13 Glycolalicin conjugation onto PLGA NPs (A) Fluorescent NPs imaged using the green filter via Cytoviva microscope (B) Cytoviva image obtained using both green and red filters.

We examined the adhesion of different sized GPIIb-conjugated NPs on P-selectin and vWF coated surfaces under different flow rates and found that the 200nm sized NPs adhered better at different shear stresses compared to 500nm and 1micron sized particles (Figure 2.14 A and B) on both surfaces. However, for the same sized particles a decrease in adhesion of the particles to the coated surfaces was seen at higher shear stresses (Figure 2.14 A and B).

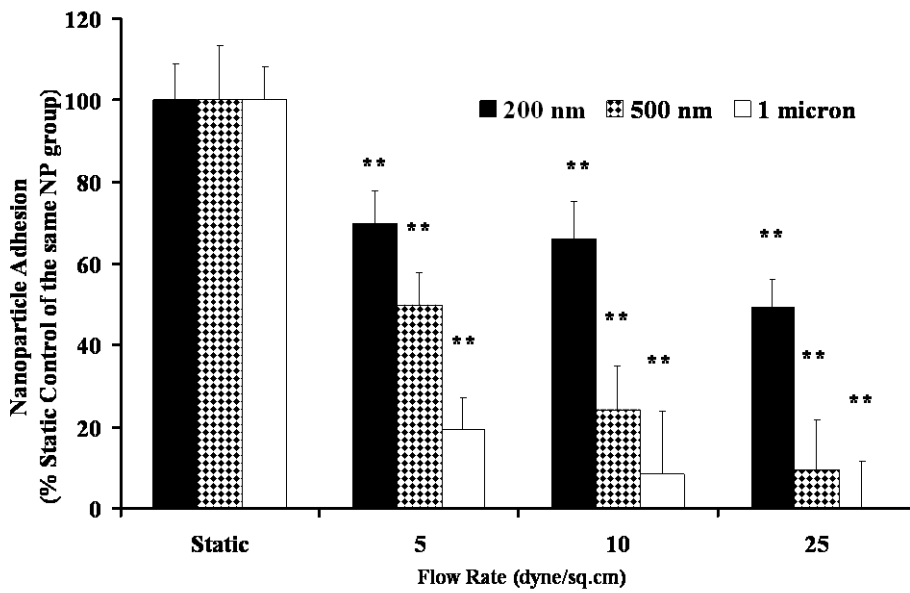
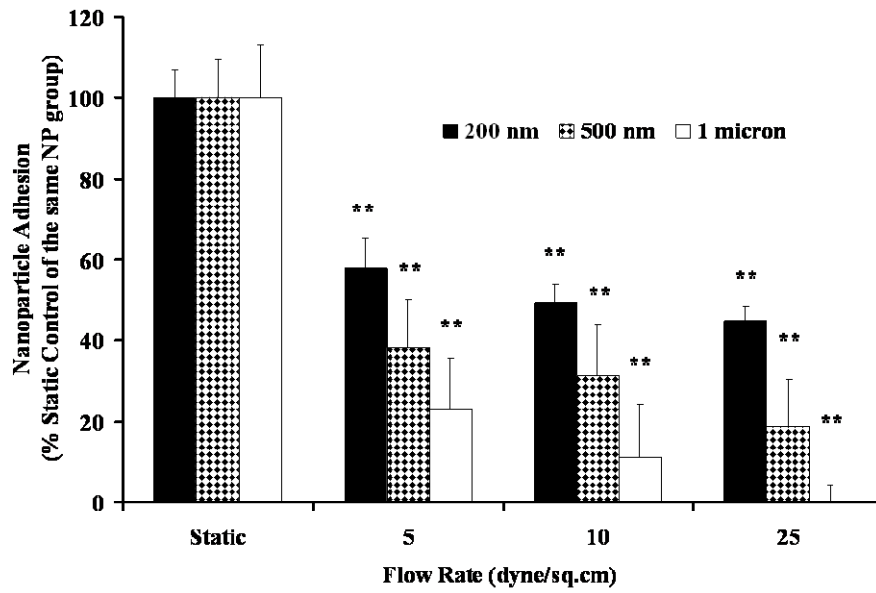


Figure 2.14 GPIb-conjugated particle adhesion to (A) P-selectin and (B) vWF coated surfaces using different size particle samples. Values represent mean \pm SD (n=4). ** denotes the significant differences with respect to the same particle group of static samples ($p < 0.001$)

We further analyzed the specific interaction of the control and GPIb conjugated NPs on P-selectin and vWF-coated surfaces under flow conditions (Figure 2.15). Nearly a two fold increase in the adhesion of GPIb-conjugated NPs to P-selectin- and vWF- coated surfaces was observed compared to the control NPs. Using antibodies against GPIb with GPIb-conjugated NPs showed that the NP adhesion to P-selectin and vWF coated surfaces was comparable to those of the control NPs, indicating the importance of GPIb binding to P-selectin and vWF under physiological flow conditions.

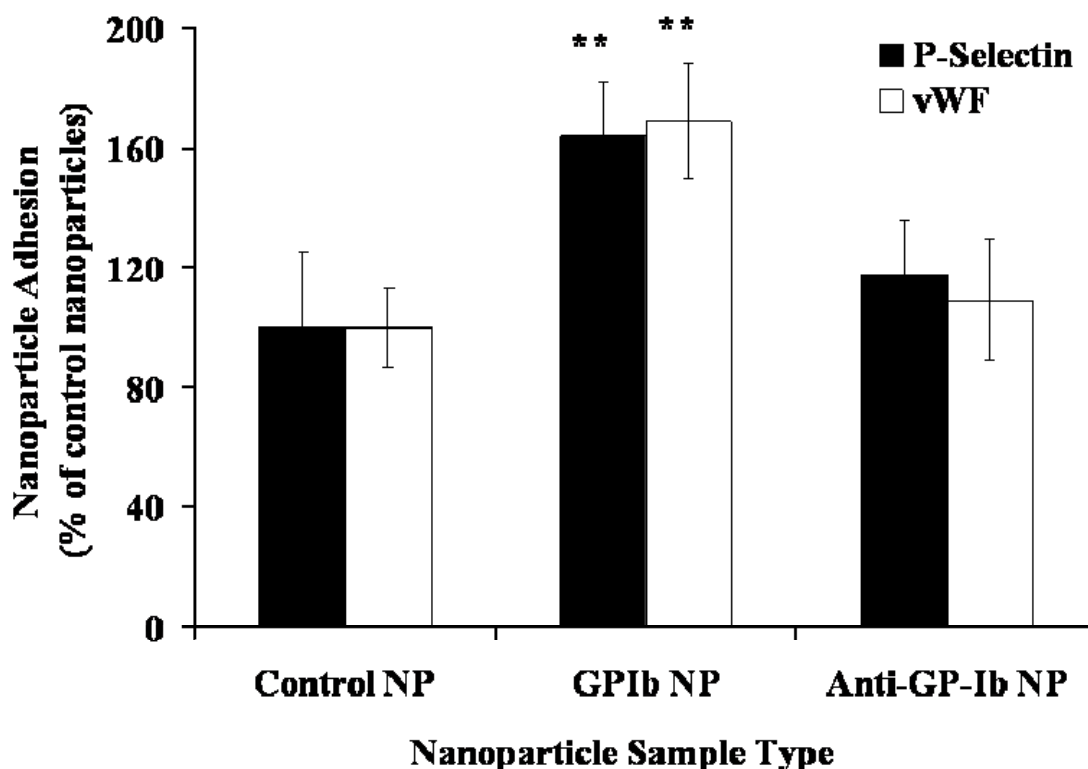


Figure 2.15 Adhesion of control and GPIb-conjugated NPs onto P-selectin and vWF coated surfaces at a shear stress of 5 dyne/sq. cm for 15 minutes. Values are represented as mean \pm SD (n=4). * indicates the significant difference compared to the control NPs samples (p < 0.05)

Investigation of effects of shear stresses on cellular uptake and binding of control (non-conjugated) and GPIb-conjugated NPs by activated HAECs exhibited significant cellular uptake of GPIb-conjugated NPs, while lesser cellular uptake of control NPs was observed (Figure 2.16).

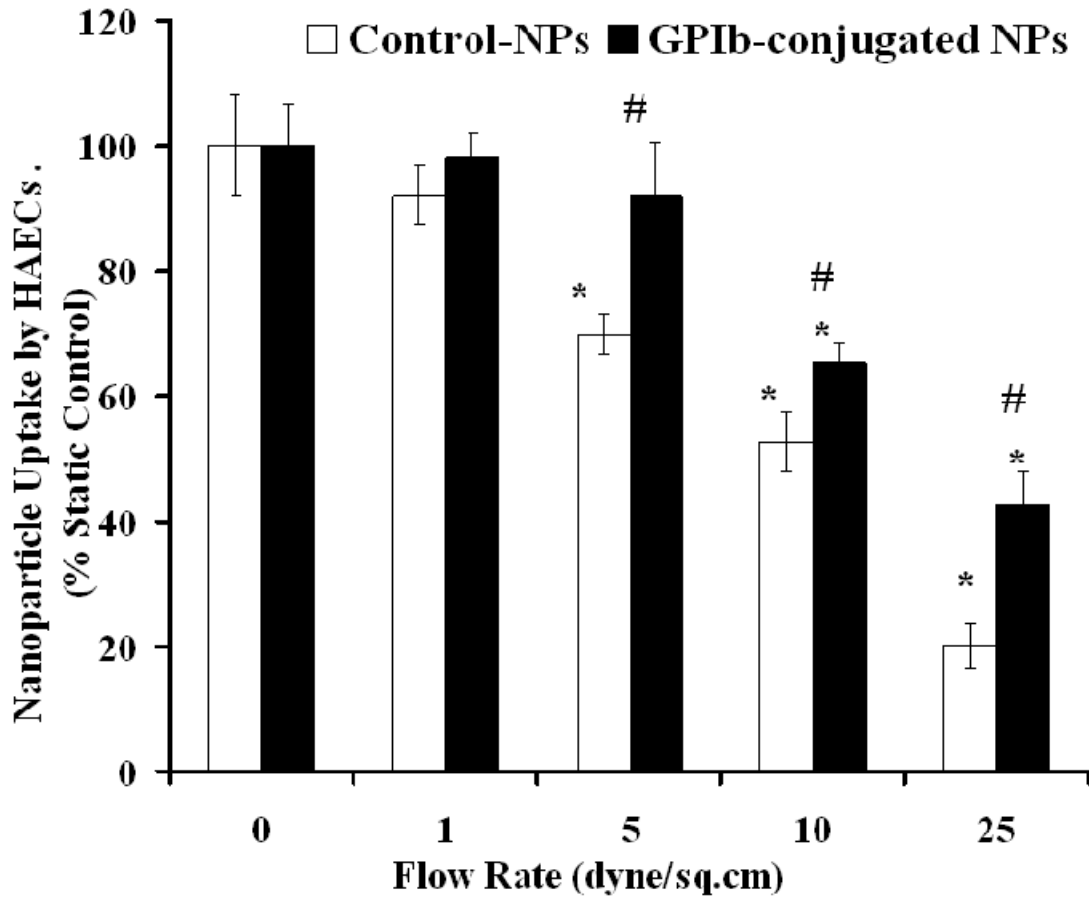


Figure 2.16 Adhesion and Uptake of GPIb-conjugated and control NPs by activated HAECs under shear stresses. Cells were activated with 25mM histamine just before flow. Measurements were made after 30 minutes of flow. Values represent mean \pm SD (n=3). * indicates the significant differences compared to the same nanoparticle group of static samples ($p < 0.05$). # denotes the significant difference between GPIb-conjugated NPs with control NPs ($p < 0.05$).

In addition, confocal images showed that unconjugated NPs were mostly detected in extracellular spaces, with minimal NPs within the cells (Figure 2.17A). In contrast, NPs conjugated with GPIb showed higher uptake as detected within cells, with a very low concentration of NPs present in extracellular spaces (Figure 2.17B). Samples were observed at the middle point of each cell using the stack imaging option, with slice thickness set at 1 μm . These observations confirm that GPIb adhesion to P-selectin of activated HAECs is essential for uptake by HAECs under flow shear stress.

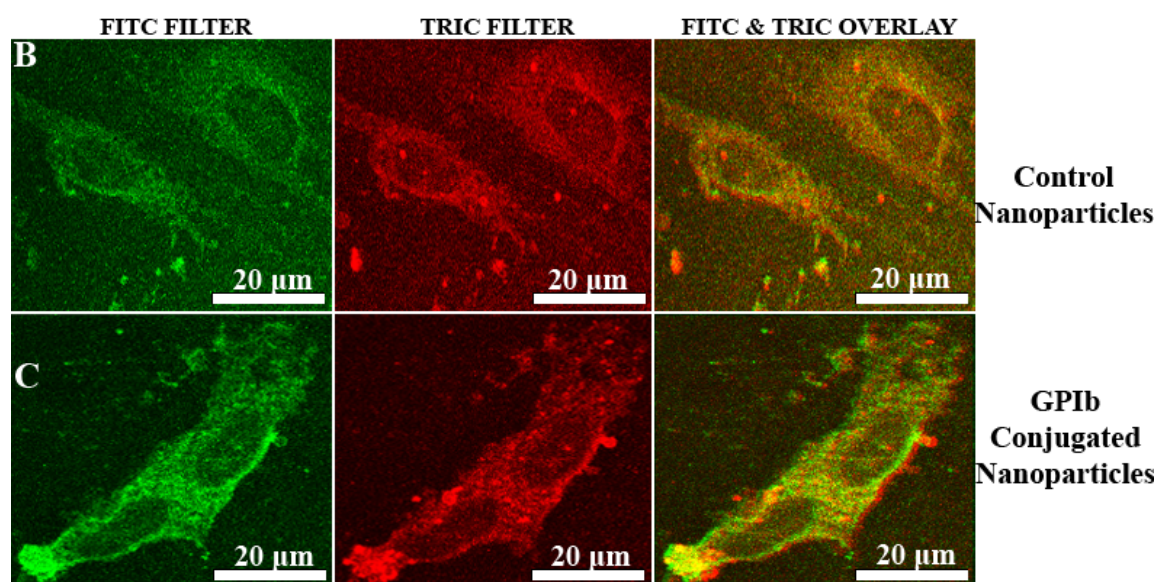


Figure 2.17 (A) Z-stack Confocal Image of cellular uptake of control NPs (B) Z-stack Confocal Image of cellular uptake of GPIb-conjugated NPs. Fluorescent NPs were imaged using a FITC filter, while plasma membranes were stained with FM[®] 4-64 FX red membrane dye and imaged using TRIC filter. Images on the far right represent the color overlay of FITC and TRIC filters. Scale Bar = 20 μm .

2.3.5 *In Vitro* Anti-inflammation Study

From the results of *in vitro* anti-inflammatory study, it is clearly observed that the cells incubated with GPIb-conjugated NPs showed a significantly lower expression

of P-selectin (marker used to study inflammation, as described previously) compared to the control cells (Figure 2.18). After 24 hours incubation with histamine containing media, control cells showed about 6 times and cells incubated with free DEX in solution showed approximately 4 times higher expression of P-selectin, compared to cells that were incubated with GPIb-conjugated NPs (Figure 2.18). These results may be explained by the fact that the drug encapsulated NPs release the encapsulated DEX slowly from the NPs even after removal of the NPs from the media, as opposed to free drug, which shows minimal effect on the cells after its removal from the media. These results indicate the promise of our GPIb-conjugated NPs as therapeutic delivery system.

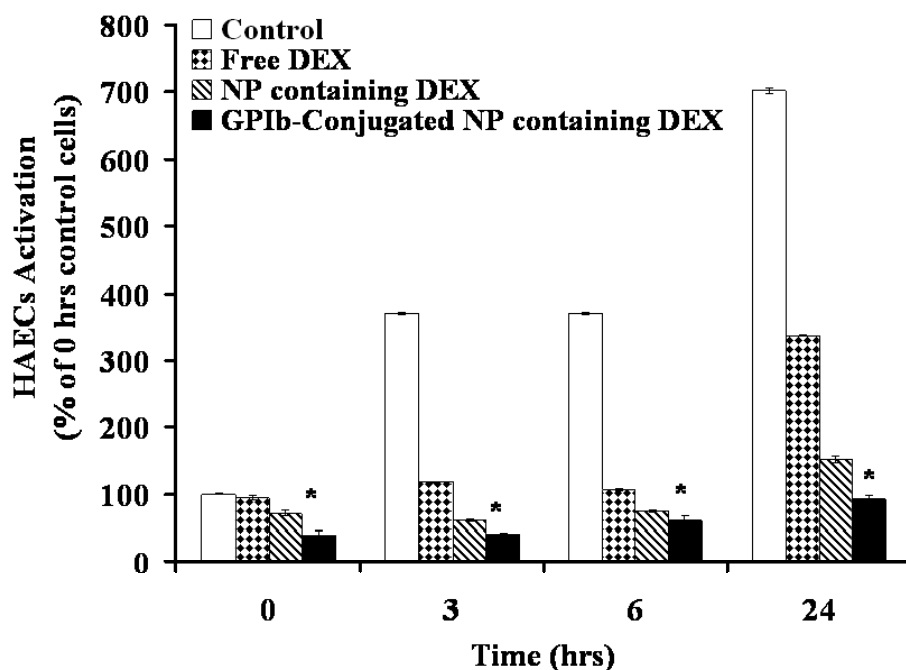


Figure 2.18 *In vitro* anti-inflammatory study comparing control, free DEX, DEX encapsulated PLGA NPs and GPIb-conjugated - DEX encapsulated PLGA NPs. Values represent mean \pm standard deviation (n=4). * indicates significant differences of GPIb-conjugated NPs compared to control NP samples (p< 0.05)

2.4 Discussion

The intent of this research was to examine a novel strategy of targeted drug delivery of nanoparticles to enhance cellular uptake by inflamed/activated HAECs. The formulated PLGA NPs were characterized for their size, surface charge and morphology. The NPs showed a sustained drug release for upto 21 days, were stable in different physiological fluids, and showed minimal cytotoxicity in HAECs. Furthermore, cellular uptake studies showed that a reduction in particle size increased cellular uptake. Additionally, the optimal nanoparticle dosage was determined to be 300 µg/ml while optimal incubation time was found to be 4 hours, under static conditions. Our results also indicated that when the NPs were conjugated with GPIb, they considerably increased their adhesion to P-selectin and vWF coated surfaces. Moreover, cellular uptake studies performed under fluid shear stress also showed an increased uptake and targeting capacity of GPIb-conjugated NPs when HAECs were activated with histamine to express P-selectin. The GPIb-conjugated NPs also exhibited a better anti-inflammatory effect compared to control NPs. Results from these cellular uptake and targeting characterization studies imply that conjugation of GPIb onto our NPs can increase nanoparticle targeting capability and endothelial cellular uptake under physiological flow conditions.

The release of the drug from our NPs showed evidence of a triphasic release – an initial burst release (about 36% in 24 hours) owing to drug desorption from the NP

surface, followed by a plateau due to drug diffusion and finally a stable sustained release attributable to both diffusion of the drug and surface erosion of the NPs. This interpretation of the results is consistent with the findings reported by several other authors.^{62, 207, 208} These results suggest that our PLGA nanoparticles can be loaded with any therapeutic reagent including anti-proliferative agents and hold promise as a viable sustained drug delivery system. To be used as a drug delivery system, the NPs must also be stable in physiological fluids. The stability of the NPs can be ascribed to the steric repulsion caused by hydrodynamic diameter of the PLGA and residual PVA chains as well as from the electrostatic repulsion of the negatively charged – COOH end groups of the PLGA chains, similar to the results observed from other studies.²⁰⁹⁻²¹¹

Similar to previous uptake studies using polystyrene particles (100nm to 1µm) on HAECs,⁹⁴ we saw a decreased uptake of the particles NPs by HAECs with an increase in the NPs size (Figure 2.8). Furthermore, previous cellular studies using NPs in our size range have shown that NPs below 200 nm are internalized by Caco-2 cells⁸⁵ and HUVEC cells.²¹² In addition, cellular uptake of nanoparticles at various sizes by the HAECs is energy-dependent. We believe that maximum cellular uptake with minimum energy consumption is observed at 37⁰C and this assumption is confirmed by the results from studies that used a range of fluorescent latex beads of defined sizes (50–1000 nm) on B16 non-phagocytic cells.²¹³ Thus, results from our and previous studies confirm the advantages of NPs for intracellular drug delivery with added benefits of minimal to no local inflammation and a lower risk of arterial occlusion.^{53, 214}

In addition to particle size-dependence, NPs uptake by HAECs was also found to be dose (300 $\mu\text{g/ml}$) and incubation time (4 hours) dependent. These results were similar to the PLGA NPs cellular uptake outcomes in previous studies using HUVECs where uptake saturated at 300 $\mu\text{g/ml}$.⁵⁹ But contrary to our studies, uptake by HUVECs saturated after two hours of exposure to NPs⁵⁹ and Caco-2 showed saturated uptake in 2 hours and at a dose of 500 $\mu\text{g/ml}$.⁸⁵ This disparity in dose and incubation time can be attributed to the variations in the NP size and cell types used for these studies. Thus, our result, in combination with previous findings suggests that encapsulated drugs can be delivered using NP concentration-based dosages. Indeed, studies via catheter-based infusion demonstrated that increasing the concentration of NPs significantly increases arterial uptake of drug-loaded NPs, leading to enhanced drug levels at the arterial wall in acute animal models.^{84, 215, 216}

Understanding the method of cellular NP uptake is important for intracellular trafficking of the NPs for enhancing the effectiveness of any internalized drug.^{198, 217-220} Confocal microscopy confirmed the intracellular localization of our NPs. We attribute this localization to endocytosis of the NPs by various cellular mechanisms and believe that the drug loaded NPs escape the endo-lysosome complex by surface charge reversal of the NPs. This is supported by well-documented studies on the mechanism of intracellular uptake of PLGA nanoparticles such as their trafficking and sorting into different intracellular compartments like early and recycling endosomes, late endosomes, lysosomes, and cell cytoplasm.^{53, 221-224} All these findings indicate that by

optimizing the NP concentration and time, we can minimize the drug side effects and enhance NP delivery.

Other factors like surface properties of NPs, high concentrations of serum, and varying shear stress levels can also influence the NP uptake by endothelial cells. For example, excessive cell exocytosis of NPs was seen when media with high serum quantity was used for studies.¹⁹⁸ This was attributed to the energy dependent nature of the exocytosis process.¹⁹⁸ Additionally, the amount of shear stress can also affect NP adhesion and uptake by endothelial cells. Similar to our results, other researchers have also found that adhesion of NPs on surfaces and/or endothelial cells is inversely related to shear stress levels.^{92, 94, 225}

To improve the adhesion of NPs to endothelial cells under physiological flow conditions, other researchers have used leukocyte-imitating particles^{129, 131, 170, 191-193} and endothelial targeting particles coated with humanized antibodies against E- and P-selectins.^{92, 225} Particles (both nano and micro) conjugated with either sialyl Lewis^x (sLe^x)^{129, 131, 191-193, 226} or with antibodies against P-selectin^{92, 225} and/or LFA-1²²⁷ were observed to adhere to P-selectin-, E-selectin- and ICAM-1 – coated surfaces as well as to activated endothelial cells. Just like these studies, our “platelet-mimicking endothelial-targeting NPs” adhered better to both P-selectin- and vWF- coated surfaces under physiological flow conditions by imitating the binding of platelets onto activated ECs. Our NPs adhere better to both P-selectin- and vWF- coated surfaces as well as to

activated HAECs owing to the higher binding strength of platelet ligands under high shear stress situations.^{99, 133, 135, 228} Additionally, GPIb-conjugated NPs were significantly better compared to control NPs in terms of adhesion, uptake, and efficiency of the released anti-inflammatory drugs. Other researchers have also found that incorporating anti-inflammatory agents into nanoparticles improved their efficacy.^{229, 230} For example, lipid nanoparticles loaded with prostaglandin E1 improved its anti-inflammatory effects in RAW264.7, HUVEC, and MDA-MB-468 cells²²⁹ while encapsulation of thymoquinone into PLGA nanoparticles enhanced its anti-inflammatory, anti-proliferative, and chemosensitizing properties.²³⁰

2.5 Limitations

Current study did not look into the correlation between bond forces upon GPIb-vWF in the presence of soluble vWF and the competitive binding of our NPs with platelets. In addition, the increase in the adhesion and uptake of our GPIb-conjugated NPs under higher shear conditions was also less compared to the static and low shear uptake. Additionally, for the flow studies, we presumed that the flow velocities of the nanoparticle solution in the flow chamber are the same all through. This may however not be the case. Future work on this project will include studies to overcome above limitations and *in vivo* studies via animal models. To increase the stealth properties of these NPs for *in vivo* application, we will also study the PEGylated formulations of these NPs.

CHAPTER 3
GPIb-TAT CONJUGATED NANOPARTICLES FOR TARGETED DRUG
DELIVERY TO VASCULATURE

3.1 Introduction

In the previous chapter, we successfully developed the GPIb-conjugated PLGA NPs that exhibited enhanced shear regulated uptake and decreased inflammation of the activated endothelial cells. The conjugated NPs also showed significantly increased adhesion to P-selectin and vWF coated surfaces over control nanoparticles. However, a vital downside of this strategy was that the increase in the adhesion and uptake of the NPs under higher shear conditions of 25 dyne/cm² for 30 minutes was only around 50% compared to the static samples.

Recently, studies using cell penetrating peptides have shown excellent results in being able to translocate spontaneously through the plasma membrane.²³¹ Various biological molecules and therapeutic substances like proteins, small peptides, DNA, siRNA, vaccines, and drugs have been delivered into cellular compartments successfully *in vitro* via these penetrating peptides.²³²⁻²³⁵ Therefore, to overcome the limitation of the previous aim, we propose to conjugate a cell penetrating peptide along

with GPIb to the PLGA NPs. Since it is proposed to use these NPs *in vivo*, we will also be conjugating polyethylene glycol (PEG) to the PLGA NPs to increase the blood circulation time and to prevent clearance by the reticulo-endothelial system.²³⁶⁻²³⁸ The scheme of our nanoparticles is shown in Figure 1.3.

In this chapter, we first evaluated five different cell penetrating peptides (CPPs) and determined TAT to be the most optimal peptide for our application. We then formulated and characterized the drug (dexamethasone)-loaded PLGA-PEG nanoparticles. We determined the optimal cellular uptake concentration and incubation time by fluorescent measurements. Furthermore, after conjugation of TAT and GPIb to the PLGA-PEG NPs, these nanoparticles were investigated for their anti-inflammation property, adhesion to P-selectin- and vWF- coated surfaces, and effectiveness of cellular uptake under high shear stress conditions. We further performed a preliminary *ex vivo* assessment of the targeting efficacy of the conjugated NPs using balloon injury rat models.

3.2 Materials and Methods

3.2.1 Materials

Poly (D, L-lactic-co-glycolic acid) (PLGA) (inherent viscosity – 0.4dl/g, copolymer ratio 50:50) with carboxyl end groups, was purchased from Lakeshore Biomaterials (Birmingham, AL). Bi-functional polyethylene glycol (NH₂-PEG-COOH)

was procured from Laysan Bio (Arab, AL). All other chemicals, if not specified, were purchased from Sigma-Aldrich (St. Louis, MO). Low serum growth supplement (LSGS, 2 % fetal bovine serum, hydrocortisone (1 $\mu\text{g/ml}$), human epidermal growth factor (10 ng/ml), basic fibroblast growth factor (3 ng/ml), and heparin (10 $\mu\text{g/ml}$)) was purchased from Invitrogen (Carlsbad, CA). HAECs were purchased from PromoCell GmbH, Germany. Cell culture media, buffers, and supplements including trypsin-EDTA, Medium 199 (M199), fetal bovine serum (FBS), and penicillin-streptomycin were acquired from Invitrogen Corporation (Carlsbad, CA). Glycocalicin was received from our collaborator at the Baylor College of Medicine, Dr. Jing-Fei Dong. For the initial experiments, the cell penetrating peptides were gifted by Dr. J.T. Hsieh of the University of Texas Southwestern Medical Center at Dallas, Texas. Biotin-TAT cell penetrating peptide was purchased from Anaspec (Fremont, CA).

3.2.2 Formulation of PLGA-PEG NPs

PLGA NPs were formulated using a double emulsion–solvent evaporation method. As described in the previous chapter, a 3% aqueous DEX solution was emulsified in 3% PLGA organic solution containing 6-coumarin to form the primary emulsion. This primary emulsion was then added dropwise into a 5% aqueous PVA solution to form the double emulsion. After overnight stirring to evaporate the organic solvent, NPs were recovered by ultracentrifugation at 30,000 rpm and then washed twice with DI water.

To conjugate PEG to the drug-loaded PLGA NPs, carboxyl groups on the surface of the PLGA NPs were activated using the standard carbodiimide chemistry (Figure 3.1). The above formulated PLGA NPs were resuspended in isotonic 0.1M MES buffer saline (pH 4.75) and allowed to react for two hours with 2.7% EDC and 4% NHS. After washing twice with PBS, the activated NPs were allowed to react with 3% NH₂-PEG-COOH in PBS for four hours after which the NPs were washed twice and freeze-dried. NPs without the drug and fluorescence dye were prepared in a similar way. For *in vivo* studies, the NPs were formulated in a similar manner. However, instead of the 6-coumarin fluorescent dye, we incorporated the near infrared fluorescent dye - NIR-797 isothiocyanate (Sigma-Aldrich Corp., St. Louis, MO) in the NPs.

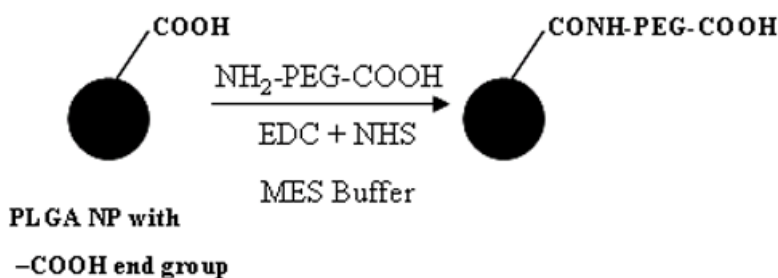


Figure 3.1 Illustration showing the reaction for conjugation of PEG to PLGA NPs

3.2.3 Characterization and *In Vitro* Stability of PLGA-PEG NPs

The PLGA-PEG NPs were characterized using TEM and DLS for their morphology and size. The size, polydispersity, and surface charge were measured using ZetaPALS DLS. The conjugation of bi-functional PEG to PLGA NPs was confirmed using Fourier Transform Infrared Spectroscopy (FTIR) (Nicolet 6700 FT-IR spectrometer, Thermo Fisher Scientific) at room temperature. Stability and protein

binding of the NPs were conducted *in vitro* in PBS and FBS. The NPs were suspended in PBS and 100% FBS for 120 hours at 37°C, and the change in particle sizes was measured every 24 hours using DLS.

3.2.4 Drug Loading and *In vitro* Drug Release Studies

To determine the loading efficiency of dexamethasone in the PLGA-PEG NPs, 1mg of the freeze-dried particles were suspended in mixture of chloroform and DI water. This allowed the drug to escape from the polymer into the water phase. The amount of drug was then quantified using a spectrophotometer and loading efficiency was calculated based on the total amount of DEX used in the initial nanoparticle formulation.

For *in vitro* drug release studies, 1ml of drug-loaded PLGA-PEG NPs were suspended in PBS and placed in dialysis bags (Spectrum Laboratories Inc.) with molecular weight cut-off of 1,000 (as the molecular weight of water soluble dexamethasone is 392.5 Da) and dialyzed against PBS at 37°C for 28 days. At a predetermined time, 1ml of dialysate was removed from each sample and replaced with 1ml of fresh PBS. The collected samples were stored at -20°C for later analysis. To determine the amount of DEX released, absorbance of the samples was read at 242 nm. The amount of released drugs was determined against a standard DEX curve and correlated to the loading amount to determine the cumulative percent drug release. The samples were prepared in quadruple.

3.2.5 Culture of Human Aortic Endothelial Cells

HAECs were grown in M199 that was complemented with 10% FBS, 1% penicillin-streptomycin, and LSGS (complete M199). Cells up to passage 10 were used for all the cellular studies. We used low serum (1% serum) M199 for all the cellular studies as previous research has revealed that using high serum (greater than 1%) media amplifies the endocytosis and exocytosis processes of PLGA NPs.^{197, 198}

3.2.6 Determination of Suitable Cell Penetrating Peptide for Conjugation to NPs

To determine the suitable peptide for our application, we used the following peptides: TAT (FITC-G-RKKRRQRRR), homopolymers of L-arginine R11 (FITC-G-RRRRRRRRRRR) and L-lysine K11 (FITC-G-KKKKKKKKKKK), penetratin (PENE; FITC-G-RQIKIWFQNRRMKWKK) and KALA (FITC-G-KLALKLALKALKALKLA). 10,000 HAECs per well were plated in 96-well plates for the experiments. The following day, different concentrations of FITC-tagged CPPs were incubated with the HAECs for one hour or indicated time. The cells were then washed with PBS and lysed using 1X-Triton[®]. The fluorescence intensity was examined by spectrophotometer (Ex-490nm, Em-525nm), and the uptake was normalized to the cell number. Additionally, to determine the effect of these CPPs on cell viability, the cells were seeded in 96-well plates at a density of 10⁴ cells/well and incubated with the respective CPPs for 24 hours. We then assessed the viability with the MTS cell proliferation assay per the manufacturer's instructions. Furthermore, we conjugated the

CPPs to the NPs using EDC chemistry and analyzed the cellular uptake and cytotoxicity of the CPP-conjugated NPs as described above.

3.2.7 Preparing P-selectin- and vWF- Coated Slides and Activation of HAECs

Coated surfaces for flow were prepared by incubating 500 μ l of 20 μ g/ml P-selectin (R&D Systems) and 500 μ l of 5 μ g/ml vWF (Calbiochem) at 4°C overnight. After washing, the surfaces were incubated with 1% BSA solution for one hour to prevent nonspecific binding. After washing the surfaces with 0.9% NaCl solution to remove any unbound ligands, the surfaces were used for experiments. To activate HAECs, cells seeded on glass slides were incubated with 25 mM histamine for 12 minutes at 37°C to promote P-selectin expression. The activated cells were used for experiments right away.

3.2.8 Cellular Studies of PLGA-PEG NPs using HAECs

The cell biocompatibility of the PLGA-PEG NPs on HAECs was assessed using the MTS assay. HAECs were exposed to varying concentrations (0–1000 μ g/ml) of NPs, and after 24 hours of exposure, the viability was assessed by adding the MTS reagent (Promega Corp.) following the manufacturer's instructions. The absorbance was measured at 490nm using the microplate reader (Infinite M200, Tecan USA, Inc.).

Dose- and time-dependent cellular uptake of PLGA-PEG NPs were determined by plating and growing HAECs in 48-well plates at a seeding density of 20,000 cells per

well. At least six hours before the experiments, the complete media was replaced with low serum media to quiescent the cells. To study the dose-dependent NPs uptake, HAECs were incubated with different concentrations of NP suspension (0–1000 $\mu\text{g/ml}$) in low serum media for one hour. For the time-dependent NP uptake, HAECs were incubated with NP suspension (300 $\mu\text{g/ml}$) in low serum media for different time periods (0–6 hours).

To explore the uptake pathways of PLGA-PEG NPs by HAECs, endocytic inhibitors were used. For this purpose, the HAECs cell cultures in 96-well plates were initially pre-incubated for one hour at 37°C with chlorpromazine (10 $\mu\text{g/ml}$) to inhibit clathrin vesicles formation, filipin III (1 $\mu\text{g/ml}$) to hinder caveolae, and/or with amiloride (50 μM) to inhibit macropinocytosis. Following this, the cells were treated with a suspension of PLGA-PEG NPs (300 $\mu\text{g/ml}$), which also had the respective inhibitors at the same concentrations, for an additional hour.

After experiments, cells were washed three times with cold PBS and then lysed by incubating them with 1% Triton[®] X-100 for 30 minutes at 37°C. The cell lysates were then processed at EX 490 nm/EM 515 nm using the microplate reader (Infinite M200, Tecan USA, Inc.). Results are expressed as μg of NPs normalized to the cell number, as described earlier.

3.2.9 Conjugation of Glycocalicin and TAT Peptide to PLGA-PEG NPs

Glycocalicin, the extracellular fraction of platelet GPIIb/IIIa and TAT peptide were attached to the PLGA-PEG NPs using carbodiimide chemistry and avidin-biotin affinity chemistry (Figure 3.2).

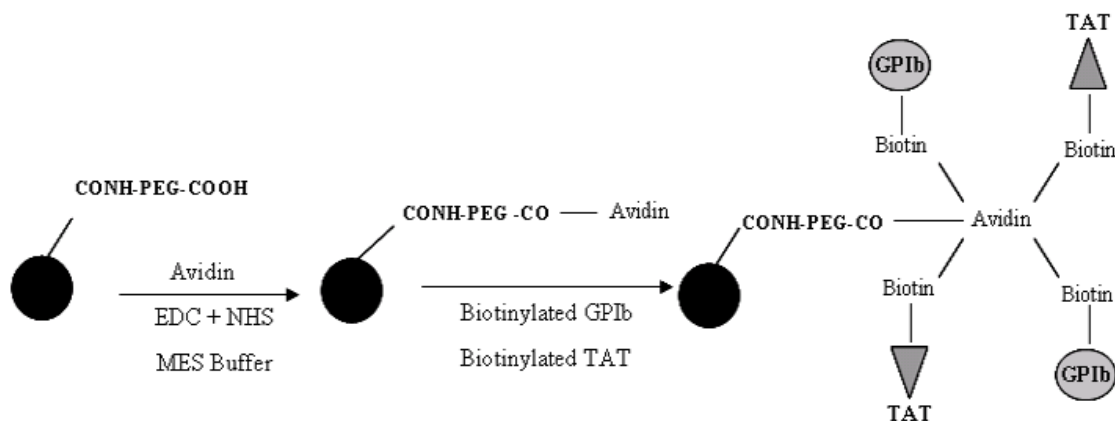


Figure 3.2 Schematic of the conjugation of GPIIb and TAT to the PLGA-PEG NPs

The first step in the process was attaching biotin to glycocalicin via the Biotin-X-NHS kit (EMD Biosciences, Inc., San Diego, CA) using the manufacturer's instructions. In the next step, PLGA-PEG NPs were suspended in 0.1 M MES buffer (pH 4.75) along with EDC to activate the carboxyl groups on the NPs. This solution was incubated at room temperature for 5 hours after which avidin (EMD Biosciences, Inc.) was added to the NP solution and the reaction was allowed to proceed overnight. The following day equal quantities of biotinylated glycocalicin (prepared in the previous step) and biotin TAT (Anaspec, Fremont, CA; used as received) were mixed with the avidin-complexed NPs and reacted for two hours at room temperature under gentle stirring. The NPs were washed and collected by ultracentrifugation.

To confirm the conjugation of glycolalicin onto the NPs, NPs were incubated with 100 μ l of 30 μ g/ml primary mouse antibody monoclonal against glycolalicin (HIP1, BioLegend) in PBS for one hour, followed by washing. Texas-Red[®] conjugated secondary antibodies (anti-mouse IgG1, BioLegend) were incubated with the NP solution for one hour followed by washing. FITC conjugated TAT peptide was used for verifying conjugation. The NPs were imaged using the Zeiss cyto viva microscope. In addition, the GPIb-TAT conjugated NPs were characterized using DLS and TEM for their size. The stability and protein binding of these nanoparticles in PBS and 100% FBS were also studied, as explained above.

3.2.10 Comparative Studies of Adhesion and Cellular Uptake of Conjugated NPs

For adhesion and cellular uptake under physiological flow conditions, P-selectin– and vWF– coated culture dishes were assembled in a circular flow chamber (GlycoTech, Gaithersburg, MD) for surface studies, where as glass slides with activated HAECs were assembled in the parallel plate flow system for cellular studies (Figure 2.2). The wall shear stress (τ) for the flow chamber was calculated using the equation given below:

$$\tau = 6Q\mu / bh^2$$

where Q is the volumetric flow rate, μ is the fluid viscosity, b is the channel width, and h is the channel height.

We compared the adhesion of NPs to P-selectin- and vWF- coated surfaces at a shear stress of 10 dyne/cm². Three groups of NPs were used, namely control NPs, GPIIb-conjugated NPs, and GPIIb-TAT-conjugated NPs. After the flow experiments, the amount of NPs bound to the culture dishes were quantified using a spectrophotometer.

We also performed cytotoxicity and cellular uptake studies of control NPs, GPIIb-conjugated NPs, and GPIIb-TAT-conjugated NPs under both static and flow conditions to assess their biocompatibility and efficiency. HAECs seeded in a 24-well plate were incubated with 300 µg/ml of respective nanoparticle solution for one hour (static uptake studies) or 24 hours (cytotoxicity studies) at 37°C. To study the targeting ability and uptake of the conjugated NPs by activated HAECs under flow, the shear stress was varied between 0-25 dyne/cm². The NPs at 300µg/ml concentration were suspended in low serum media. The activated HAECs on glass slides were exposed to the respective groups of NPs under varying shear stress. Static samples served as controls. Following the experiments, cells were washed with PBS, lysed, and analyzed for cellular uptake or cytotoxicity of the NPs as described above.

For confocal experiments, after the completion of the experiments, cells were prepared by washing with cold PBS, followed by incubation with ice-cold FM[®] 4-64 FX (5 µg/ml, Invitrogen) in PBS for 5 minutes to stain cell membranes red. Cells were then fixed with 4% paraformaldehyde and imaged using confocal laser scanning microscope (Leica) outfitted with FITC (Ex(λ) 488 nm/Em(λ) 525 nm) and TRIC filters

(Ex(λ) 565 nm/Em(λ) 744 nm). An average of 32 slices per cell was taken with a slice thickness of 0.1 μ m. The images were then analyzed using ImageJ software (NIH, ImageJ 1.42).

3.2.11 In Vitro Anti-Inflammatory Study

To compare the anti-inflammatory property of the GPIb-TAT conjugated DEX encapsulated NPs and free DEX in media, we carried out an *in vitro* anti-inflammatory study. HAECs were seeded in T-25 culture flasks at a density of 10,000 cells per cm² for two days followed by cell quiescence. Cells were first activated with 25 mM histamine. HAECs were then incubated for one hour with respective NPs and free DEX samples prepared in low serum growth media containing histamine, while HAECs incubated with low serum media containing histamine and without DEX or NPs served as control. After one hour, the cells were washed and further incubated with media containing histamine for pre-determined time periods. After experiments, the cells were detached using EDTA and washed. The cells were then incubated with APC-conjugated monoclonal primary mouse antibodies (BD Pharmingen, San Jose, California) against P-selectin for one hour, washed, and fixed in 4% paraformaldehyde. The mean fluorescence intensity of the cells was measured by flow cytometry. As over-expressed P-selectin^{145, 203-206} has been implicated in inflammation of vascular endothelium, we preferred using P-selectin as the indicator for measuring the anti-inflammation property of the dexamethasone-loaded GPIb-TAT-conjugated NPs.

3.2.12 Ex vivo localization and retention of the GPIIb-TAT-conjugated NPs

All animal experiments were performed in accordance with the animal welfare policy and IACUC approved protocols (Protocol Number: A07.005) of the University of Texas at Arlington. For these studies, NIR-797 loaded NPs were used to determine the localization and persistence of NPs in the injured blood vessel after a single local infusion of NPs. Carotid balloon injury was induced in 10 male Sprague-Dawley rats weighing between 300 to 600 g. For creating the balloon injury, general anesthesia was induced with a mixture of ketamine (80 mg/kg) and xylazine (8 mg/kg) given intraperitoneally. Then, through a midline neck incision, the common, external, and internal carotid arteries were exposed by blunt dissection. This was followed by introduction of a 2F Fogarty balloon catheter into the external carotid artery via an arteriotomy and advanced to the origin of the left common carotid artery. The balloon was then gradually inflated to 7atm to cause a balloon injury and then deflated. This process was repeated thrice to consistently produce endothelial activation along the length of the common carotid artery similar to a standard angioplasty procedure. After removal of the balloon catheter, the injured artery was excised and the distal end of the artery was clamped using vascular clamps. 50 μ l of either 5 mg/ml of control NPs or GPIIb-TAT-conjugated NPs suspended in PBS was then infused over 3 minutes using a 1 ml syringe. After the NPs were delivered, the apical end was also clamped with a vascular clamp. This created a closed loop system that allowed the contact of the NPs with the injured vessel wall. The NPs were allowed to interact with the injured wall for 30 minutes, after which the vascular clamps were removed and the nanoparticles

solution was collected. The vessel was then washed with 500 μ l of PBS over 3 minutes. The amount of NPs adhering to the carotid vessel wall was quantified by indirect measurement of the NPs fluorescence intensity (using TECAN microplate reader, EX – 760 nm/EM – 830 nm). The arteries were also imaged using the same wavelength by means of the KODAK FX Pro imaging system (Carestream) before and after washing with the buffer solution for 3 minutes. A total of six arteries per group were used for the experiments.

3.2.13 Statistical Analysis

Analysis of results was done with StatView 5.0 software (SAS Institute) using one way ANOVA and t-tests with $p < 0.05$. Post-hoc comparisons were made by means of the Fisher's least significant differences (LSD). Results are presented as mean \pm SD.

3.3 Results

3.3.1 Characterization and *In Vitro* stability of the NPs

After preparation of PLGA-PEG NPs, the attachment of PEG to PLGA was confirmed by FTIR (Figure 3.3). The FT-IR spectra of both PLGA and PLGA-PEG NPs showed sharp peaks at 1750 cm^{-1} , which are characteristic of carbonyl groups of the ester bond. Transmittance peak at around 3000 cm^{-1} is attributed to stretching of amine bound hydrogen in the PEG polymer alone, and this peak is absent in both PLGA and PLGA-PEG NPs. Additionally, amide I and amide II vibrations were also observed at

1670 cm^{-1} and 1560 cm^{-1} , respectively in PEG polymer and were noticeably absent in the PLGA-PEG NPs spectrum. In addition, presence of twin peaks between 2215-2240 cm^{-1} in the PLGA-PEG NPs spectra indicated the presence of C= N stretching vibration that points to the presence of a peptide bond.

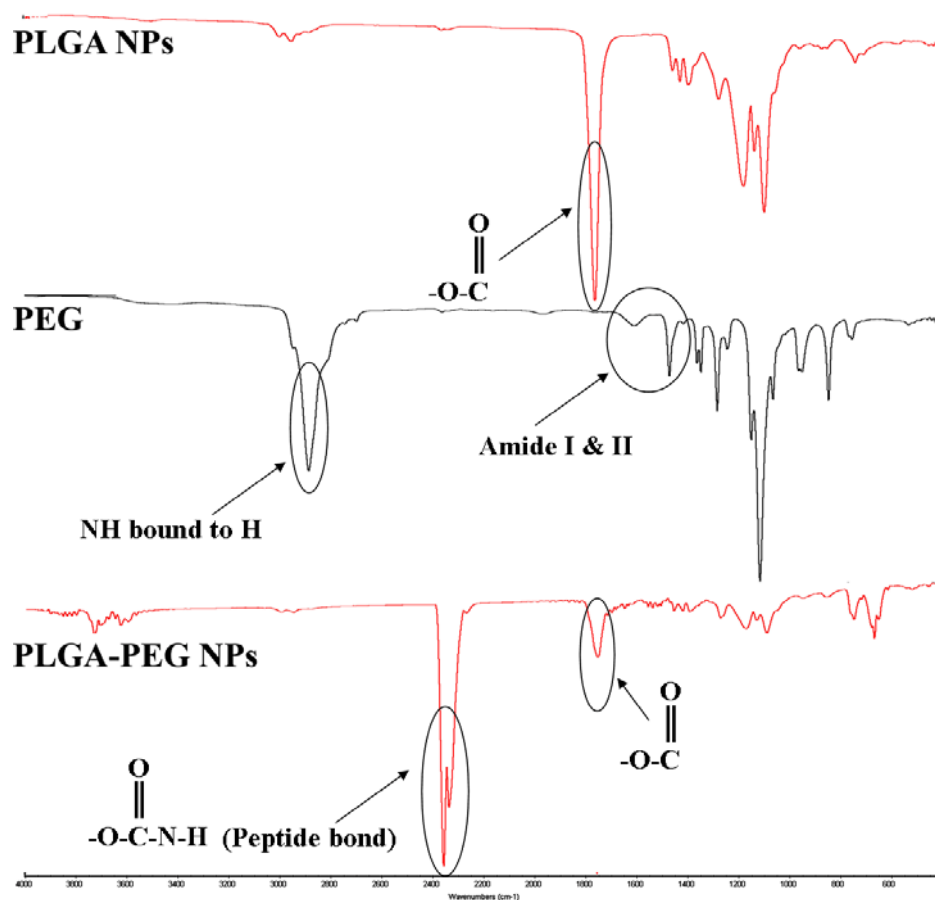


Figure 3.3 FTIR spectra of PLGA NPs, PEG polymer and PLGA-PEG NPs

Furthermore, the NPs were characterized for size and surface charge. *In vitro* studies were used to establish the stability in various physiological fluids. The mean hydrodynamic diameter along with the polydispersity and zeta potential of the NPs are

listed in Table 3.1 while the TEM images (Figure 3.4) of the various formulated NPs show the morphology and size range of the particles.

Table 3.1 Size, polydispersity and Zeta potential of various NP formulations

Type	Size (nm)	Polydispersity	Zeta (ζ) Potential (mV)
PLGA NPs	187.8 \pm 2.0	0.136 \pm 0.005	-26.27 \pm 0.51
PLGA-PEG NPs	197.7 \pm 1.6	0.150 \pm 0.023	-12.08 \pm 0.62
GPIIb conjugated PLGA-PEG NPs	249.9 \pm 25.0	0.303 \pm 0.016	-8.27 \pm 0.25
GPIIb-TAT conjugated PLGA-PEG NPs	241.1 \pm 25.6	0.311 \pm 0.012	-6.46 \pm 0.63

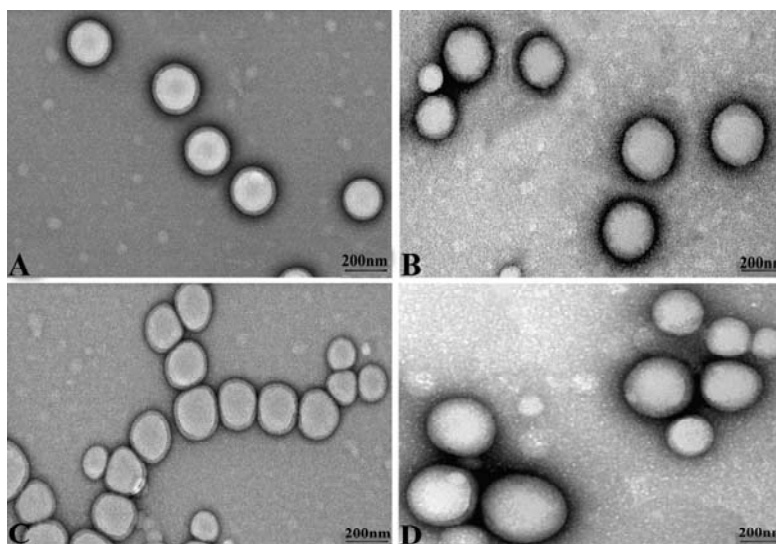


Figure 3.4 Nanoparticle Characterization using TEM (A) PLGA NPs (B) PLGA-PEG NPs (C) GPIIb-conjugated PLGA-PEG NPs (D) GPIIb-TAT-conjugated PLGA-PEG NPs

Control and conjugated NPs suspended in PBS remained stable behaviour during the 5-day study with no apparent change in size (Figure 3.5A). Furthermore,

after an initial 20-30 nm increase in size, all the NPs maintained their stability in 100% FBS, and no aggregates were formed (Figure 3.5B).

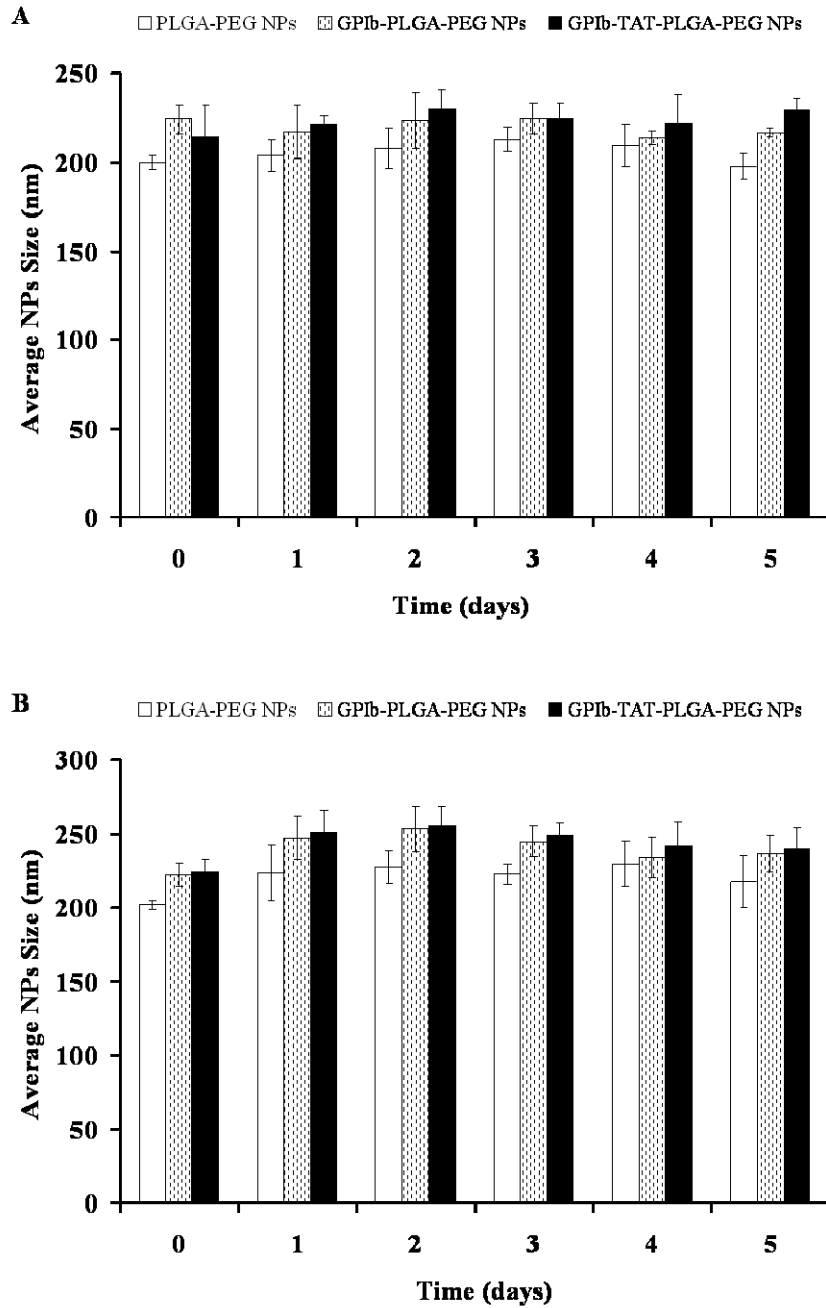


Figure 3.5 Stability of formulated NPs over 5 days at 37°C (A) PBS and (B) 100% FBS. Values represent mean \pm standard deviation (n=3)

3.3.2 Drug Release Profile

The suitability of the drug – loaded PLGA-PEG NPs for sustained drug delivery was ascertained by an *in vitro* drug release study. The amount of DEX released from the NPs at pre-determined periods was quantified and correlated to the initial amount of the drug loaded in the formulation to obtain the cumulative drug release. The drug release showed three stages and the NPs maintained the release for 4 weeks (Figure 3.6). The NPs had a loading efficiency of about 63.5%.

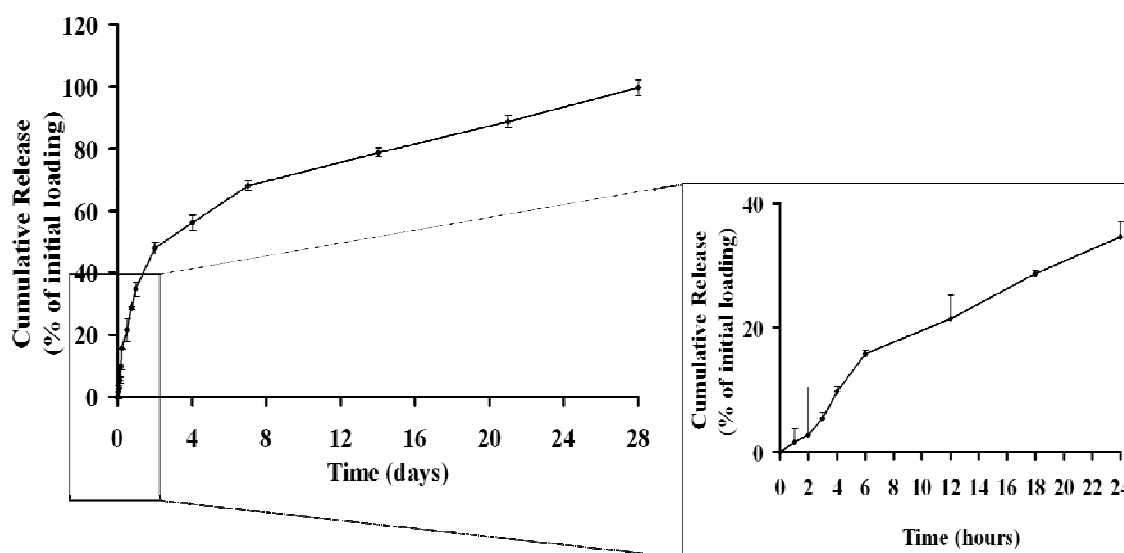


Figure 3.6 *In vitro* Release Curve of Dexamethasone from PLGA-PEG NPs at 37°C. Values represent mean \pm standard deviation (n=4)

3.3.3 Determination of suitable cell penetrating peptide for conjugation to NPs

We measured the zeta potential of the five CPPs used in the study, and the results are tabulated in Table 3.2.

Table 3.2 Zeta Potential of various cell penetrating peptides

CPP	Name/Source	Sequence	Mean Zeta Potential ± Std Error
TAT	Trans-activating transcripter derived from HIV-1	G-RKKRRQRRR	14.00 ± 3.16 mV
R11	Polyarginine peptide	G-RRRRRRRRRRR	17.18 ± 2.10 mV
PENE	Derived from the <i>Antennapedia</i> gene of <i>Drosophila</i> flies	G-RQIKIWFQNRRMKWKK	5.65 ± 1.96 mV
K11	Polylysine peptide	G-KKKKKKKKKKK	18.13 ± 2.50 mV
KALA	Synthetic cationic amphipathic peptide	G-KLALKLALKALKAALKLA	24.55 ± 2.96 mV

To determine the most suitable peptide for our studies, cellular uptake efficiency and intracellular cytotoxicity of five different CPPs, TAT, R11, K11, PENE and KALA, were evaluated. TAT and R11 peptides showed the highest cellular uptake at 5 μ M (Figure 3.7); however, cell uptake of R11 peptides also revealed significant toxicity compared to the control cells (Figure 3.8). All CPPs exhibited a dose dependent uptake and cytotoxicity.

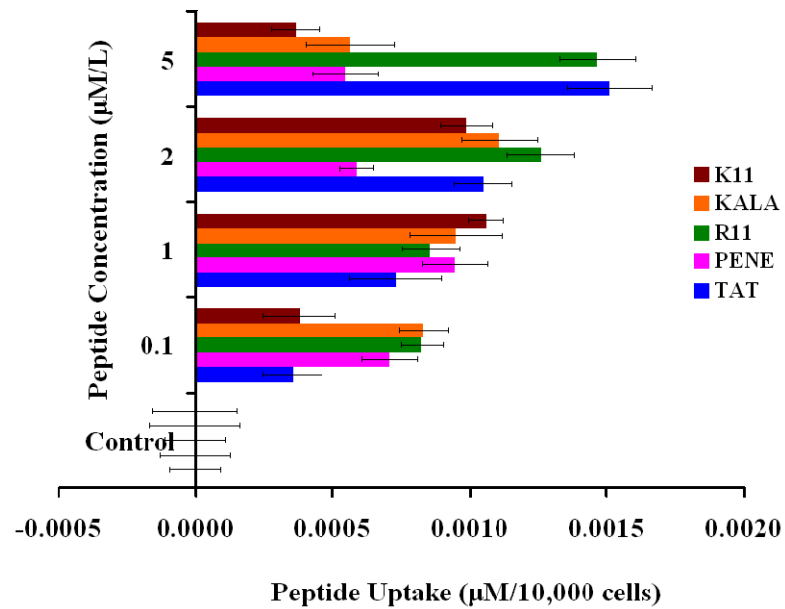


Figure 3.7 Uptake of various CPPs in HAECs after incubation for one hour. FITC intensity was determined by normalizing fluorescence intensity of each treatment with its cell numbers. Values are represented as mean \pm standard deviation (n=4)

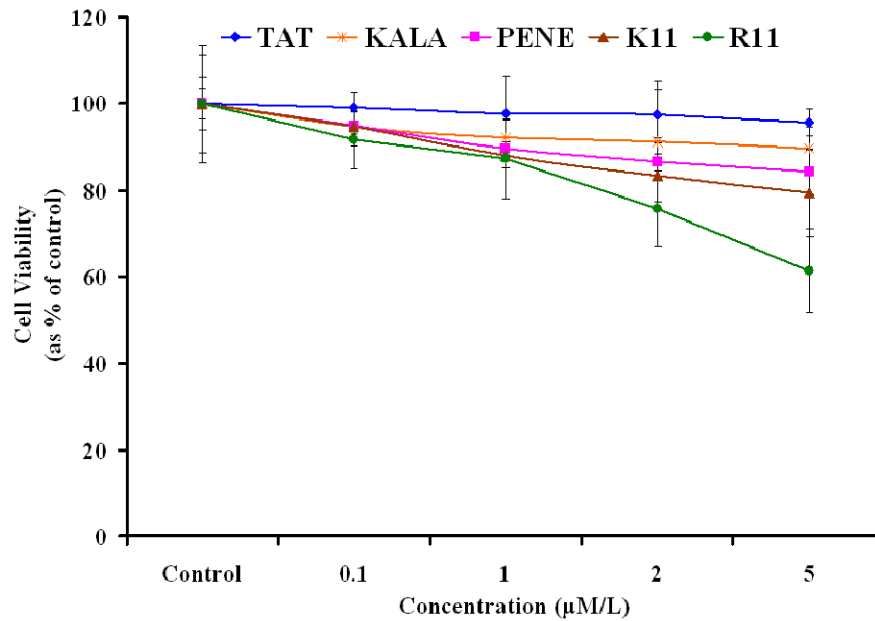


Figure 3.8 Cytotoxicity of various CPPs in HAECs as determined by MTS assays after incubation for 24 hours. Values are represented as mean \pm standard deviation (n=4)

To test if the synergic effect of CPPs with NPs decreases the cytotoxicity of the peptides, we conjugated the CPPs to PLGA NPs. We then examined the uptake and cell viability of these NPs on HAECs. From the results it is seen that the TAT and K11 conjugated NPs had a higher uptake compared to the other three peptides (Figure 3.9). Cells exposed to TAT and K11 conjugated NPs also showed slightly decreased cell viability compared to the cells that were exposed to KALA (76% cell viability of the control cells), PENE (showing ~ 80% cell viability of the control cells) and R11 conjugated NPs (less than 70% cell viability of the control cells) exhibited a much higher level of toxicity compared to the control cells (Figure 3.10).

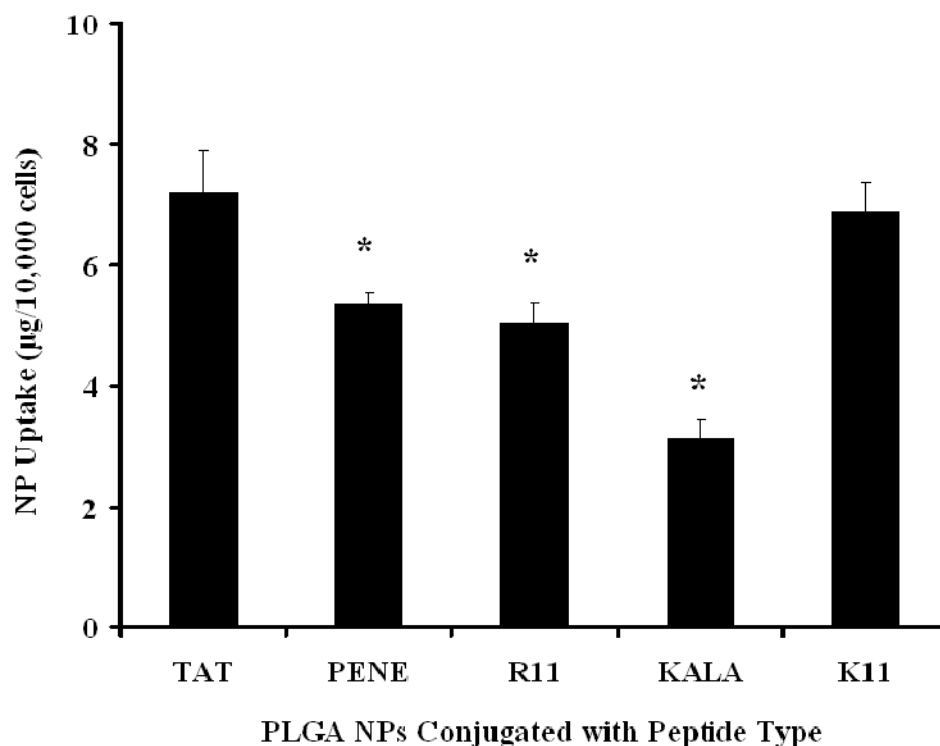


Figure 3.9 Uptake of various CPP-conjugated PLGA NPs by HAECs after incubation for one hour (200 µg/ml). Uptake was determined by normalizing FITC fluorescence intensity with respective cell numbers. Values represent mean ± standard deviation (n=4). * indicates significant differences compared to the control samples (p < 0.05)

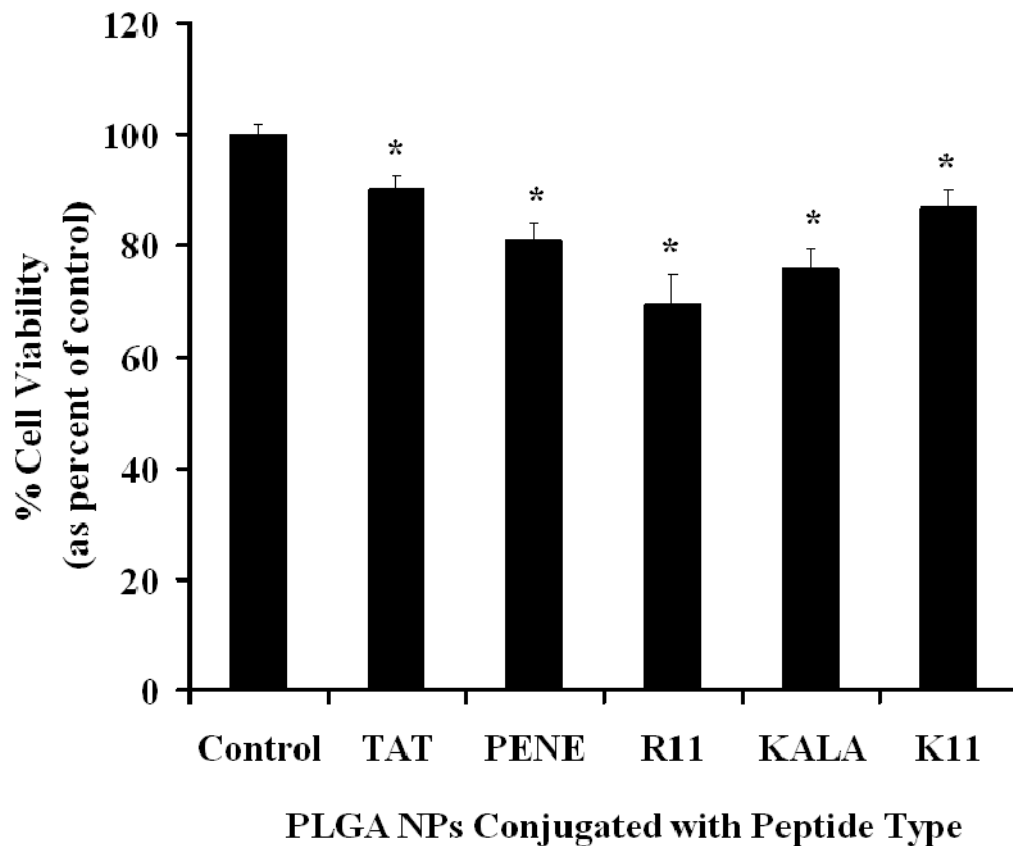


Figure 3.10 Cytotoxicity of various CPP-conjugated PLGA NPs in HAECs after incubation for 24 hours at a concentration of 200 $\mu\text{g/ml}$. Viability was assessed by MTS assay. Values are represented as mean \pm standard deviation ($n=4$). * indicates significant differences compared to the control samples ($p < 0.05$)

From the above results, we determined that the TAT peptide shows minimal cytotoxicity even at higher concentrations and exhibited a higher uptake by the HAECs. We further determined the dose and time dependent uptake of the free TAT peptide by the HAECs and observed a dose and time dependent uptake with uptake peaking at 5 μM concentration and saturating at 30 minutes of incubation (Figure 3.11).

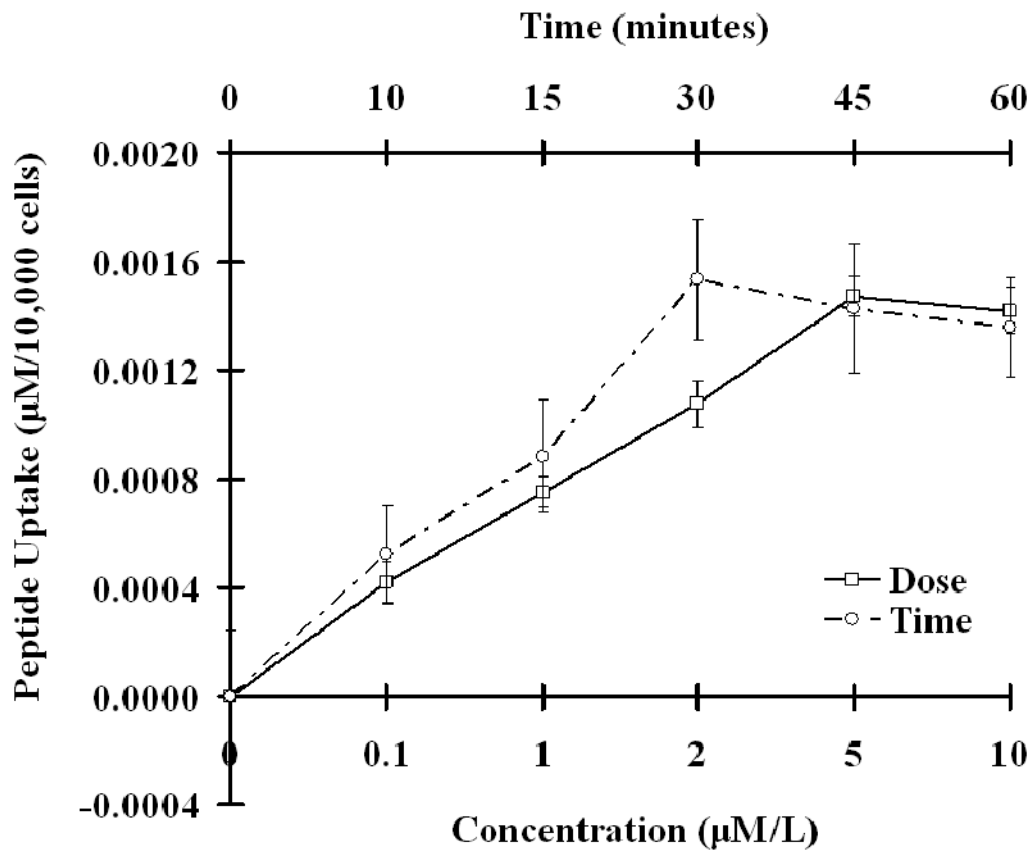


Figure 3.11 Effect of dose and incubation time on cellular uptake of TAT peptide. Values were obtained after incubating with TAT for either upto 1 hour or upto 5 µM

We exposed the HAECs to varying concentrations of the TAT peptide and found the peptide to be biocompatible even at higher concentrations (10µM) when compared to the control using MTS assay measurements (Figure 3.12). We also determined the half-life of the TAT peptide to be 32.6 hrs by incubating HAECs with optimal concentration of 5 µM/L of free fluorescent peptide for 72 hours (Figure 3.13).

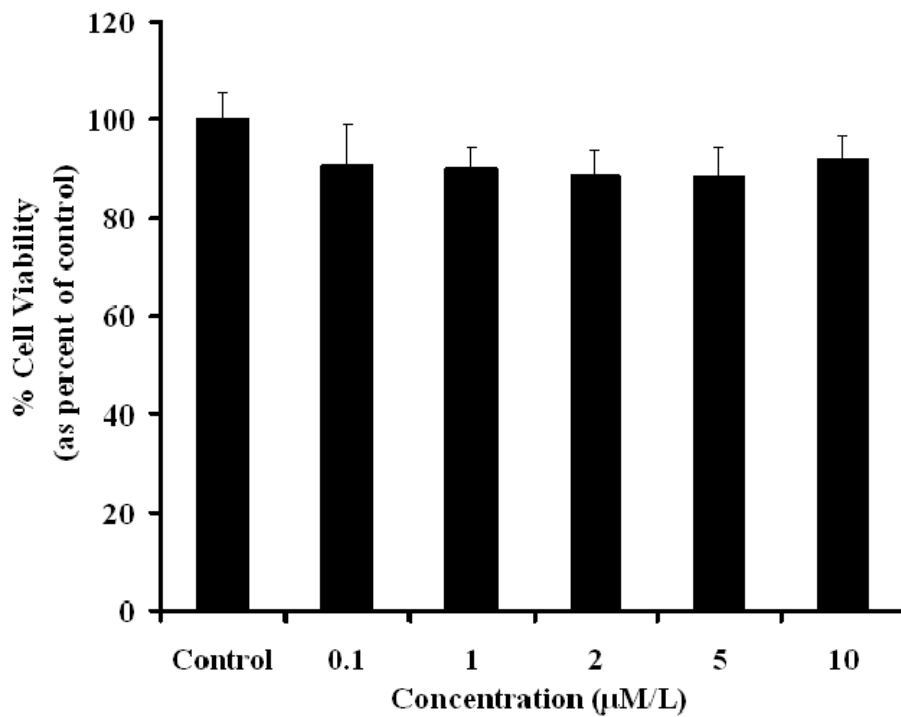


Figure 3.12 HAEC viability after exposure to TAT peptides for 24 hours at 37°C

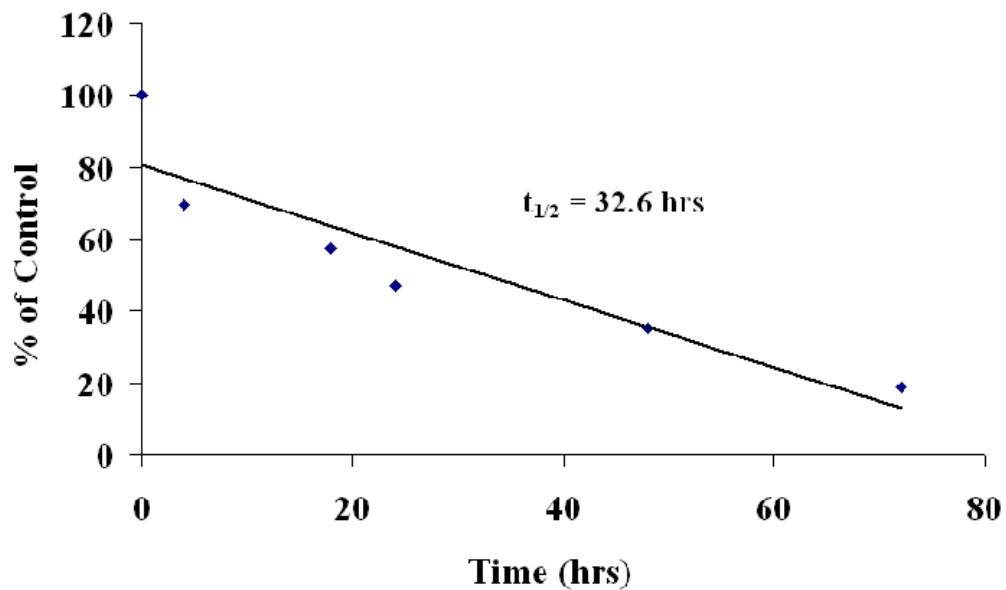


Figure 3.13 Half-life of TAT peptides in HAECs

The internalization of the TAT peptide was confirmed by fluorescence microscope image (Figure 3.14).

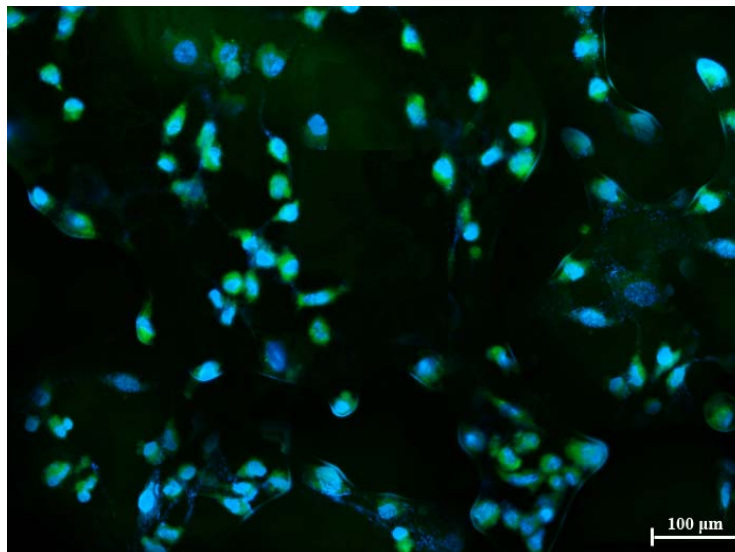


Figure 3.14 Fluorescence microscope image of cellular uptake of FITC-labeled TAT by HAECs. Cells were incubated with 5 μM of peptide for 30 minutes. After fixation, cells were counterstained with DAPI and the cellular distribution of peptide was visualized with fluorescence microscope. Scale = 100 μm

3.3.4 Characteristics of cellular studies of PLGA-PEG NPs by HAECs

We evaluated the cellular viability of PLGA-PEG NPs using the MTS assay. Relative to the control cells, around 90% of cells remained viable even upto concentrations of 1000 $\mu\text{g/ml}$ (Figure 3.15), pointing to the virtual biocompatibility of the PLGA-PEG NPs.

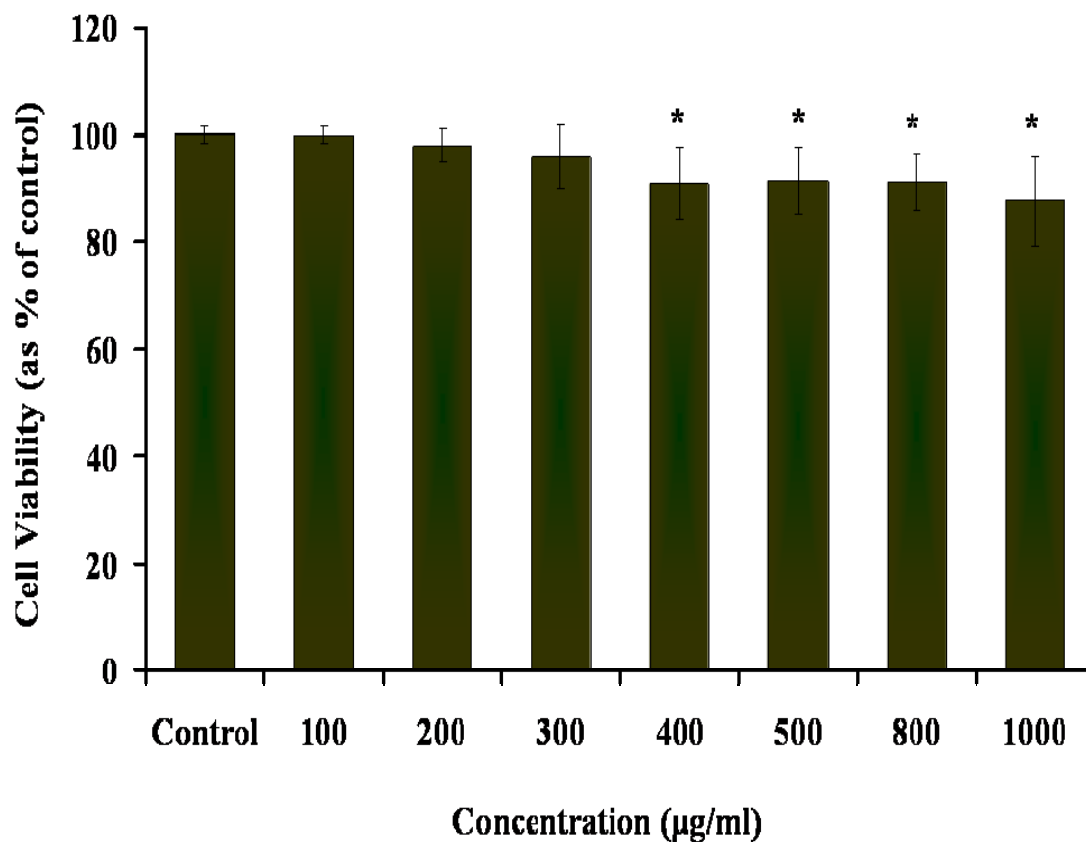


Figure 3.15 PLGA-PEG NPs biocompatibility study. Cells not exposed to NPs act as controls (100% cell viability). * indicates significant differences compared to the control samples ($p < 0.05$). Values are expressed as mean \pm SD (n=4)

The results of cellular uptake of PLGA-PEG NPs exhibited both dose- and time-dependence in uptake with cellular uptake saturating at 400 µg/ml. Significant uptake was observed after 30 minutes of exposure to NPs and uptake saturated after one hour of incubation (Figure 3.16).

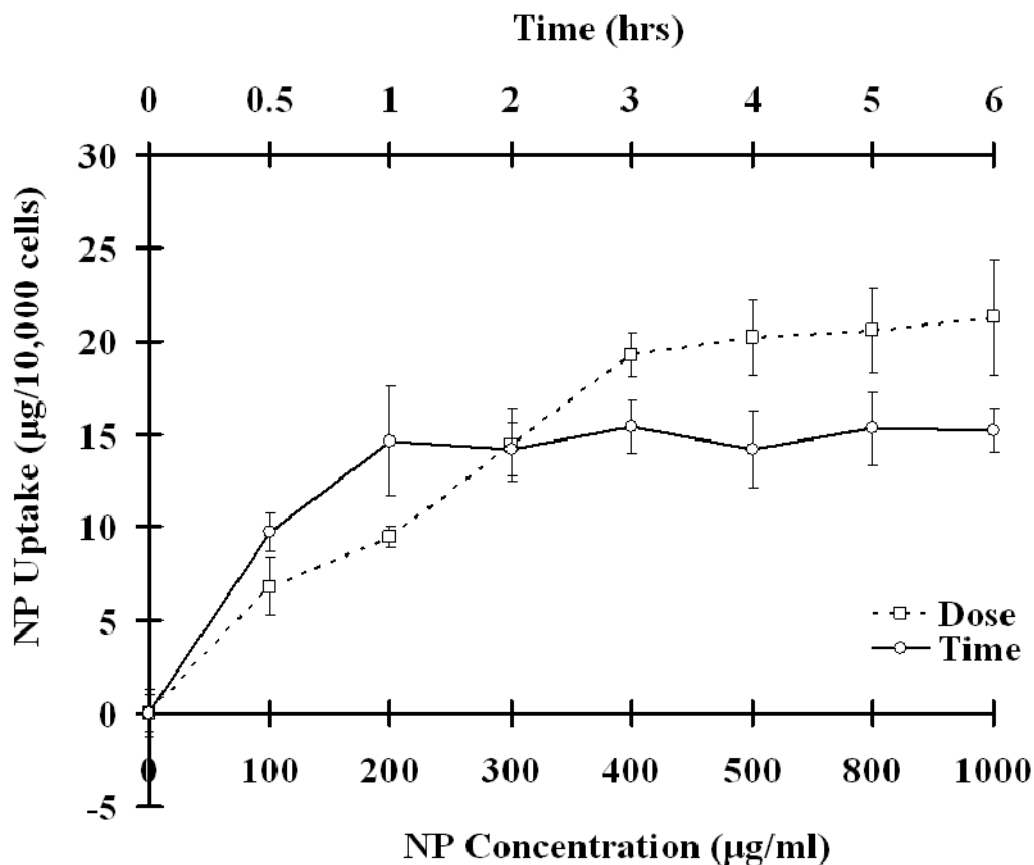


Figure 3.16 Effect of PLGA-PEG NP dose and incubation time on HAEC uptake. Values were obtained after incubating with NPs solutions either for one hour or with 300 µg/ml of NPs

3.3.5 Comparative Studies with GPIb-TAT conjugated NPs under static and physiological flow conditions

Conjugation of the two ligands, glycolalicin (GPIb) and TAT peptide was verified by Cytoviva imaging. Cytoviva images (Figure 3.17) confirmed the presence of green fluorescence in the region of the NPs, which is characteristic of the FITC TAT peptide. Red fluorescence around the NPs attributable to the existence of Texas Red[®]

fluorescent secondary antibodies against GPIb antibodies confirms the conjugation of glycolalicin to the NPs.

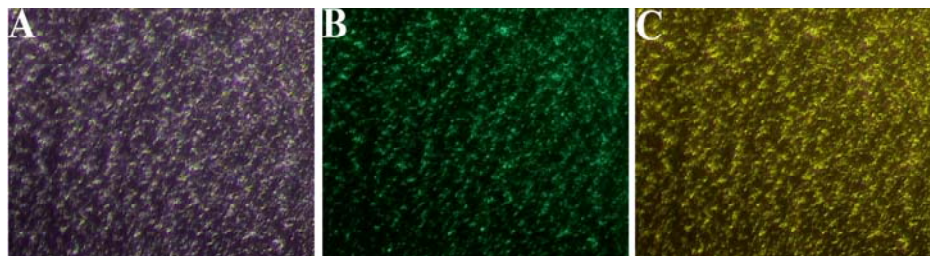


Figure 3.17 Evidence of TAT peptide and GPIb conjugation to PLGA-PEG NPs using CytoViva imaging (A) PLGA-PEG NPs (B) Fluorescent NPs imaged using green filter (C) Image obtained using both green and red filters

Stability of the ligands conjugated onto the NPs was studied over a week under physiological conditions and only about 20% of the ligand detached from NPs surface (Figure 3.18). This detachment was most likely due to NPs degradation. The total amount of ligand conjugated on the NPs served as the control.

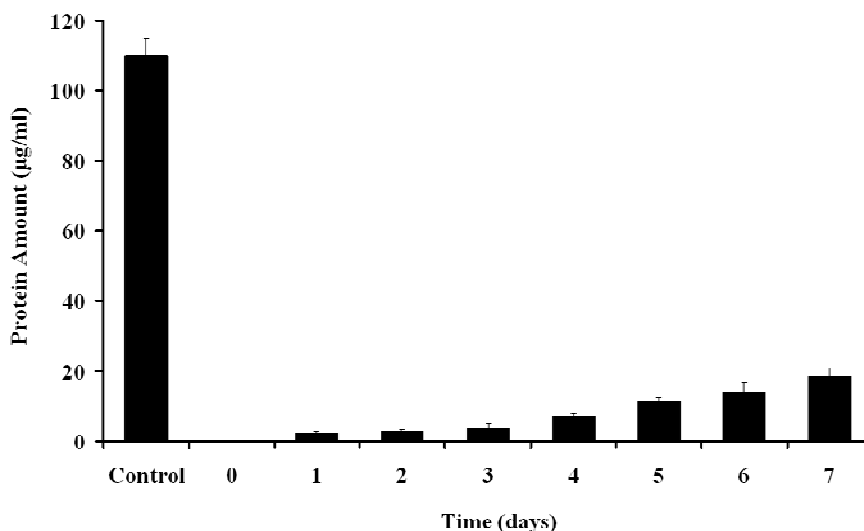


Figure 3.18 Quantification of ligand detachment from the conjugated NPs over one week. Values are presented as mean \pm SD (n=4). The total amount of protein bound to the nanoparticles served as the control sample

We also quantified the surface coating efficiency of both P-selectin and vWF (Table 3.3) using protein assays.

Table 3.3 Coating Efficiency using Passive Coating Method

Sample	Coating Efficiency (% of Initial Amount)
P-Selectin	75.25 ± 14.45
vWF	68.52 ± 19.96

We further analyzed the adhesion of control, GPIb-conjugated NPs, and GPIb-TAT-conjugated NPs on P-selectin- and vWF- coated surfaces under flow conditions to verify that presence of TAT peptide does not interfere with the binding of GPIb to the P-selectin- and vWF- coated surfaces. As seen from Figure 3.19, both the single and double ligands attached NPs exhibit similar binding behaviour compared to the control NPs. These results suggest that presence of TAT peptide does not hinder the function of GPIb.

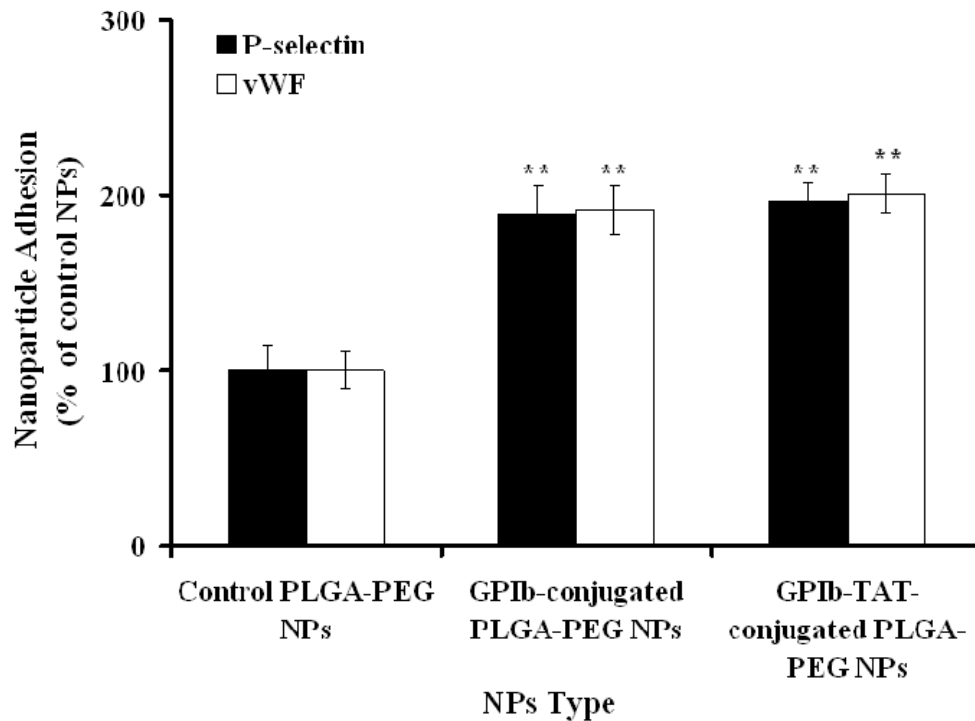


Figure 3.19 Adhesion of control, GPIb-conjugated NPs and GPIb-TAT conjugated NPs on P-selectin and vWF coated surfaces at shear stress of 10 dyne/cm² for 30 minutes. Values represent mean \pm SD (n=4). ** indicates the significant difference compared to the control NPs samples (p< 0.001)

We also performed comparative uptake and cytotoxicity studies on HAECs (control and activated cells) using PLGA-PEG NPs (as control NPs), PLGA-PEG-GPIb (single conjugation) and PLGA-PEG-GPIb-TAT (double conjugation) under static conditions. Results of these studies indicated that all three groups of NPs showed good biocompatibility (Figure 3.20) with the double ligand NPs showing a significant increase (%) of nanoparticle adhesion and uptake in both control and activated HAECs compared to the control NPs (Figure 3.21).

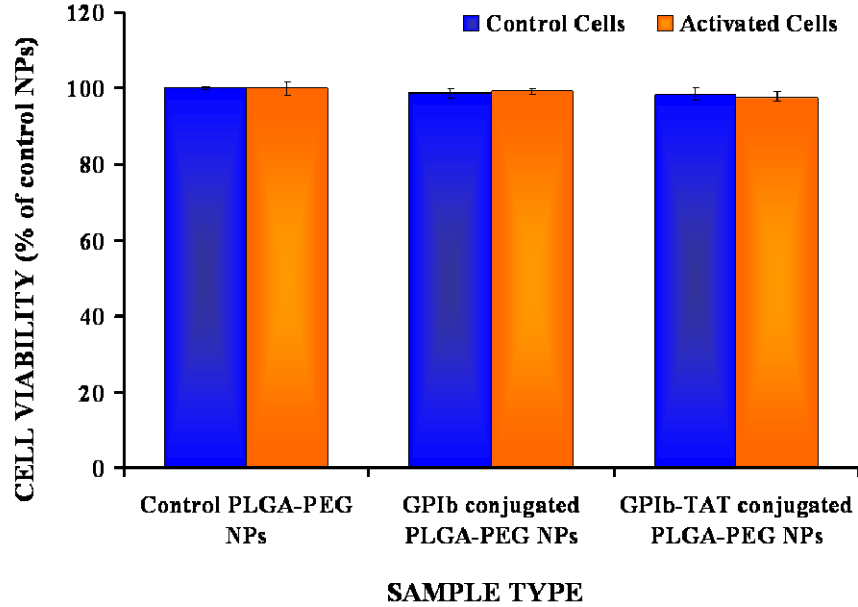


Figure 3.20 Comparison of cellular biocompatibility of control, GPIb-conjugated and GPIb-TAT-conjugated NPs (NP concentration = 300 µg/ml) on control and activated HAECs. Values are represented as mean ± SD (n=4)

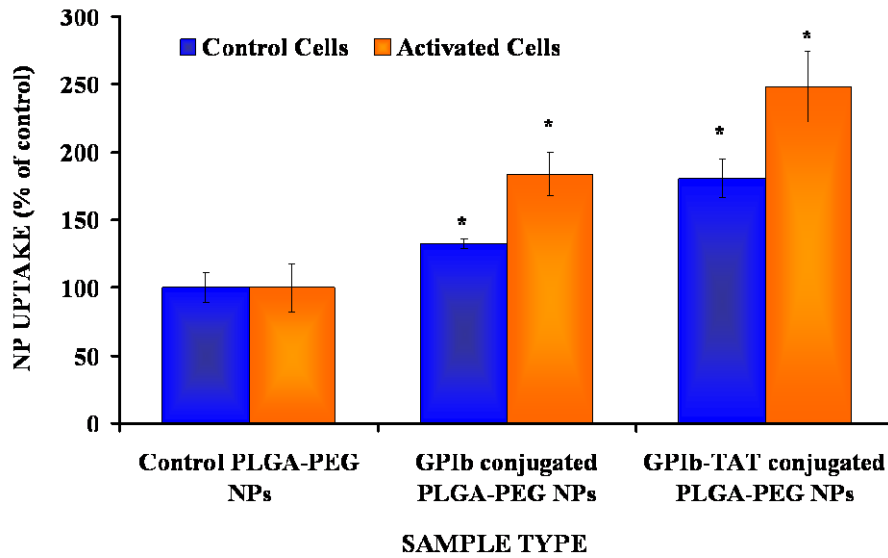


Figure 3.21 Comparison of uptake of control, GPIb-conjugated, and GPIb-TAT-conjugated NPs by either control or activated HAECs under static experimental conditions. Values represent mean ± SD (n=4). * indicates the significant differences compared to the control NPs of respective cell type

Furthermore, the analysis of shear stress effects on activated HAEC uptake and binding of control (PLGA-PEG NPs), GPIIb-conjugated, and GPIIb-TAT-conjugated NPs under flow revealed that at 25 dyne/cm², the perfusion of GPIIb-TAT-conjugated NPs had a significantly higher uptake (~ 4 times higher) compared to the control NPs (Figure 3.22) indicating that the presence of TAT peptide aids in the cellular uptake.

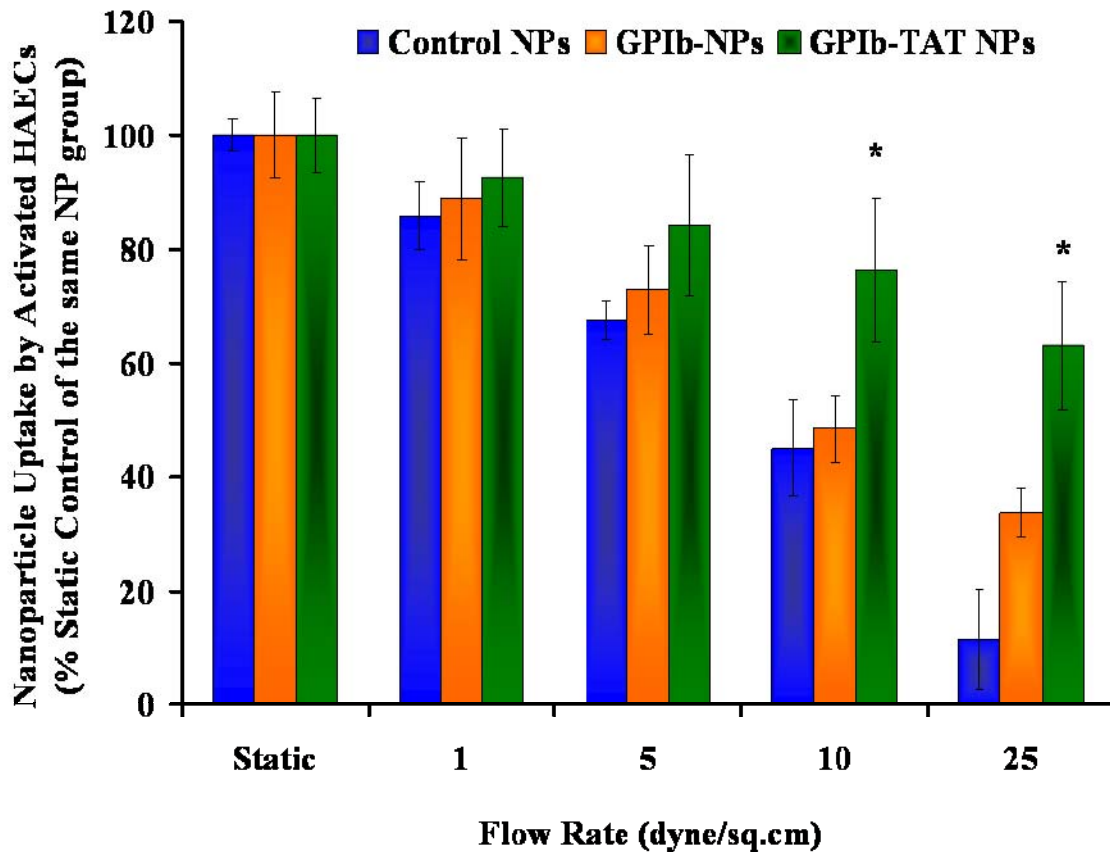


Figure 3.22 Shear stress regulated uptake of double-conjugation, single-conjugation and control NPs by activated HAECs. 25 mM histamine was used to activate the cells just before flow. After 30 minutes of flow, the NPs were quantified as described in section 3.2.8. Values represent mean \pm SD (n=3). * indicates the significant differences compared to the static control NP sample

Additionally, the confocal images showed minimal control NPs inside the cells while the GPIb-TAT-conjugated NPs exhibited a significantly higher accumulation inside HAECs (Figure 3.23).

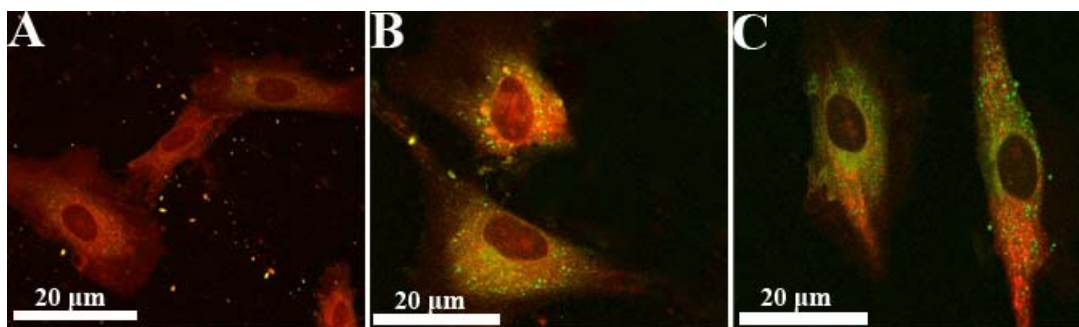


Figure 3.23 Confocal Images of cellular uptake of (A) control NPs (B) GPIb-conjugated NPs, and (C) GPIb-TAT-conjugated NPs. The fluorescent NPs were imaged via a FITC filter, while the FM 4-64 FX[®] stained plasma membranes were imaged with a TRIC filter. Images represent the overlay of both the filters

3.3.6 *In Vitro* Anti-inflammation Study

Results from the *in vitro* anti-inflammatory study clearly showed that the cells incubated with GPIb-TAT-conjugated NPs had a significantly lower P-selectin expression (inflammation biomarker, as described previously) compared to the control samples. After 24 hours of incubation with histamine containing media, control cells had approximately eight times higher P-selectin expression while cells exposed to free DEX in solution exhibited a three fold increased P-selectin expression compared to the zero hour control samples (Figure 3.24). Incubation of cells with either free DEX or GPIb-TAT-NPs containing DEX significantly reduced the P-selectin expression. These results show the feasibility of the GPIb-TAT-conjugated NPs as targeted and sustained drug delivery carriers to treat activated endothelial cells.

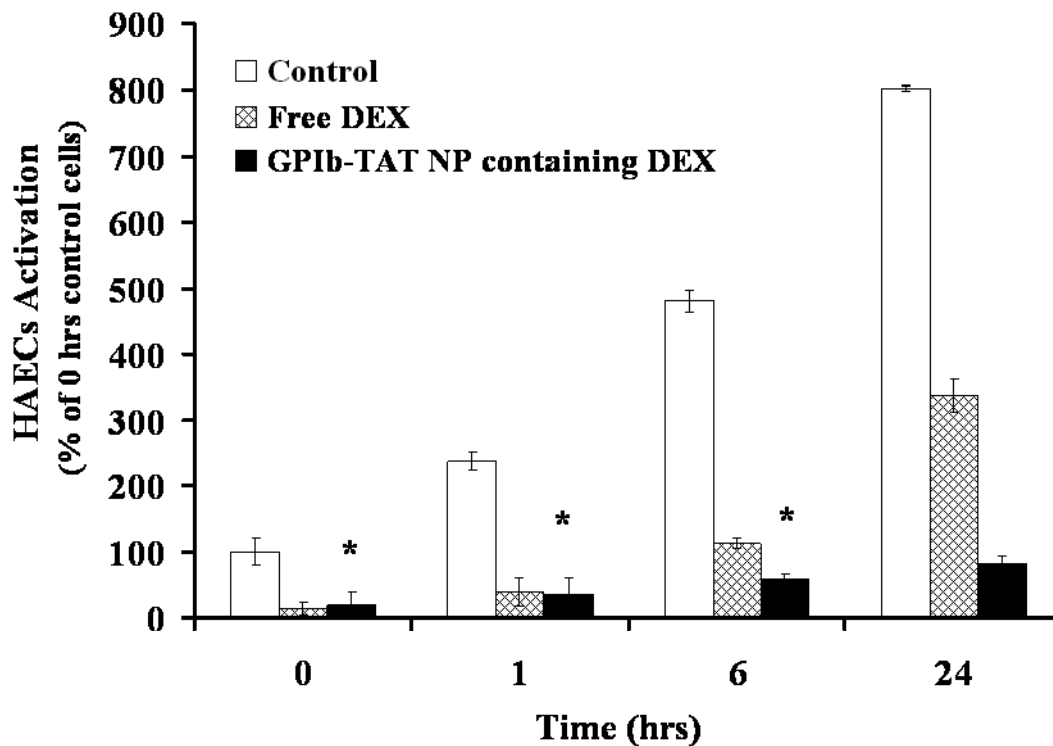


Figure 3.24 *In vitro* anti-inflammatory study comparing control, free DEX, and GPIb-TAT-conjugated DEX-encapsulated NPs. Values are represented as mean \pm standard deviation (n=4). * indicates significant differences compared to 0 hour control NP samples ($p < 0.05$)

3.3.7 Mechanisms of Nanoparticle Uptake

In an effort to identify the mechanisms of uptake that could be involved in the cellular entry of PLGA-PEG NPs and GPIb-TAT-conjugated PLGA-PEG NPs, we used several endocytic inhibitors, each of which is known to be explicit for a particular endocytic pathway. When the formation of clathrin-coated pits was inhibited by use of chlorpromazine, $\sim 50\%$ decrease in GPIb-TAT-conjugated NPs uptake was observed (Figure 3.25). However, inhibition of caveola-coated pit endocytosis by use of filipin did not have any effect on either of the NP uptake. In addition, when the HAECs were

treated with amiloride – a known inhibitor of Na^+/H^+ exchange mechanism of macropinocytosis, both groups of NPs exhibited a marked decline in the cellular uptake compared to the control samples. Additionally, in the presence of both chlorpromazine and amiloride, the cellular uptake of GPIIb-TAT conjugated NPs showed more than 50% reduction by HAECs (Figure 3.25), suggesting that the two endocytic processes, clathrin-mediated endocytosis and macropinocytosis, play a significant role in the NP cellular uptake. The various combinations of inhibitors (Inb.1+ Inb.2, Inb.1+ Inb.3 and Inb.2+ Inb.3) were used to study the synergistic effect of the inhibitors on the cellular uptake of the NPs.

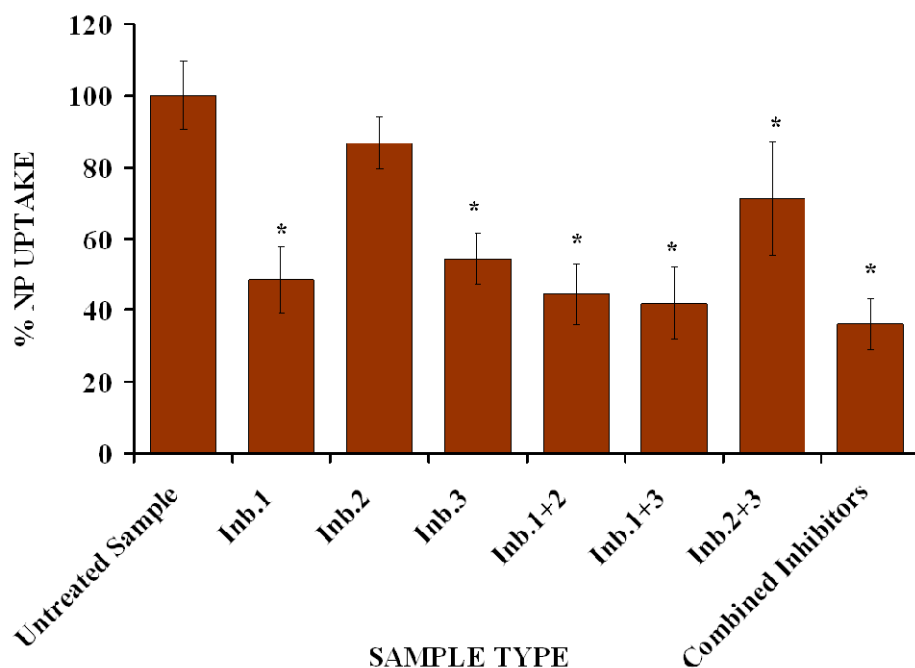


Figure 3.25 Effects of various inhibitory agents on cellular uptake of GPIIb-TAT-conjugated PLGA-PEG NPs. *Inb.1* (chlorpromazine), *Inb.2* (filipin) and *Inb. 3* (amiloride). Positive control represents cells incubated with all three inhibitors while negative controls were not exposed to any of the inhibitors. Values represent mean \pm standard deviation (n=4). * indicates significant differences compared to the negative control sample ($p < 0.05$)

3.3.8 *Ex Vivo* Retention Study

Preliminary *ex vivo* adhesion studies using the rat carotid injury model showed a significantly higher adhesion (13 fold retention) of the PLGA-PEG-GPIIb-TAT NPs to the injured vascular wall compared to the control NPs after washing for 3 minutes (Figure 3.26). Images of the retention of PLGA-PEG, GPIIb-conjugated NPs and GPIIb-TAT conjugated NPs after washing is shown in Figure 3.27.

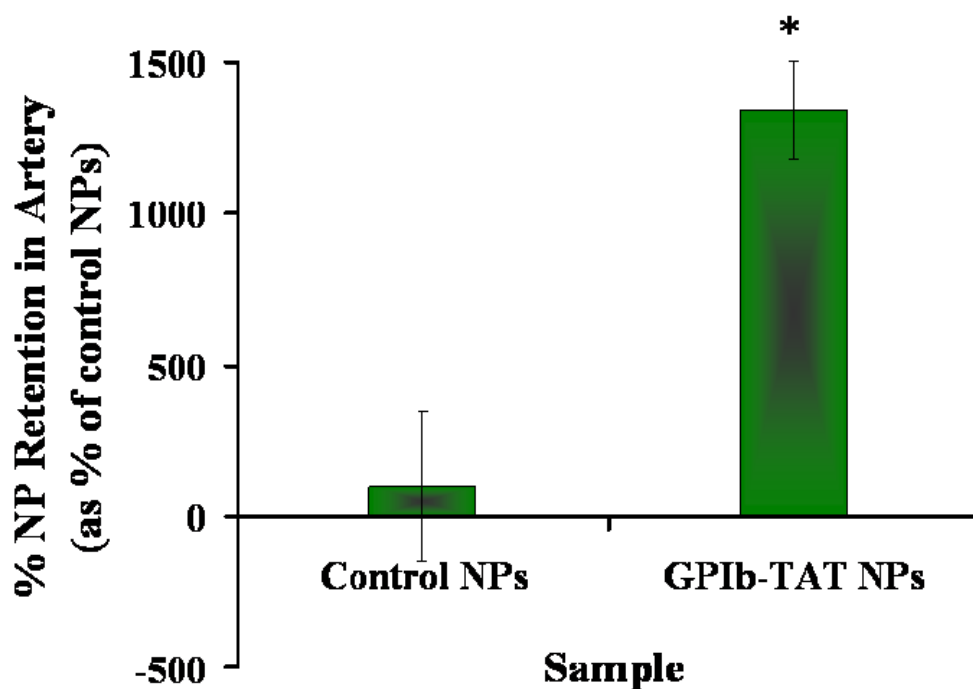


Figure 3.26 Retention of PLGA-PEG NPs and GPIIb-TAT conjugated NPs in rat carotid artery injury model. Values are correspond to mean \pm standard deviation (n=6). * indicates significant differences compared to the control NPs sample ($p < 0.05$)

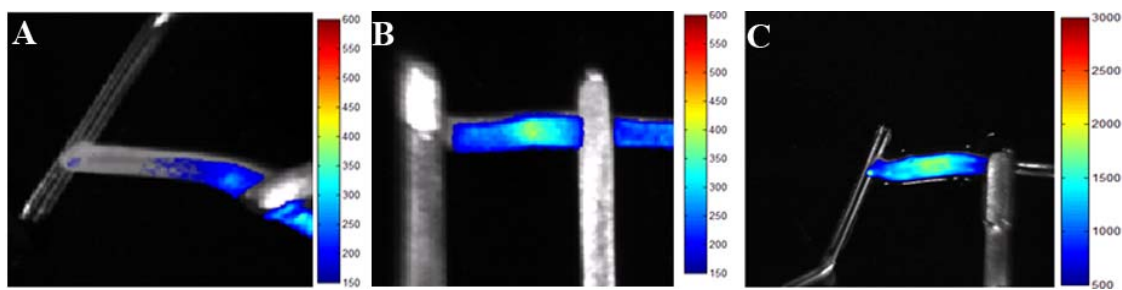


Figure 3.27 *Ex vivo* images of rat carotid arteries using (A) Control NPs, (B) GPIb NPs and (C) GPIb-TAT NPs imaged using the KODAK FX Pro imaging system, after washing with PBS for 3 minutes

3.4 Discussion

Recent approaches for an effective site-specific drug delivery have moved towards a local delivery system rather than systemic drug administration in an effort to achieve and maintain high levels of the drug at the target site. In this work, our aim was to develop and characterize a unique drug targeting strategy to the injured vascular wall and/or the inflamed HAECs. The novel nanoparticle system used the binding ability of GPIb to anchor the nanoparticles to the blood vessel under physiological flow conditions while the cell penetrating peptide TAT aided as a facilitator to enhance the intracellular nanoparticle uptake by the cells similar to the invasive properties of HIV-1 virus into the cell membrane. The formulated GPIb-TAT-conjugated PLGA-PEG NPs were characterized for size and cellular behaviour *in vitro*. Compared to the control NPs, our GPIb-TAT-conjugated PLGA-PEG NPs exhibited increased cellular uptake under both static and dynamic conditions along with better anti-inflammatory effect. These nanoparticles were internalized primarily by clathrin aided endocytosis and

macropinocytosis. Preliminary *in vivo* results also indicated that the GPIb-TAT-conjugated NPs have a considerably better retention to the vascular wall. Our data suggests that attaching both GPIb ligand and TAT peptide to NPs can increase the targeting capability and enhance particle uptake under fluid shear stress *in vivo*.

The release of the drug from the PLGA-PEG NPs showed three stages – a burst release of around 34% in the first 24 hours. This burst release might be due to the desorption of the drug from the NP surface. This stage is followed by a plateau that is attributed to the drug diffusion. The third stage is a steady release attained from both diffusion of the drug and surface erosion of the NPs. Our findings are consistent with the results reported by several researchers using PLGA as the material for formulating NPs for controlled drug delivery.²³⁹⁻²⁴¹

Our results point towards the TAT peptide having the highest uptake with minimal cytotoxicity in the HAECs. This result is in contrast to those reported by Zhou et al.,²⁴² and the difference could be due to the difference in the cell type used in our studies (HAECs) and other studies (prostate cancer cells – LNCaP, C4-2, LAPC4, and PC3 cells). Additionally, the lower cytotoxicity of the TAT peptide can be credited to the fact that it contains only the basic region TAT (47–57), and this region does not induce significant toxicity on cells, even when used at high concentrations of upto 100 μ M as shown by previous studies.^{243, 244}

The PLGA-PEG NP uptake by HAECs was found to be dose- and incubation time-dependent. Our results were comparable to other cellular uptake studies of PLGA-PEG NPs²⁴⁵ and of PLGA NPs.⁵⁹ However, contrary to these studies, uptake of our NPs reached equilibrium after one hour of incubation. This difference in saturation time may be due to the particle composition as well as different cell types used. These results imply that the cellular uptake pathway of PLGA-PEG NPs for endothelial cells is more active at lower incubation time and reaches the saturation limit more rapidly. Additionally, our findings with TAT-conjugated NPs are supported by results from other studies.²⁴⁶⁻²⁵⁰ Moreover, the use of known endocytic inhibitors in blocking the cellular uptake mechanisms showed a marked change in uptake. Chlorpromazine is a chemical that dissociates clathrin from the membrane surface to inhibit the clathrin-mediated endocytosis, filipin III is a selective inhibitor that prevents caveolae formation, and amiloride is a potent inhibitor of macropinocytosis. Our observations with these inhibitors suggest the existence of two distinct primary endocytic mechanisms, namely clathrin-mediated endocytosis and macropinocytosis, that aid in the NP cellular uptake. These findings indicate that the majority of our NPs are internalized by non-destructive cellular means, and this is substantiated by other research findings.^{53, 220, 221, 251-254}

Varying levels of shear stress can also influence the uptake of NPs by HAECs. Comparable to our results, other research has also indicated that the adhesion of NPs on ligand coated surface and uptake by endothelial cells shows an inverse correlation to

shear stress.^{92, 94, 225} Similar to nanoparticle adhesion and cellular studies using antibodies against P-selectins,^{92, 225} our studies found that the GPIb-attached and GPIb-TAT-conjugated NPs exhibited increased adhesion to P-selectin- and vWF- coated surfaces and to activated HAECs. This could be due to the higher binding strength of platelet ligands under high shear conditions.^{99, 133, 135, 228} The inhibitory effects of GPIb-TAT-conjugated drug loaded NPs on the expression of P-selectin was more pronounced compared to control and GPIb-conjugated drug loaded NPs. Higher retention of GPIb-TAT-conjugated PLGA-PEG NPs by local administration of the NPs in the injured carotid artery of rats supports our hypothesis that modifying the NPs with platelet GPIb and TAT peptides would enhance the arterial endothelial retention of drug-loaded agents to treat restenosis.

3.5 Conclusions

We have developed a novel multi-ligand nanoparticle system to target the endothelial cells and the subendothelium with the ability to deliver therapeutic agents like the anti-inflammatory drug, dexamethasone, to the injured vascular wall and/or activated endothelial cells. These multi-ligand nanoparticles also showed promising results in arresting the nanoparticles to the activated cells *in vitro* under flow as well as *ex vivo* in injured arteries in animal studies. Pending additional qualification studies, it is possible that this dual targeting nanoparticle system could serve as an efficient therapeutic carrier, in particular for delivering drugs to the injured vascular wall.

CHAPTER 4

CONCLUSIONS, LIMITATIONS AND FUTURE WORK

In summary, we successfully formulated and characterized the platelet-mimicking multi-ligand drug-loaded, dual targeting nanoparticles for improved and efficient therapeutic delivery. These nanoparticles have shown enhanced adhesion and uptake by activated endothelial cells under high flow conditions. Preliminary *ex vivo* studies using rat carotid injury model exhibited higher retention of these novel nanoparticles. Other results involving formulation of multi-ligand nanoparticles have shown that they possess positive qualities for a suitable drug delivery system. We could successfully load and deliver the anti-inflammatory agent – dexamethasone, via the nanoparticles with high efficiency. With the aid of *in vitro* experiments using endocytic inhibitors, we demonstrated that in addition to diffusion, the internalization of the nanoparticles can be mediated by two distinct uptake pathways – clathrin mediated-endocytosis and macropinocytosis. All these results support our hypothesis of using platelet GPIIb α for arresting the nanoparticles onto the injured endothelial cells under flow along with TAT peptides to increase internalization of the nanoparticles by the activated/injured endothelial cells.

Given the favorable results including low toxicity, coupled with efficient adhesion and uptake under flow as well as nondestructive endocytic pathways of uptake, our multi-ligand nanoparticles could act as versatile carriers for targeted intracellular delivery of therapeutic agents under physiological flow as well as lead to the creation of novel drug delivery nanoparticles which can be used as alternative or as complementary treatments to oral drugs and drug eluting stents to reduce thrombosis, inflammation, and restenosis associated with injured vascular wall.

Though the novel platelet mimicking multi-ligand conjugated nanoparticles developed in this project demonstrated a superior adhesion and uptake by activated endothelial cells under physiological flow, the applicability of this targeting strategy might have some limitations. Some of these limitations are listed below:

- The amount of targeting ligands bound to the nanoparticle surfaces may be limited due to inadequate number of exposed free carboxyl groups on the polymer surface (even though we use PLGA and PEG with carboxyl groups in the formulation of the NPs). A possible alternative to this inadequacy would be coating of monomers/polymers containing more carboxyl groups on the surfaces of the polymeric NPs using a pulsed plasma polymerization process.
- Just like other glycoproteins,²⁵⁵⁻²⁵⁹ our GPIb-TAT-conjugated nanoparticles may present unwanted effects elicited by interaction with blood cells like platelets and inflammation cells. Experiments using human blood containing these particles will be performed to see whether this is the case. An alternative

strategy for this limitation would be the incorporation of the peptide (sequences of GPIb) that is shear-stress regulated and binds only to the regions of P-selectin expressed on the activated endothelium, instead of glycofibrinogen (the whole extracellular fraction of GPIb) onto NPs.

- Although we have estimated the delivery dose of NPs for *in vivo* studies based on previous research and our preliminary *in vitro* studies, it is possible that the optimal dose will not be achieved in animal studies within the studied range. If this is the case, re-evaluation of doses and time points will be performed for our drug delivery carriers using animal models.
- We used dexamethasone as our model drug to test the efficacy of the targeted and controlled drug delivery approach using GPIb-TAT-conjugated NPs. Dexamethasone has shown in various studies to inhibit endothelial activation and in-stent restenosis.^{167, 189, 190, 260-264} However, drug-eluting stents using dexamethasone did not show any significant clinical benefits.²⁶⁵⁻²⁶⁷ If a potential limitation of drug efficiency is encountered, other established therapeutic agents such as anti-platelet/anti-thrombotic drugs like Cilostazol, Prasugrel, Clopidogrel and Aspirin¹⁸⁴ as well as anti-inflammatory/anti-proliferative agents like Cilostazol, Paclitaxel, Actinomycin-D, Mycophenolic acid, Estradiol and Sirolimus and its analogues like Everolimus, Tacrolimus¹⁸⁵ will be studied as alternatives.

Future work on this project will involve more *in vitro* and *in vivo* studies to optimize the drug delivery formulations. Future studies will include:

- Variation of P-selectin and vWF coating densities and studying their effects on the nanoparticle adhesion.
- Varying the amount of the conjugating ligand densities on the nanoparticle surface and studying their effects on the nanoparticle cellular uptake.
- Flow cytometric analysis on the conjugated nanoparticles to determine ligand surface densities.
- Investigation on the attachment and detachment kinetics of GPIb-TAT-conjugated NPs on coated surfaces.
- Study of competitive binding of GPIb-TAT-conjugated NPs with soluble GPIb protein and platelets.
- *In vivo* biodistribution and biocompatibility.
- Evaluation of the pharmacological efficiency of multi-ligand NPs using rat injury models.
- Study of interactions of GPIb-TAT-conjugated NPs on blood cells such as platelets and leukocytes, and on injured arteries.

REFERENCES

1. Fact Sheets and At-a-Glance Reports. Available at: http://www.cdc.gov/dhdsp/library/fs_heart_disease.htm.
2. Lloyd-Jones D, Adams RJ, Brown TM, Carnethon M, Dai S, De Simone G, Ferguson TB, Ford E, Furie K, Gillespie C, Go A, Greenlund K, Haase N, Hailpern S, Ho PM, Howard V, Kissela B, Kittner S, Lackland D, Lisabeth L, Marelli A, McDermott MM, Meigs J, Mozaffarian D, Mussolino M, Nichol G, Roger VL, Rosamond W, Sacco R, Sorlie P, Stafford R, Thom T, Wasserthiel-Smoller S, Wong ND, Wylie-Rosett J. Heart disease and stroke statistics--2010 update: a report from the American Heart Association. *Circulation*. Feb 23;121(7):e46-e215.
3. Samara WM, Gurbel PA. The role of platelet receptors and adhesion molecules in coronary artery disease. *Coronary artery disease*. Feb 2003;14(1):65-79.
4. Libby P. Inflammation and cardiovascular disease mechanisms. *The American journal of clinical nutrition*. Feb 2006;83(2):456S-460S.
5. Rocha VZ, Libby P. Obesity, inflammation, and atherosclerosis. *Nature reviews*. Jun 2009;6(6):399-409.
6. Heart Disease Facts. Available at: <http://www.cdc.gov/heartdisease/facts.htm>.

7. Heron M. Deaths: leading causes for 2004. *Natl Vital Stat Rep.* Nov 20 2007;56(5):1-95.
8. Minino AM, Heron MP, Murphy SL, Kochanek KD. Deaths: final data for 2004. *Natl Vital Stat Rep.* Aug 21 2007;55(19):1-119.
9. Klugmann S, Barbieri L. [Coronary stenting: indications and results]. *Cardiologia (Rome, Italy)*. Dec 1993;38(12 Suppl 1):377-381.
10. Cardiac Medications At-A-Glance.
American Heart Association. Available at:
<http://www.americanheart.org/presenter.jhtml?identifier=3038846>.
11. Sleight P. Current options in the management of coronary artery disease. *The American journal of cardiology*. Nov 7 2003;92(9B):4N-8N.
12. Liddicoat JR, De La Torre R, Ho KK, Nathan S, Levitsky S, Krempin J, Sellke F. Initial impact of drug-eluting stents on coronary artery bypass graft surgery. *The Annals of thoracic surgery*. Apr 2006;81(4):1239-1242; discussion 1242.
13. Harjai KJ, Grines CL. Management of multivessel coronary disease: let us not shortchange drug-eluting stents. *Journal of interventional cardiology*. Jun 2008;21(3):213-217.

14. Forteza A, Rabinstein A. [Angioplasty and stenting in carotid stenosis. Therapeutic alternative or technical possibility?]. *Revista de neurologia*. Feb 1-15 2001;32(3):270-275.
15. Mauro LS, Borovicka MC, Kline SS. Introduction to coronary artery stents and their pharmacotherapeutic management. *The Annals of pharmacotherapy*. Dec 1997;31(12):1490-1498.
16. Nageh T, Meier B. Treatment of in-stent restenosis. *International journal of cardiology*. Oct 10 2005;104(3):245-250.
17. Tsakiris DA, Tschopl M, Jager K, Haefeli WE, Wolf F, Marbet GA. Circulating cell adhesion molecules and endothelial markers before and after transluminal angioplasty in peripheral arterial occlusive disease. *Atherosclerosis*. Jan 1999;142(1):193-200.
18. Tsakiris DA, Tschopl M, Wolf F, Labs KH, Jager KA, Marbet GA. Platelets and cytokines in concert with endothelial activation in patients with peripheral arterial occlusive disease. *Blood Coagul Fibrinolysis*. Mar 2000;11(2):165-173.
19. Ellozy SH, Carroccio A. Drug-eluting stents in peripheral vascular disease: eliminating restenosis. *Mt Sinai J Med*. Nov 2003;70(6):417-419.
20. Winslow RD, Sharma SK, Kim MC. Restenosis and drug-eluting stents. *The Mount Sinai journal of medicine, New York*. Mar 2005;72(2):81-89.

21. Rectenwald JE, Moldawer LL, Huber TS, Seeger JM, Ozaki CK. Direct evidence for cytokine involvement in neointimal hyperplasia. *Circulation*. Oct 3 2000;102(14):1697-1702.
22. Kornowski R, Hong MK, Tio FO, Bramwell O, Wu H, Leon MB. In-stent restenosis: contributions of inflammatory responses and arterial injury to neointimal hyperplasia. *J Am Coll Cardiol*. Jan 1998;31(1):224-230.
23. Smith SCJ, Feldman TE, Hirshfeld JW, al. e. ACC/AHA/SCAI 2005 guideline update for percutaneous coronary intervention: a report of the American College of Cardiology/American Heart Association Task Force on Practice Guidelines (ACC/AHA/SCAI Writing Committee to Update 2001 Guidelines for Percutaneous Coronary Intervention). *Circulation*. 2006;113(7):166-286.
24. Badimon JJ, Fuster V, Chesebro JH, Badimon L. Coronary atherosclerosis. A multifactorial disease. *Circulation*. Mar 1993;87(3 Suppl):II3-16.
25. Indolfi C, Coppola C, Torella D, Arcucci O, Chiariello M. Gene therapy for restenosis after balloon angioplasty and stenting. *Cardiology in review*. Nov-Dec 1999;7(6):324-331.
26. Ip JH, Fuster V, Badimon L, Badimon J, Taubman MB, Chesebro JH. Syndromes of accelerated atherosclerosis: role of vascular injury and smooth muscle cell proliferation. *Journal of the American College of Cardiology*. Jun 1990;15(7):1667-1687.

27. Rivard A, Andres V. Vascular smooth muscle cell proliferation in the pathogenesis of atherosclerotic cardiovascular diseases. *Histology and histopathology*. Apr 2000;15(2):557-571.
28. Serruys PW, de Jaegere P, Kiemeneij F, et al. A comparison of balloon-expandable stent implantation with balloon angioplasty in patients with coronary artery disease. *N. Engl. J. Med.* 1994;331:489-495.
29. Fischman DL, Leon M, Baim DS, et al. A randomized comparison of coronary stent placement and balloon angioplasty in the treatment of coronary artery disease. *N. Engl. J. Med.* 1994;331:496-501.
30. Gaspardone A, Versaci F. Coronary stenting and inflammation. *The American journal of cardiology*. Dec 19 2005;96(12A):65L-70L.
31. Versaci F, Gaspardone A. Prevention of restenosis after stenting: the emerging role of inflammation. *Coronary artery disease*. Sep 2004;15(6):307-311.
32. Harder S, Klinkhardt U, Alvarez JM. Avoidance of bleeding during surgery in patients receiving anticoagulant and/or antiplatelet therapy: pharmacokinetic and pharmacodynamic considerations. *Clin Pharmacokinet*. 2004;43(14):963-981.
33. Kidane AG, Salacinski H, Tiwari A, Bruckdorfer KR, Seifalian AM. Anticoagulant and antiplatelet agents: their clinical and device application(s) together with usages to engineer surfaces. *Biomacromolecules*. May-Jun 2004;5(3):798-813.

34. Burt HM, Hunter WL. Drug-eluting stents: a multidisciplinary success story. *Adv Drug Deliv Rev.* Jun 3 2006;58(3):350-357.
35. Nguyen KT, Su SH, Sheng A, Wawro D, Schwade ND, Brouse CF, Greilich PE, Tang L, Eberhart RC. In vitro hemocompatibility studies of drug-loaded poly-(L-lactic acid) fibers. *Biomaterials.* Dec 2003;24(28):5191-5201.
36. Alexis F, Venkatraman SS, Rath SK, Boey F. In vitro study of release mechanisms of paclitaxel and rapamycin from drug-incorporated biodegradable stent matrices. *Journal of Controlled Release.* Jul 23 2004;98(1):67-74.
37. Kipshidze N, Leon MB, Tsapenko M, Falotico R, Kopia GA, Moses J. Update on sirolimus drug-eluting stents. *Current Pharmaceutical Design.* 2004;10(4):337-348.
38. Vogt F, Stein A, Rettmeier G, Krott N, Hoffmann R, vom Dahl J, Bosserhoff AK, Michaeli W, Hanrath P, Weber C, Blindt R. Long-term assessment of a novel biodegradable paclitaxel-eluting coronary polylactide stent. *Eur Heart J.* Aug 2004;25(15):1330-1340.
39. Dalal AR, D'Souza S, Shulman MS. Brief review: Coronary drug-eluting stents and anesthesia. *Canadian Journal of Anaesthesia-Journal Canadien D Anesthesie.* Dec 2006;53(12):1230-1243.
40. Pan M, Suarez de Lezo J, Medina A, Romero M, Delgado A, Segura J, Ojeda S, Mazuelos F, Hernandez E, Melian F, Pavlovic D, Esteban F, Herrador J. Drug-

eluting stents for the treatment of bifurcation lesions: a randomized comparison between paclitaxel and sirolimus stents. *American heart journal*. Jan 2007;153(1):15 e11-17.

41. Pires NM, Eefting D, de Vries MR, Quax PH, Jukema JW. Sirolimus and paclitaxel provoke different vascular pathological responses after local delivery in a murine model for restenosis on underlying atherosclerotic arteries. *Heart (British Cardiac Society)*. Aug 2007;93(8):922-927.
42. Ruef J, Storger H, Schwarz F, Haase J. Comparison of a polymer-free rapamycin-eluting stent (YUKON) with a polymer-based paclitaxel-eluting stent (TAXUS) in real-world coronary artery lesions. *Catheter Cardiovasc Interv*. Feb 15 2008;71(3):333-339.
43. Saia F, Degertekin M, Lemos PA, Serruys PW. Drug-eluting stents: from randomized trials to the real world. *Minerva cardioangiologica*. Oct 2004;52(5):349-363.
44. Kedia G, Lee MS. Stent thrombosis with drug-eluting stents: a re-examination of the evidence. *Catheter Cardiovasc Interv*. May 1 2007;69(6):782-789.
45. Luscher TF, Steffel J, Eberli FR, Joner M, Nakazawa G, Tanner FC, Virmani R. Drug-eluting stent and coronary thrombosis: biological mechanisms and clinical implications. *Circulation*. Feb 27 2007;115(8):1051-1058.

46. Leon MB. Late thrombosis a concern with drug-eluting stents. *Journal of interventional cardiology*. Feb 2007;20(1):26-29.
47. Wenaweser P, Dorffler-Melly J, Imboden K, Windecker S, Togni M, Meier B, Haerberli A, Hess OM. Stent thrombosis is associated with an impaired response to antiplatelet therapy. *Journal of the American College of Cardiology*. Jun 7 2005;45(11):1748-1752.
48. Park DW, Park SW, Lee SW, Kim YH, Lee CW, Hong MK, Kim JJ, Park SJ. Frequency of coronary arterial late angiographic stent thrombosis (LAST) in the first six months: outcomes with drug-eluting stents versus bare metal stents. *The American journal of cardiology*. Mar 15 2007;99(6):774-778.
49. Petrak K. Essential properties of drug-targeting delivery systems. *Drug Discovery Today*. 2005;10(23/24):1667-1673.
50. Feng SS. Nanoparticles of biodegradable polymers for new-concept chemotherapy. *Expert review of medical devices*. Sep 2004;1(1):115-125.
51. Farokhzad OC, Cheng J, Teply BA, Sherifi I, Jon S, Kantoff PW, Richie JP, Langer R. Targeted nanoparticle-aptamer bioconjugates for cancer chemotherapy in vivo. *Proceedings of the National Academy of Sciences of the United States of America*. Apr 18 2006;103(16):6315-6320.

52. Yannas IV. Chapter 2.8. Natural Materials. *Biomaterials Science*. Second Edition, Edited by Ratner, B., Hoffman, A., Schoen, F., Lemons, J. Elsevier Inc., San Diego, CA, (2004): p. 127-128.
53. Panyam J, Labhasetwar V. Biodegradable nanoparticles for drug and gene delivery to cells and tissue. *Advanced drug delivery reviews*. Feb 24 2003;55(3):329-347.
54. Hoerstrup SP, Vacanti JP. Overview of Tissue Engineering. In: Ratner B, Hoffman A, Schoen F, Lemons J, eds. *Biomaterials Science*. Second ed. San Diego: Elsevier Inc; 2004:712-714.
55. Moshfeghi AA, Peyman GA. Micro- and nanoparticulates. *Advanced drug delivery reviews*. 2005;57(14):2047-2052.
56. Eniola AO, Rodgers SD, Hammer DA. Characterization of biodegradable drug delivery vehicles with the adhesive properties of leukocytes. *Biomaterials*. May 2002;23(10):2167-2177.
57. Kohn JK, Abramson S, Langer R. Chapter 2.7. Bioresorbable and Bioerodible Materials. *Biomaterials Science*. Second Edition, Edited by Ratner, B., Hoffman, A., Schoen, F., Lemons, J. Elsevier Inc., San Diego, CA, (2004): p. 115-125.
58. Chorny M, Fishbein I, Danenberg HD, Golomb G. Lipophilic drug loaded nanospheres prepared by nanoprecipitation: effect of formulation variables on

- size, drug recovery and release kinetics. *J Control Release*. Oct 30 2002;83(3):389-400.
59. Davda J, Labhasetwar V. Characterization of nanoparticle uptake by endothelial cells. *Int J Pharm*. Feb 21 2002;233(1-2):51-59.
60. Dong Y, Feng SS. Nanoparticles of poly(D,L-lactide)/methoxy poly(ethylene glycol)-poly(D,L-lactide) blends for controlled release of paclitaxel. *Journal of biomedical materials research*. Jul 2006;78(1):12-19.
61. Hans ML, Lowman AM. Biodegradable nanoparticles for drug delivery and targeting. *Current Opinion in Solid State and Materials Science*. 2002;6(4):319-327.
62. Song CX, Labhasetwar V, Murphy H, Qu X, Humphrey WR, Shebuski RJ, Levy RJ. Formulation and characterization of biodegradable nanoparticles for intravascular local drug delivery. *Journal of Controlled Release*. 1997;43(2-3):197-212.
63. Fessi H, Puisieux F, Devissaguet JP, Ammoury N, Benita S. Nanocapsule formation by interfacial polymer deposition following solvent displacement. *International journal of pharmaceutics*. 1989;55(1):R1-R4.
64. Feng SS. New-concept chemotherapy by nanoparticles of biodegradable polymers: where are we now? *Nanomedicine (London, England)*. Oct 2006;1(3):297-309.

65. Sakhalkar HS, Dalal MK, Salem AK, Ansari R, Fu J, Kiani MF, Kurjiaka DT, Hanes J, Shakesheff KM, Goetz DJ. Leukocyte-inspired biodegradable particles that selectively and avidly adhere to inflamed endothelium in vitro and in vivo. *Proceedings of the National Academy of Sciences of the United States of America*. Dec 23 2003;100(26):15895-15900.
66. Yan F, Xue J, Zhu J, Marchant RE, Guo Z. Synthesis of a lipid conjugate of SO₃Le(a) and its enhancement on liposomal binding to activated platelets. *Bioconjugate chemistry*. Jan-Feb 2005;16(1):90-96.
67. Chang DK, Chiu CY, Kuo SY, Lin WC, Lo A, Wang YP, Li PC, Wu HC. Antiangiogenic targeting liposomes increase therapeutic efficacy for solid tumors. *The Journal of biological chemistry*. May 8 2009;284(19):12905-12916.
68. Kessner S, Krause A, Rothe U, Bendas G. Investigation of the cellular uptake of E-Selectin-targeted immunoliposomes by activated human endothelial cells. *Biochimica et biophysica acta*. Oct 1 2001;1514(2):177-190.
69. Oku N, Asai T, Watanabe K, Kuromi K, Nagatsuka M, Kurohane K, Kikkawa H, Ogino K, Tanaka M, Ishikawa D, Tsukada H, Momose M, Nakayama J, Taki T. Anti-neovascular therapy using novel peptides homing to angiogenic vessels. *Oncogene*. Apr 18 2002;21(17):2662-2669.

70. Maeda H, Bharate GY, Daruwalla J. Polymeric drugs for efficient tumor-targeted drug delivery based on EPR-effect. *Eur J Pharm Biopharm.* Mar 2009;71(3):409-419.
71. Greish K. Enhanced permeability and retention of macromolecular drugs in solid tumors: a royal gate for targeted anticancer nanomedicines. *Journal of drug targeting.* Aug-Sep 2007;15(7-8):457-464.
72. Spragg DD, Alford DR, Greferath R, Larsen CE, Lee KD, Gurtner GC, Cybulsky MI, Tosi PF, Nicolau C, Gimbrone MA, Jr. Immunotargeting of liposomes to activated vascular endothelial cells: a strategy for site-selective delivery in the cardiovascular system. *Proceedings of the National Academy of Sciences of the United States of America.* Aug 5 1997;94(16):8795-8800.
73. Dufresne MH, Garrec DL, Sant V, Leroux JC, Ranger M. Preparation and characterization of water-soluble pH-sensitive nanocarriers for drug delivery. *International journal of pharmaceutics.* Jun 11 2004;277(1-2):81-90.
74. Fournier E, Dufresne MH, Smith DC, Ranger M, Leroux JC. A novel one-step drug-loading procedure for water-soluble amphiphilic nanocarriers. *Pharm Res.* Jun 2004;21(6):962-968.
75. Couvreur P, Puisieux F. Nano- and microparticles for the delivery of polypeptides and proteins. *Advanced drug delivery reviews.* 1993/6//;10(2-3):141-162.

76. Eniola AO, Hammer DA. Artificial polymeric cells for targeted drug delivery. *Journal of controlled release : official journal of the Controlled Release Society*. Feb 21 2003;87(1-3):15-22.
77. Eniola AO, Hammer DA. Characterization of biodegradable drug delivery vehicles with the adhesive properties of leukocytes II: effect of degradation on targeting activity. *Biomaterials*. Feb 2005;26(6):661-670.
78. Alexis F, Pridgen E, Molnar LK, Farokhzad OC. Factors affecting the clearance and biodistribution of polymeric nanoparticles. *Molecular pharmaceutics*. Jul-Aug 2008;5(4):505-515.
79. Cho K, Wang X, Nie S, Chen ZG, Shin DM. Therapeutic nanoparticles for drug delivery in cancer. *Clin Cancer Res*. Mar 1 2008;14(5):1310-1316.
80. Yang YY, Wang Y, Powell R, Chan P. Polymeric core-shell nanoparticles for therapeutics. *Clinical and experimental pharmacology & physiology*. May-Jun 2006;33(5-6):557-562.
81. Brannon-Peppas L, Blanchette JO. Nanoparticle and targeted systems for cancer therapy. *Advanced drug delivery reviews*. Sep 22 2004;56(11):1649-1659.
82. Maruyama K. [PEG-liposome in DDS and clinical studies]. *Nippon rinsho*. Mar 1998;56(3):632-637.
83. Douglas SJ, Davis SS, Illum L. Nanoparticles in drug delivery. *Critical reviews in therapeutic drug carrier systems*. 1987;3(3):233-261.

84. Labhasetwar V, Song C, Humphrey W, Shebuski R, Levy RJ. Arterial uptake of biodegradable nanoparticles: effect of surface modifications. *Journal of pharmaceutical sciences*. Oct 1998;87(10):1229-1234.
85. Desai MP, Labhasetwar V, Walter E, Levy RJ, Amidon GL. The mechanism of uptake of biodegradable microparticles in Caco-2 cells is size dependent. *Pharmaceutical research*. Nov 1997;14(11):1568-1573.
86. Win KY, Feng SS. Effects of particle size and surface coating on cellular uptake of polymeric nanoparticles for oral delivery of anticancer drugs. *Biomaterials*. May 2005;26(15):2713-2722.
87. Chester K, Pedley B, Tolner B, Violet J, Mayer A, Sharma S, Boxer G, Green A, Nagl S, Begent R. Engineering antibodies for clinical applications in cancer. *Tumour Biol*. Jan-Apr 2004;25(1-2):91-98.
88. Cheifetz A, Mayer L. Monoclonal antibodies, immunogenicity, and associated infusion reactions. *The Mount Sinai journal of medicine, New York*. Jul 2005;72(4):250-256.
89. Grabarek Z, Gergely J. Zero-length crosslinking procedure with the use of active esters. *Analytical Biochemistry*. 1990;185(1):131-135.
90. Hermanson GT, Mallia AK, Smith KP. *Immobilized affinity ligand techniques*. San Diego Academic Press; 1992.

91. Piercenet.
<http://www.piercenet.com/Objects/View.cfm?type=ProductFamily&ID=02030312>.
92. Blackwell JE, Dagia NM, Dickerson JB, Berg EL, Goetz DJ. Ligand coated nanosphere adhesion to E- and P-selectin under static and flow conditions. *Annals of biomedical engineering*. Jun 2001;29(6):523-533.
93. Nguyen KT, Shukla KP, Moctezuma M, Braden AR, Zhou J, Hu Z, Tang L. Studies of the cellular uptake of hydrogel nanospheres and microspheres by phagocytes, vascular endothelial cells, and smooth muscle cells. *Journal of biomedical materials research*. Mar 15 2009;88(4):1022-1030.
94. Lin A, Sabnis A, Kona S, Nattama S, Patel H, Dong JF, Nguyen KT. Shear-regulated uptake of nanoparticles by endothelial cells and development of endothelial-targeting nanoparticles. *Journal of biomedical materials research*. Aug 3 2009.
95. Doshi N, Zahr AS, Bhaskar S, Lahann J, Mitragotri S. Red blood cell-mimicking synthetic biomaterial particles. *Proceedings of the National Academy of Sciences of the United States of America*. Dec 22 2009;106(51):21495-21499.
96. Eniola AO, Hammer DA. In vitro characterization of leukocyte mimetic for targeting therapeutics to the endothelium using two receptors. *Biomaterials*. Dec 2005;26(34):7136-7144.

97. Lee SY, Ferrari M, Decuzzi P. Design of bio-mimetic particles with enhanced vascular interaction. *Journal of biomechanics*. Aug 25 2009;42(12):1885-1890.
98. Andre P, Hainaud P, Bal dit Sollier C, Garfinkel LI, Caen JP, Drouet LO. Relative involvement of GPIb/IX-vWF axis and GPIIb/IIIa in thrombus growth at high shear rates in the guinea pig. *Arteriosclerosis, thrombosis, and vascular biology*. May 1997;17(5):919-924.
99. Chen J, Lopez JA. Interactions of platelets with subendothelium and endothelium. *Microcirculation*. Apr-May 2005;12(3):235-246.
100. Lopez JA, Dong JF. Shear stress and the role of high molecular weight von Willebrand factor multimers in thrombus formation. *Blood Coagul Fibrinolysis*. Apr 2005;16 Suppl 1:S11-16.
101. Lindblom A, Bengtsson-Olivecrona G, Fransson LA. Domain structure of endothelial heparan sulphate. *The Biochemical journal*. Nov 1 1991;279 (Pt 3):821-829.
102. Myers PR, Tanner MA. Vascular endothelial cell regulation of extracellular matrix collagen: role of nitric oxide. *Arteriosclerosis, thrombosis, and vascular biology*. May 1998;18(5):717-722.
103. Rubanyi GM, Botelho LH. Endothelins. *Faseb J*. Sep 1991;5(12):2713-2720.
104. Vapaatalo H, Mervaala E. Clinically important factors influencing endothelial function. *Med Sci Monit*. Sep-Oct 2001;7(5):1075-1085.

105. Blum A, Miller HI. The role of inflammation in atherosclerosis. *Israel journal of medical sciences*. Nov 1996;32(11):1059-1065.
106. Holvoet P, Collen D. Thrombosis and atherosclerosis. *Current opinion in lipidology*. Oct 1997;8(5):320-328.
107. Kriegelstein CF, Granger DN. Adhesion molecules and their role in vascular disease. *American journal of hypertension*. Jun 2001;14(6 Pt 2):44S-54S.
108. Langer HF, Gawaz M. Platelet-vessel wall interactions in atherosclerotic disease. *Thrombosis and haemostasis*. Mar 2008;99(3):480-486.
109. Mitrovic S, Mitrovic D, Todorovic V, Videnovic A. [Platelet function]. *Srpski arhiv za celokupno lekarstvo*. Nov-Dec 1998;126(11-12):478-487.
110. Nabel EG. Biology of the impaired endothelium. *The American journal of cardiology*. Nov 4 1991;68(12):6C-8C.
111. Preda I, Bencze J, Vargova K. [Endothelial function and ischemic heart disease]. *Orvosi hetilap*. May 15 2005;146(20 Suppl 2):1047-1053.
112. Mannarino E, Pirro M. Endothelial injury and repair: a novel theory for atherosclerosis. *Angiology*. Apr-May 2008;59(2 Suppl):69S-72S.
113. Sprague AH, Khalil RA. Inflammatory cytokines in vascular dysfunction and vascular disease. *Biochemical pharmacology*. Sep 15 2009;78(6):539-552.

114. Versari D, Lerman LO, Lerman A. The importance of reendothelialization after arterial injury. *Current pharmaceutical design*. 2007;13(17):1811-1824.
115. Chen M, Geng JG. P-selectin mediates adhesion of leukocytes, platelets, and cancer cells in inflammation, thrombosis, and cancer growth and metastasis. *Archivum immunologiae et therapiae experimentalis*. Mar-Apr 2006;54(2):75-84.
116. Geng JG, Chen M, Chou KC. P-selectin cell adhesion molecule in inflammation, thrombosis, cancer growth and metastasis. *Current medicinal chemistry*. Aug 2004;11(16):2153-2160.
117. Piro M, Giubilato G, Pinnelli M, Giordano Sciacca P, Biasucci LM. Endothelium and inflammation. *Panminerva medica*. Jun 2005;47(2):75-80.
118. van Gils JM, Zwaginga JJ, Hordijk PL. Molecular and functional interactions among monocytes, platelets, and endothelial cells and their relevance for cardiovascular diseases. *Journal of leukocyte biology*. Feb 2009;85(2):195-204.
119. Vandendries ER, Furie BC, Furie B. Role of P-selectin and PSGL-1 in coagulation and thrombosis. *Thrombosis and haemostasis*. Sep 2004;92(3):459-466.
120. Bradbury AW, Murie JA, Ruckley CV. Role of the leucocyte in the pathogenesis of vascular disease. *The British journal of surgery*. Dec 1993;80(12):1503-1512.

121. Dosquet C, Weill D, Wautier JL. Cytokines and thrombosis. *Journal of cardiovascular pharmacology*. 1995;25 Suppl 2:S13-19.
122. Subramaniam M, Saffaripour S, Van De Water L, Frenette PS, Mayadas TN, Hynes RO, Wagner DD. Role of endothelial selectins in wound repair. *The American journal of pathology*. May 1997;150(5):1701-1709.
123. Vizcaino-Salazar G. [Platelet physiology. Advances in platelet reactivity. Review]. *Investigacion clinica*. Mar 1994;35(1):41-62.
124. Newman PJ. The role of PECAM-1 in vascular cell biology. *Annals of the New York Academy of Sciences*. Apr 18 1994;714:165-174.
125. Gawaz M, Langer H, May AE. Platelets in inflammation and atherogenesis. *The Journal of clinical investigation*. Dec 2005;115(12):3378-3384.
126. Langer H, Gawaz M. [The role of platelets for the pathophysiology of acute coronary syndromes]. *Hamostaseologie*. May 2006;26(2):114-118.
127. Lindemann S, Kramer B, Seizer P, Gawaz M. Platelets, inflammation and atherosclerosis. *J Thromb Haemost*. Jul 2007;5 Suppl 1:203-211.
128. Siegel-Axel D, Langer H, Lindemann S, Gawaz M. [Role of platelets in atherosclerosis and inflammation]. *Med Klin (Munich)*. Jun 15 2006;101(6):467-475.

129. Eniola OA, Hammer DA. In vitro characterization of leukocyte mimetic for targeting therapeutics to the endothelium using two receptors. *Biomaterials*. Dec 2005;26(34):7136-7144.
130. Sakhalkar HS, Hanes J, Fu J, Benavides U, Malgor R, Borruso CL, Kohn LD, Kurjiaka DT, Goetz DJ. Enhanced adhesion of ligand-conjugated biodegradable particles to colitic venules. *Faseb J*. May 2005;19(7):792-794.
131. Zou X, Shinde Patil VR, Dagia NM, Smith LA, Wargo MJ, Interliggi KA, Lloyd CM, Tees DF, Walcheck B, Lawrence MB, Goetz DJ. PSGL-1 derived from human neutrophils is a high-efficiency ligand for endothelium-expressed E-selectin under flow. *American journal of physiology*. Aug 2005;289(2):C415-424.
132. Burch EE, Shinde Patil VR, Camphausen RT, Kiani MF, Goetz DJ. The N-terminal peptide of PSGL-1 can mediate adhesion to trauma-activated endothelium via P-selectin in vivo. *Blood*. Jul 15 2002;100(2):531-538.
133. Nesbitt WS, Mangin P, Salem HH, Jackson SP. The impact of blood rheology on the molecular and cellular events underlying arterial thrombosis. *Journal of molecular medicine (Berlin, Germany)*. Dec 2006;84(12):989-995.
134. Andrews RK, Berndt MC. Platelet physiology and thrombosis. *Thrombosis research*. 2004;114(5-6):447-453.

135. Andrews RK, Shen Y, Gardiner EE, Berndt MC. Platelet adhesion receptors and (patho)physiological thrombus formation. *Histology and histopathology*. Jul 2001;16(3):969-980.
136. Elstad MR, McIntyre TM, Prescott SM, Zimmerman GA. The interaction of leukocytes with platelets in blood coagulation. *Current opinion in hematology*. Jan 1995;2(1):47-54.
137. McIntyre TM, Prescott SM, Weyrich AS, Zimmerman GA. Cell-cell interactions: leukocyte-endothelial interactions. *Current opinion in hematology*. Mar 2003;10(2):150-158.
138. Zimmerman GA, McIntyre TM, Prescott SM. Adhesion and signaling in vascular cell-cell interactions. *The Journal of clinical investigation*. Oct 15 1996;98(8):1699-1702.
139. Zimmerman GA, McIntyre TM, Prescott SM. Adhesion and signaling in vascular cell-cell interactions. *The Journal of clinical investigation*. Dec 1 1997;100(11 Suppl):S3-5.
140. Solum NO. Procoagulant expression in platelets and defects leading to clinical disorders. *Arteriosclerosis, thrombosis, and vascular biology*. Dec 1999;19(12):2841-2846.
141. Andrews RK, Gardiner EE, Shen Y, Berndt MC. Platelet interactions in thrombosis. *IUBMB life*. Jan 2004;56(1):13-18.

142. Andrews RK, Gardiner EE, Shen Y, Whisstock JC, Berndt MC. Glycoprotein Ib-IX-V. *The international journal of biochemistry & cell biology*. Aug 2003;35(8):1170-1174.
143. Yip J, Shen Y, Berndt MC, Andrews RK. Primary platelet adhesion receptors. *IUBMB Life*. Feb 2005;57(2):103-108.
144. Gawaz M. Role of platelets in coronary thrombosis and reperfusion of ischemic myocardium. *Cardiovascular research*. Feb 15 2004;61(3):498-511.
145. Baruch D. [Platelet--vessel wall interactions]. *Therapie*. Sep-Oct 2006;61(5):371-378.
146. Massberg S, Brand K, Gruner S, Page S, Muller E, Muller I, Bergmeier W, Richter T, Lorenz M, Konrad I, Nieswandt B, Gawaz M. A critical role of platelet adhesion in the initiation of atherosclerotic lesion formation. *The Journal of experimental medicine*. Oct 7 2002;196(7):887-896.
147. Cook S, Togni M, Schaub MC, Wenaweser P, Hess OM. High heart rate: a cardiovascular risk factor? *European heart journal*. Oct 2006;27(20):2387-2393.
148. Malek AM, Alper SL, Izumo S. Hemodynamic Shear Stress and Its Role in Atherosclerosis. Vol 282; 1999:2035-2042.
149. Thorin E, Thorin-Trescases N. Vascular endothelial ageing, heartbeat after heartbeat. *Cardiovascular research*. Oct 1 2009;84(1):24-32.

150. Kroll MH, Hellums JD, McIntire LV, Schafer AI, Moake JL. Platelets and shear stress. *Blood*. Sep 1 1996;88(5):1525-1541.
151. Deshayes S, Morris MC, Divita G, Heitz F. Cell-penetrating peptides: tools for intracellular delivery of therapeutics. *Cell Mol Life Sci*. Aug 2005;62(16):1839-1849.
152. Morris MC, Deshayes S, Heitz F, Divita G. Cell-penetrating peptides: from molecular mechanisms to therapeutics. *Biology of the cell / under the auspices of the European Cell Biology Organization*. Apr 2008;100(4):201-217.
153. Pooga M, Langel U. Synthesis of cell-penetrating peptides for cargo delivery. *Methods in molecular biology (Clifton, N.J.)* 2005;298:77-89.
154. Fawell S, Seery J, Daikh Y, Moore C, Chen LL, Pepinsky B, Barsoum J. Tat-mediated delivery of heterologous proteins into cells. *Proceedings of the National Academy of Sciences of the United States of America*. Jan 18 1994;91(2):664-668.
155. Moy P, Daikh Y, Pepinsky B, Thomas D, Fawell S, Barsoum J. Tat-mediated protein delivery can facilitate MHC class I presentation of antigens. *Molecular biotechnology*. Oct 1996;6(2):105-113.
156. Abes R, Arzumanov AA, Moulton HM, Abes S, Ivanova GD, Iversen PL, Gait MJ, Lebleu B. Cell-penetrating-peptide-based delivery of oligonucleotides: an overview. *Biochemical Society transactions*. Aug 2007;35(Pt 4):775-779.

157. Fonseca SB, Pereira MP, Kelley SO. Recent advances in the use of cell-penetrating peptides for medical and biological applications. *Advanced drug delivery reviews*. Sep 30 2009;61(11):953-964.
158. Veldhoen S, Laufer SD, Restle T. Recent developments in Peptide-based nucleic Acid delivery. *International journal of molecular sciences*. Jun 2008;9(7):1276-1320.
159. Foged C, Nielsen HM. Cell-penetrating peptides for drug delivery across membrane barriers. *Expert opinion on drug delivery*. Jan 2008;5(1):105-117.
160. Torchilin VP. Tatp-mediated intracellular delivery of pharmaceutical nanocarriers. *Biochemical Society transactions*. Aug 2007;35(Pt 4):816-820.
161. Torchilin VP. Cell penetrating peptide-modified pharmaceutical nanocarriers for intracellular drug and gene delivery. *Biopolymers*. 2008;90(5):604-610.
162. Koppelhus U, Awasthi SK, Zachar V, Holst HU, Ebbesen P, Nielsen PE. Cell-dependent differential cellular uptake of PNA, peptides, and PNA-peptide conjugates. *Antisense & nucleic acid drug development*. Apr 2002;12(2):51-63.
163. Rao KS, Labhasetwar V. Trans-Activating Transcriptional Activator (TAT) Peptide-Mediated Brain Drug Delivery. *Journal of Biomedical Nanotechnology*. 2006;2:173-185.

164. Rao KS, Reddy MK, Horning JL, Labhasetwar V. TAT-conjugated nanoparticles for the CNS delivery of anti-HIV drugs. *Biomaterials*. Nov 2008;29(33):4429-4438.
165. Rinne J, Albarran B, Jylhava J, Ihalainen TO, Kankaanpaa P, Hytonen VP, Stayton PS, Kulomaa MS, Vihinen-Ranta M. Internalization of novel non-viral vector TAT-streptavidin into human cells. *BMC biotechnology*. 2007;7:1.
166. Petrik PV, Law MM, Moore WS, Colburn MD, Quinones-Baldrich W, Gelabert HA. Dexamethasone and enalapril suppress intimal hyperplasia individually but have no synergistic effect. *Ann Vasc Surg*. May 1998;12(3):216-220.
167. Liu X, De Scheerder I, Desmet W. Dexamethasone-eluting stent: an anti-inflammatory approach to inhibit coronary restenosis. *Expert Rev Cardiovasc Ther*. Sep 2004;2(5):653-660.
168. Lutters BC, Leeuwenburgh MA, Appeldoorn CC, Molenaar TJ, Van Berkel TJ, Biessen EA. Blocking endothelial adhesion molecules: a potential therapeutic strategy to combat atherogenesis. *Curr Opin Lipidol*. Oct 2004;15(5):545-552.
169. Thiemeermann C. Nitric oxide and septic shock. *General pharmacology*. Aug 1997;29(2):159-166.
170. Sakhalkar HS, Dalal MK, Salem AK, Ansari R, Fu J, Kiani MF, Kurjiaka DT, Hanes J, Shakesheff KM, Goetz DJ. Leukocyte-inspired biodegradable particles

that selectively and avidly adhere to inflamed endothelium in vitro and in vivo.

Proc Natl Acad Sci U S A. Dec 23 2003;100(26):15895-15900.

171. Clark P, Boswell F, Greer IA. The neutrophil and preeclampsia. *Seminars in reproductive endocrinology.* 1998;16(1):57-64.
172. Polek A, Sobiczewski W, Matowicka-Karna J. [P-selectin and its role in some diseases]. *Postepy higieny i medycyny doswiadczalnej (Online).* 2009;63:465-470.
173. Sluiter W, Pietersma A, Lamers JM, Koster JF. Leukocyte adhesion molecules on the vascular endothelium: their role in the pathogenesis of cardiovascular disease and the mechanisms underlying their expression. *Journal of cardiovascular pharmacology.* 1993;22 Suppl 4:S37-44.
174. Giddings JC, Banning AP, Ralis H, Lewis MJ. Redistribution of von Willebrand factor in porcine carotid arteries after balloon angioplasty. *Arteriosclerosis, thrombosis, and vascular biology.* Oct 1997;17(10):1872-1878.
175. Tsakiris DA, Tschèopl M, Jèager K, Haefeli WE, Wolf F, Marbet GA. Circulating cell adhesion molecules and endothelial markers before and after transluminal angioplasty in peripheral arterial occlusive disease. *Atherosclerosis.* Jan 1999;142(1):193-200.
176. Dong J, Ye P, Schade AJ, Gao S, Romo GM, Turner NT, McIntire LV, Lâopez JA. Tyrosine sulfation of glycoprotein I(b)alpha. Role of electrostatic

- interactions in von Willebrand factor binding. *J Biol Chem.* May 18 2001;276(20):16690-16694.
- 177.** Fredrickson BJ, Dong JF, McIntire LV, L opez JA. Shear-dependent rolling on von Willebrand factor of mammalian cells expressing the platelet glycoprotein Ib-IX-V complex. *Blood.* Nov 15 1998;92(10):3684-3693.
- 178.** Li CQ, Dong JF, L opez JA. The mucin-like macroglycopeptide region of glycoprotein Ib α is required for cell adhesion to immobilized von Willebrand factor (VWF) under flow but not for static VWF binding. *Thromb Haemost.* Oct 2002;88(4):673-677.
- 179.** Chen J, L opez JA. Interactions of platelets with subendothelium and endothelium. *Microcirculation.* Apr-May 2005;12(3):235-246.
- 180.** Rao KS, Labhasetwar V. Trans-Activating Transcriptional Activator (TAT) Peptide-Mediated Brain Drug Delivery. *Journal of Biomedical Nanotechnology.* October/December 2006;2(3-4):173-185.
- 181.** Chen C, Hu JT, Tu YJ, Wu JC, Liang J, Gao LL, Wang ZG, Yang BF, Dong DL. Effects of isosorbide mononitrate on the restoration of injured artery in mice in vivo. *European journal of pharmacology.* Aug 25;640(1-3):150-156.
- 182.** Haynes WG. Hyperhomocysteinemia, vascular function and atherosclerosis: effects of vitamins. *Cardiovascular drugs and therapy / sponsored by the*

International Society of Cardiovascular Pharmacotherapy. Sep 2002;16(5):391-399.

183. Kurowska EM. Nitric oxide therapies in vascular diseases. *Current pharmaceutical design*. 2002;8(3):155-166.
184. Meadows TA, Bhatt DL. Clinical aspects of platelet inhibitors and thrombus formation. *Circ Res*. May 11 2007;100(9):1261-1275.
185. Charron T, Nili N, Strauss BH. The cell cycle: a critical therapeutic target to prevent vascular proliferative disease. *The Canadian journal of cardiology*. Feb 2006;22 Suppl B:41B-55B.
186. Berk BC, Gordon JB, Alexander RW. Pharmacologic roles of heparin and glucocorticoids to prevent restenosis after coronary angioplasty. *Journal of the American College of Cardiology*. May 1991;17(6 Suppl B):111B-117B.
187. Celik T, Iyisoy A, Barindik N, Isik E. Glucocorticoids in the prevention of in-stent restenosis: the role of inflammation. *International journal of cardiology*. Jul 10 2009;135(3):403-405.
188. Ferrero V, Ribichini F, Pesarini G, Brunelleschi S, Vassanelli C. Glucocorticoids in the prevention of restenosis after coronary angioplasty: therapeutic potential. *Drugs*. 2007;67(9):1243-1255.
189. Han SH, Ahn TH, Kang WC, Oh KJ, Chung WJ, Shin MS, Koh KK, Choi IS, Shin EK. The favorable clinical and angiographic outcomes of a high-dose

- dexamethasone-eluting stent: randomized controlled prospective study. *American heart journal*. Nov 2006;152(5):887 e881-887.
- 190.** Radke PW, Weber C, Kaiser A, Schober A, Hoffmann R. Dexamethasone and restenosis after coronary stent implantation: new indication for an old drug? *Current pharmaceutical design*. 2004;10(4):349-355.
- 191.** Eniola AO, Hammer DA. Artificial polymeric cells for targeted drug delivery. *J Control Release*. Feb 21 2003;87(1-3):15-22.
- 192.** Eniola AO, Hammer DA. Characterization of biodegradable drug delivery vehicles with the adhesive properties of leukocytes II: effect of degradation on targeting activity. *Biomaterials*. Feb 2005;26(6):661-670.
- 193.** Eniola AO, Rodgers SD, Hammer DA. Characterization of biodegradable drug delivery vehicles with the adhesive properties of leukocytes. *Biomaterials*. May 2002;23(10):2167-2177.
- 194.** Nguyen KT, Shukla KP, Moctezuma M, Braden AR, Zhou J, Hu Z, L. T. Studies of the cellular uptake of hydrogel nanospheres and microspheres by phagocytes, vascular endothelial cells, and smooth muscle cells. *J Biomed Mater Res A*. 2009;88(4):1022-1030.
- 195.** Dong JF, Moake JL, Bernardo A, Fujikawa K, Ball C, Nolasco L, Lopez JA, Cruz MA. ADAMTS-13 metalloprotease interacts with the endothelial cell-

- derived ultra-large von Willebrand factor. *The Journal of biological chemistry*. Aug 8 2003;278(32):29633-29639.
- 196.** Romo GM, Dong JF, Schade AJ, Gardiner EE, Kansas GS, Li CQ, McIntire LV, Berndt MC, Lopez JA. The glycoprotein Ib-IX-V complex is a platelet counterreceptor for P-selectin. *The Journal of experimental medicine*. Sep 20 1999;190(6):803-814.
- 197.** Chithrani BD, Chan WC. Elucidating the mechanism of cellular uptake and removal of protein-coated gold nanoparticles of different sizes and shapes. *Nano letters*. Jun 2007;7(6):1542-1550.
- 198.** Panyam J, Labhasetwar V. Dynamics of endocytosis and exocytosis of poly(D,L-lactide-co-glycolide) nanoparticles in vascular smooth muscle cells. *Pharmaceutical research*. Feb 2003;20(2):212-220.
- 199.** Reneman RS, Hoeks AP. Wall shear stress as measured in vivo: consequences for the design of the arterial system. *Medical & biological engineering & computing*. May 2008;46(5):499-507.
- 200.** Chung WB, Hamburg NM, Holbrook M, Shenouda SM, Dohadwala MM, Terry DF, Gokce N, Vita JA. The Brachial Artery Remodels to Maintain Local Shear Stress Despite the Presence of Cardiovascular Risk Factors. Vol 29; 2009:606-612.

- 201.** Stone PH, Coskun AU, Kinlay S, Popma JJ, Sonka M, Wahle A, Yeghiazarians Y, Maynard C, Kuntz RE, Feldman CL. Regions of low endothelial shear stress are the sites where coronary plaque progresses and vascular remodelling occurs in humans: an in vivo serial study. *Vol 28; 2007:705-710.*
- 202.** Nguyen KT, Eskin SG, Patterson C, Runge MS, McIntire LV. Shear stress reduces protease activated receptor-1 expression in human endothelial cells. *Annals of biomedical engineering.* Feb 2001;29(2):145-152.
- 203.** Ludwig RJ, Schon MP, Boehncke WH. P-selectin: a common therapeutic target for cardiovascular disorders, inflammation and tumour metastasis. *Expert opinion on therapeutic targets.* Aug 2007;11(8):1103-1117.
- 204.** Smith CW. Endothelial adhesion molecules and their role in inflammation. *Canadian journal of physiology and pharmacology.* Jan 1993;71(1):76-87.
- 205.** Strukova S. Blood coagulation-dependent inflammation. Coagulation-dependent inflammation and inflammation-dependent thrombosis. *Front Biosci.* 2006;11:59-80.
- 206.** Zarbock A, Polanowska-Grabowska RK, Ley K. Platelet-neutrophil-interactions: linking hemostasis and inflammation. *Blood reviews.* Mar 2007;21(2):99-111.

- 207.** Cascone MG, Pot PM, Lazzeri L, Zhu Z. Release of dexamethasone from PLGA nanoparticles entrapped into dextran/poly(vinyl alcohol) hydrogels. *Journal of materials science*. Mar 2002;13(3):265-269.
- 208.** Kim DH, Martin DC. Sustained release of dexamethasone from hydrophilic matrices using PLGA nanoparticles for neural drug delivery. *Biomaterials*. May 2006;27(15):3031-3037.
- 209.** Chan JM, Zhang L, Yuet KP, Liao G, Rhee JW, Langer R, Farokhzad OC. PLGA-lecithin-PEG core-shell nanoparticles for controlled drug delivery. *Biomaterials*. Mar 2009;30(8):1627-1634.
- 210.** Sahu A, Bora U, Kasoju N, Goswami P. Synthesis of novel biodegradable and self-assembling methoxy poly(ethylene glycol)-palmitate nanocarrier for curcumin delivery to cancer cells. *Acta biomaterialia*. Nov 2008;4(6):1752-1761.
- 211.** Talelli M, Rijcken CJ, Lammers T, Seevinck PR, Storm G, van Nostrum CF, Hennink WE. Superparamagnetic iron oxide nanoparticles encapsulated in biodegradable thermosensitive polymeric micelles: toward a targeted nanomedicine suitable for image-guided drug delivery. *Langmuir*. Feb 17 2009;25(4):2060-2067.

- 212.** Frohlich E, Samberger C, Kueznik T, Absenger M, Roblegg E, Zimmer A, Pieber TR. Cytotoxicity of nanoparticles independent from oxidative stress. *The Journal of toxicological sciences*. Oct 2009;34(4):363-375.
- 213.** Rejman J, Oberle V, Zuhorn IS, Hoekstra D. Size-dependent internalization of particles via the pathways of clathrin- and caveolae-mediated endocytosis. *The Biochemical journal*. Jan 1 2004;377(Pt 1):159-169.
- 214.** Vasir JK, Labhasetwar V. Polymeric nanoparticles for gene delivery. *Expert opinion on drug delivery*. May 2006;3(3):325-344.
- 215.** Guzman LA, Labhasetwar V, Song C, Jang Y, Lincoff AM, Levy R, Topol EJ. Local intraluminal infusion of biodegradable polymeric nanoparticles. A novel approach for prolonged drug delivery after balloon angioplasty. *Circulation*. Sep 15 1996;94(6):1441-1448.
- 216.** Song C, Labhasetwar V, Cui X, Underwood T, Levy RJ. Arterial uptake of biodegradable nanoparticles for intravascular local drug delivery: results with an acute dog model. *J Control Release*. Jul 31 1998;54(2):201-211.
- 217.** Muro S, Cui X, Gajewski C, Murciano JC, Muzykantov VR, Koval M. Slow intracellular trafficking of catalase nanoparticles targeted to ICAM-1 protects endothelial cells from oxidative stress. *Am J Physiol Cell Physiol*. Nov 2003;285(5):C1339-1347.

- 218.** Muro S, Koval M, Muzykantov V. Endothelial endocytic pathways: gates for vascular drug delivery. *Curr Vasc Pharmacol*. Jul 2004;2(3):281-299.
- 219.** Muro S, Wiewrodt R, Thomas A, Koniaris L, Albelda SM, Muzykantov VR, Koval M. A novel endocytic pathway induced by clustering endothelial ICAM-1 or PECAM-1. *Journal of cell science*. Apr 15 2003;116(Pt 8):1599-1609.
- 220.** Qaddoumi MG, Gukasyan HJ, Davda J, Labhasetwar V, Kim KJ, Lee VH. Clathrin and caveolin-1 expression in primary pigmented rabbit conjunctival epithelial cells: role in PLGA nanoparticle endocytosis. *Molecular vision*. Oct 15 2003;9:559-568.
- 221.** Panyam J, Zhou WZ, Prabha S, Sahoo SK, Labhasetwar V. Rapid endo-lysosomal escape of poly(DL-lactide-co-glycolide) nanoparticles: implications for drug and gene delivery. *Faseb J*. Aug 2002;16(10):1217-1226.
- 222.** Qaddoumi MG, Ueda H, Yang J, Davda J, Labhasetwar V, Lee VH. The characteristics and mechanisms of uptake of PLGA nanoparticles in rabbit conjunctival epithelial cell layers. *Pharmaceutical research*. Apr 2004;21(4):641-648.
- 223.** Wiewrodt R, Thomas AP, Cipelletti L, Christofidou-Solomidou M, Weitz DA, Feinstein SI, Schaffer D, Albelda SM, Koval M, Muzykantov VR. Size-dependent intracellular immunotargeting of therapeutic cargoes into endothelial cells. *Blood*. Feb 1 2002;99(3):912-922.

224. Xu P, Gullotti E, Tong L, Highley CB, Errabelli DR, Hasan T, Cheng JX, Kohane DS, Yeo Y. Intracellular drug delivery by poly(lactic-co-glycolic acid) nanoparticles, revisited. *Molecular pharmaceutics*. Jan-Feb 2009;6(1):190-201.
225. Dickerson JB, Blackwell JE, Ou JJ, Shinde Patil VR, Goetz DJ. Limited adhesion of biodegradable microspheres to E- and P-selectin under flow. *Biotechnology and bioengineering*. Jun 20 2001;73(6):500-509.
226. Eniola AO, Willcox PJ, Hammer DA. Interplay between rolling and firm adhesion elucidated with a cell-free system engineered with two distinct receptor-ligand pairs. *Biophysical journal*. Oct 2003;85(4):2720-2731.
227. Eniola AO, Krasik EF, Smith LA, Song G, Hammer DA. I-domain of lymphocyte function-associated antigen-1 mediates rolling of polystyrene particles on ICAM-1 under flow. *Biophysical journal*. Nov 2005;89(5):3577-3588.
228. Grabowski EF. Thrombolysis, flow, and vessel wall interactions. *J Vasc Interv Radiol*. Nov-Dec 1995;6(6 Pt 2 Su):25S-29S.
229. Gao Y, Xu P, Chen L, Li Y. Prostaglandin E1 encapsulated into lipid nanoparticles improves its anti-inflammatory effect with low side-effect. *International journal of pharmaceutics*. Mar 15;387(1-2):263-271.
230. Ravindran J, Nair HB, Sung B, Prasad S, Tekmal RR, Aggarwal BB. Thymoquinone poly (lactide-co-glycolide) nanoparticles exhibit enhanced anti-

- proliferative, anti-inflammatory, and chemosensitization potential. *Biochemical pharmacology*. Jun 1;79(11):1640-1647.
- 231.** Vivès E, Schmidt J, Pèlerin A. Cell-penetrating and cell-targeting peptides in drug delivery. *Biochimica et Biophysica Acta (BBA) - Reviews on Cancer*. 2008;1786(2):126-138.
- 232.** Brooks NA, Pouniotis DS, Tang C-K, Apostolopoulos V, Pietersz GA. Cell-penetrating peptides: Application in vaccine delivery. *Biochimica et Biophysica Acta (BBA) - Reviews on Cancer*. 1805(1):25-34.
- 233.** Temsamani J, Vidal P. The use of cell-penetrating peptides for drug delivery. *Drug Discovery Today*. 2004;9(23):1012-1019.
- 234.** Gupta B, Levchenko TS, Torchilin VP. Intracellular delivery of large molecules and small particles by cell-penetrating proteins and peptides. *Advanced drug delivery reviews*. 2005;57(4):637-651.
- 235.** Meade BR, Dowdy SF. Exogenous siRNA delivery using peptide transduction domains/cell penetrating peptides. *Advanced drug delivery reviews*. 2007;59(2-3):134-140.
- 236.** Avgoustakis K, Beletsi A, Panagi Z, Klepetsanis P, Livaniou E, Evangelatos G, Ithakissios DS. Effect of copolymer composition on the physicochemical characteristics, in vitro stability, and biodistribution of PLGA-mPEG

- nanoparticles. *International journal of pharmaceutics*. Jun 18 2003;259(1-2):115-127.
237. Klibanov AL, Maruyama K, Torchilin VP, Huang L. Amphipathic polyethyleneglycols effectively prolong the circulation time of liposomes. *FEBS letters*. Jul 30 1990;268(1):235-237.
238. Mosqueira VC, Legrand P, Morgat JL, Vert M, Mysiakine E, Gref R, Devissaguet JP, Barratt G. Biodistribution of long-circulating PEG-grafted nanocapsules in mice: effects of PEG chain length and density. *Pharmaceutical research*. Oct 2001;18(10):1411-1419.
239. Li Y, Pei Y, Zhang X, Gu Z, Zhou Z, Yuan W, Zhou J, Zhu J, Gao X. PEGylated PLGA nanoparticles as protein carriers: synthesis, preparation and biodistribution in rats. *J Control Release*. Apr 2 2001;71(2):203-211.
240. Perez C, Sanchez A, Putnam D, Ting D, Langer R, Alonso MJ. Poly(lactic acid)-poly(ethylene glycol) nanoparticles as new carriers for the delivery of plasmid DNA. *J Control Release*. Jul 10 2001;75(1-2):211-224.
241. Shin SB, Cho HY, Kim DD, Choi HG, Lee YB. Preparation and evaluation of tacrolimus-loaded nanoparticles for lymphatic delivery. *Eur J Pharm Biopharm*. Feb;74(2):164-171.
242. Zhou J, Fan J, Hsieh JT. Inhibition of mitogen-elicited signal transduction and growth in prostate cancer with a small peptide derived from the functional

- domain of DOC-2/DAB2 delivered by a unique vehicle. *Cancer research*. Sep 15 2006;66(18):8954-8958.
- 243.** Jia H, Lohr M, Jezequel S, Davis D, Shaikh S, Selwood D, Zachary I. Cysteine-rich and basic domain HIV-1 Tat peptides inhibit angiogenesis and induce endothelial cell apoptosis. *Biochemical and biophysical research communications*. May 4 2001;283(2):469-479.
- 244.** Vives E, Brodin P, Lebleu B. A truncated HIV-1 Tat protein basic domain rapidly translocates through the plasma membrane and accumulates in the cell nucleus. *The Journal of biological chemistry*. Jun 20 1997;272(25):16010-16017.
- 245.** Xu F, Lu W, Wu H, Fan L, Gao X, Jiang X. Brain delivery and systemic effect of cationic albumin conjugated PLGA nanoparticles. *Journal of drug targeting*. Jul 2009;17(6):423-434.
- 246.** Berry CC, de la Fuente JM, Mullin M, Chu SW, Curtis AS. Nuclear localization of HIV-1 tat functionalized gold nanoparticles. *IEEE transactions on nanobioscience*. Dec 2007;6(4):262-269.
- 247.** Liu L, Venkatraman SS, Yang YY, Guo K, Lu J, He B, Mochhala S, Kan L. Polymeric micelles anchored with TAT for delivery of antibiotics across the blood-brain barrier. *Biopolymers*. 2008;90(5):617-623.

- 248.** Martin AL, Bernas LM, Rutt BK, Foster PJ, Gillies ER. Enhanced cell uptake of superparamagnetic iron oxide nanoparticles functionalized with dendritic guanidines. *Bioconjugate chemistry*. Dec 2008;19(12):2375-2384.
- 249.** Peetla C, Rao KS, Labhasetwar V. Relevance of biophysical interactions of nanoparticles with a model membrane in predicting cellular uptake: study with TAT peptide-conjugated nanoparticles. *Molecular pharmaceutics*. Sep-Oct 2009;6(5):1311-1320.
- 250.** Zhang K, Fang H, Chen Z, Taylor JS, Wooley KL. Shape effects of nanoparticles conjugated with cell-penetrating peptides (HIV Tat PTD) on CHO cell uptake. *Bioconjugate chemistry*. Sep 2008;19(9):1880-1887.
- 251.** Mo Y, Lim LY. Mechanistic study of the uptake of wheat germ agglutinin-conjugated PLGA nanoparticles by A549 cells. *Journal of pharmaceutical sciences*. Jan 2004;93(1):20-28.
- 252.** Nam HY, Kwon SM, Chung H, Lee SY, Kwon SH, Jeon H, Kim Y, Park JH, Kim J, Her S, Oh YK, Kwon IC, Kim K, Jeong SY. Cellular uptake mechanism and intracellular fate of hydrophobically modified glycol chitosan nanoparticles. *J Control Release*. May 5 2009;135(3):259-267.
- 253.** Richard JP, Melikov K, Brooks H, Prevot P, Lebleu B, Chernomordik LV. Cellular uptake of unconjugated TAT peptide involves clathrin-dependent

- endocytosis and heparan sulfate receptors. *The Journal of biological chemistry*. Apr 15 2005;280(15):15300-15306.
- 254.** Wadia JS, Stan RV, Dowdy SF. Transducible TAT-HA fusogenic peptide enhances escape of TAT-fusion proteins after lipid raft macropinocytosis. *Nature medicine*. Mar 2004;10(3):310-315.
- 255.** Takeoka S, Teramura Y, Ohkawa H, Ikeda Y, Tsuchida E. Conjugation of von Willebrand factor-binding domain of platelet glycoprotein Ib alpha to size-controlled albumin microspheres. *Biomacromolecules*. Summer 2000;1(2):290-295.
- 256.** Teramura Y, Okamura Y, Takeoka S, Tsuchiyama H, Narumi H, Kainoh M, Handa M, Ikeda Y, Tsuchida E. Hemostatic effects of polymerized albumin particles bearing rGPIa/IIa in thrombocytopenic mice. *Biochem Biophys Res Commun*. Jun 20 2003;306(1):256-260.
- 257.** Ikeda Y, Handa M, Murata M, Goto S. A new approach to antiplatelet therapy: inhibitor of GPIb/V/IX-vWF interaction. *Haemostasis*. 2000;30:44-52.
- 258.** Nishiya T, Kainoh M, Murata M, Handa M, Ikeda Y. Reconstitution of adhesive properties of human platelets in liposomes carrying both recombinant glycoproteins Ia/IIa and Ib alpha under flow conditions: specific synergy of receptor-ligand interactions. *Blood*. Jul 1 2002;100(1):136-142.

- 259.** Takeoka S, Teramura Y, Okamura Y, Handa M, Ikeda Y, Tsuchida E. Fibrinogen-conjugated albumin polymers and their interaction with platelets under flow conditions. *Biomacromolecules*. Winter 2001;2(4):1192-1197.
- 260.** Alisky JM. Dexamethasone could improve myocardial infarction outcomes and provide new therapeutic options for non-interventional patients. *Medical hypotheses*. 2006;67(1):53-56.
- 261.** Fiarresga AJ, Fernandes R, Feliciano J, de Sousa L, Cacela D, Bernardes L, Patricio L, Ferreira RC, Quininha J. Drug-eluting stents in primary angioplasty long-term clinical outcomes. *Rev Port Cardiol*. Mar 2007;26(3):211-222.
- 262.** Hoffmann R, Langenberg R, Radke P, Franke A, Blindt R, Ortlepp J, Popma JJ, Weber C, Hanrath P. Evaluation of a high-dose dexamethasone-eluting stent. *The American journal of cardiology*. Jul 15 2004;94(2):193-195.
- 263.** Lincoff AM, Furst JG, Ellis SG, Tuch RJ, Topol EJ. Sustained local delivery of dexamethasone by a novel intravascular eluting stent to prevent restenosis in the porcine coronary injury model. *Journal of the American College of Cardiology*. Mar 15 1997;29(4):808-816.
- 264.** Muller DW, Golomb G, Gordon D, Levy RJ. Site-specific dexamethasone delivery for the prevention of neointimal thickening after vascular stent implantation. *Coronary artery disease*. May 1994;5(5):435-442.

- 265.** Ribichini F, Tomai F, Paloscia L, Di Sciascio G, Carosio G, Romano M, Verna E, Galli M, Tamburino C, De Cesare N, Pirisi R, Piscione F, Lanteri G, Ferrero V, Vassanelli C. Steroid-eluting stents in patients with acute coronary syndrome: the dexamethasone eluting stent Italian registry. *Heart (British Cardiac Society)*. May 2007;93(5):598-600.
- 266.** Culpitt SV, Rogers DF, Shah P, De Matos C, Russell RE, Donnelly LE, Barnes PJ. Impaired inhibition by dexamethasone of cytokine release by alveolar macrophages from patients with chronic obstructive pulmonary disease. *American journal of respiratory and critical care medicine*. Jan 1 2003;167(1):24-31.
- 267.** van der Hoeven BL, Pires NM, Warda HM, Putter H, Quax PH, Schaliij MJ, Jukema JW. Dexamethasone-eluting stents for the prevention of in-stent restenosis: evidence for a differential effect in insulin-dependent and non-insulin-dependent diabetic patients. *International journal of cardiology*. Feb 29 2008;124(2):166-171.

BIOGRAPHICAL INFORMATION

Soujanya Kona received her Master of Science in 2001 in Biomedical Engineering from Jadavpur University, Kolkata, India. She also earned her Bachelor of Science in Zoology Honors from Utkal University, India in 1996 and graduated with her first Master of Science Degree in Bioinstrumentation from the Birla Institute of Technology, Mesra, India in 1999. Soujanya was born in Andhra Pradesh, India. Following the completion of her second Master's degree, she worked as an Assistant Professor in an engineering college for five years before enrolling in the PhD program. Soujanya was accepted into the Bioengineering Doctoral Program at the University of Texas at Arlington in summer 2006 where she began her research under the guidance of Dr. Kytai Nguyen. Her research interests include drug delivery, biomaterials and tissue engineering applications, with focus on nanoparticle-based therapeutic systems.